
Electronic Thesis and Dissertation Repository

12-14-2015 12:00 AM

Towards the Development of a Wearable Tremor Suppression Glove

Yue Zhou

The University of Western Ontario

Supervisor

Dr. Ana Luisa Trejos

The University of Western Ontario Joint Supervisor

Dr. Michael D. Naish

The University of Western Ontario

Graduate Program in Electrical and Computer Engineering

A thesis submitted in partial fulfillment of the requirements for the degree in Master of Engineering Science

© Yue Zhou 2015

Follow this and additional works at: <https://ir.lib.uwo.ca/etd>



Part of the [Biological Engineering Commons](#), [Biomedical Commons](#), [Biomedical Devices and Instrumentation Commons](#), [Electro-Mechanical Systems Commons](#), [Nervous System Diseases Commons](#), and the [Signal Processing Commons](#)

Recommended Citation

Zhou, Yue, "Towards the Development of a Wearable Tremor Suppression Glove" (2015). *Electronic Thesis and Dissertation Repository*. 3432.

<https://ir.lib.uwo.ca/etd/3432>

This Dissertation/Thesis is brought to you for free and open access by Scholarship@Western. It has been accepted for inclusion in Electronic Thesis and Dissertation Repository by an authorized administrator of Scholarship@Western. For more information, please contact wlsadmin@uwo.ca.

Towards the Development of a Wearable Tremor Suppression Glove

(Thesis format: Monograph)

by

Yue Zhou

Faculty of Engineering
Department of Electrical and Computer Engineering

A thesis submitted in partial fulfillment
of the requirements for the degree of
Master of Engineering Science

The School of Graduate and Postdoctoral Studies
The University of Western Ontario
London, Ontario, Canada

© Yue Zhou, 2015

Abstract

Patients diagnosed with Parkinson's disease (PD) often associate with tremor. Among other symptoms of PD, tremor is the most aggressive symptom and it is difficult to control with traditional treatments. This thesis presents the assessment of Parkinsonian hand tremor in both the time domain and the frequency domain, the performance of a tremor estimator using different tremor models, and the development of a novel mechatronic transmission system for a wearable tremor suppression device. This transmission system functions as a mechatronic splitter that allows a single power source to support multiple independent applications. Unique features of this transmission system include low power consumption and adjustability in size and weight. Tremor assessment results showed that the hand tremor signal often presents a multi-harmonics pattern. The use of a multi-harmonics tremor model produced a better estimation result than using a monoharmonic tremor model.

Keywords

Parkinson's disease, tremor, Parkinsonian tremor, pathological tremor, hand tremor, resting tremor, postural tremor, tremor assessment, tremor suppression, tremor estimation, tremor cancellation, tremor suppression glove, mechatronic splitter, single-input-multiple-output mechanism, wearable device.

Acknowledgments

A gentle breeze delivered the smell of April grass to a *grus japonensis*. At that moment, a ripple appeared in his heart.

Without the support, criticism and approval from everyone in my life, I couldn't have made it this far.

I believe success consists of two parts, 99% perspiration and 1% luck. I also believe that this 1% luck is crucial to one's success. I always consider myself blessed to have the opportunity of working and learning from my supervisors, Dr. Ana Luisa Trejos and Dr. Michael D. Naish. Their constant support brought me the space to progress; their honest suggestions kept my feet on the ground; and their approvals have brought the sweetest fruit to me. I would like to express my sincere gratitude to both of them. Without them, I couldn't have made it this far.

I also want to thank Prof. Mu Zhang from Tianjin Polytechnic University, Tianjin, China. He is my mentor, my friend and like a father to me. His care, direction and encouragement have always accompanied me. If Dr. Trejos and Dr. Naish were the ones who brought me the sky, Dr. Zhang was the one who gave me the wings. Furthermore, I want to thank Tianjin Polytechnic University, which provided me the platform and opportunity to learn and progress.

Growth is never by mere chance; it is the result of forces working together. I believe this quote expresses the secret of James C. Penny's success. In the past two years, I have experienced a lot of great moments with my colleagues. I would like to thank Abelardo Escoto Murillo, who not only provided technical support for this project including 3D printing and machining, but gave me suggestive ideas and encouragement. Discussion with Anastasia Kyrylova always inspired me. Her suggestions and opinions were always honest and pertinent. Similarly, Doran Avivi's expertise in mechanical engineering has provided me with many useful references. I also want to send my thanks to Tyler Desplenter, Raneem Haddara and Myles Mathew Lidka for their encouragement and help

in this project. One more special thanks goes out to Dr. Mary Jenkins (University Hospital, University of Western Ontario). The patient trial of this project could not have been finished without her dedicated support. Furthermore, her knowledge in Parkinson's disease has provided me with the insight I couldn't find elsewhere. Without them, I couldn't have made it this far.

Having some place to go is home; having someone to love is family; having both is blessing. I would like to express my sincere gratitude to the Maclean's who are like a family to me. It is my fortune to have met them. Their care and company are the bliss of my life.

It may only need one second to meet someone, one day to know someone, and one year to understand someone, but it needs one life to love someone. I want to thank my beloved Lule Aliraj. Her love, consideration and patience have been given to me unconditionally. Thank you for being in my life.

Finally, I want to express my most sincere gratitude to my parents, Zhenkuan Zhou and Jinming Li. You brought me life, you taught me how to think, you raised me up and you gave me all your love. Being your son is the greatest bliss of my life. I also want to give my sincere gratitude to my brother, Bin Zhou. Without him, there's no place for me in this world. Thank you for always being the big brother for me, looking after me, covering for me throughout our life and thank you for always being the backbone of our family. Without you, my life would be quite different. Special thanks goes out to my sister in law, Chen Liang, my nephew and niece, Jinglin Zhou and Chunyu Zhou. You have always brought happiness and joy to our family. It is my fortune to have all of you in my life. I love you all so much.

Table of Contents

Abstract	ii
Acknowledgments.....	iii
Table of Contents	v
List of Tables	viii
List of Figures	ix
Nomenclature and Acronyms	xii
Chapter 1	1
1 INTRODUCTION	1
1.1 Motivation.....	1
1.2 General Problem Statement	2
1.3 Research Objectives.....	3
1.4 Thesis Outline	3
Chapter 2.....	5
2 LITERATURE REVIEW AND BACKGROUND INFORMATION.....	5
2.1 Parkinsonian Tremor	5
2.2 Tremor Suppression Devices: State of the Art	6
2.2.1 Wrist Tremor Suppression Devices.....	7
2.2.2 Elbow Tremor Suppression Devices	9
2.3 Tremor Estimation	13
2.4 Conclusion	15
Chapter 3	16
3 TREMOR MOTION ACQUISITION	16
3.1 Subjects	16

3.2	Experiment Procedure.....	17
3.3	Data Recording and Processing	19
3.4	Calibration and Graavity Compensation for the Accelerometer.....	20
3.5	Results.....	25
3.5.1	Time-domain Characteristics of PD Tremor	25
3.5.2	Frequency Characteristics of PD Tremor	26
3.6	Discussion	29
3.7	Conclusion	31
Chapter 4	32
4	TREMOR ESTIMATION.....	32
4.1	Tremor model.....	32
4.2	Adaptive Tremor Estimator	36
4.2.1	Weighted Fourier Linear Combiner	36
4.2.2	WFLC-based Kalman Filter	40
4.3	The Effect of the PD Tremor Model's Harmonics on Tremor Estimation	44
4.4	Conclusion	47
Chapter 5	48
5	DESIGN OF A MULTI-CHANNEL MECHANICAL SPLITTER FOR TREMOR SUPPRESSION	48
5.1	Literature Review.....	48
5.2	Concept Generation	52
5.3	Design Specification	56
5.4	First-Generation MMS.....	56
5.4.1	MMS Conceptual Model.....	56
5.4.2	MMS CAD model	57
5.4.3	MMS Prototype	63

5.5 Second-Generation MMS	64
5.5.1 MMS Model	64
5.5.2 Cable Installation.....	68
5.5.3 Power Motor Selection.....	69
5.5.4 MMS Prototype	70
5.6 Experimental Evaluation	73
5.6.1 Experimental Setup	73
5.6.2 Data Recording and Processing.....	73
5.6.3 Coating Material for the Disc and Cylinder	74
5.6.4 Performance Evaluation	76
5.6.5 Motion Tracing.....	81
5.7 Conclusion	83
Chapter 6.....	85
6 CONCLUSION AND FUTURE RESEARCH.....	85
6.1 Contributions.....	85
6.2 Future Research	86
REFERENCES	88
Appendix A.....	95
Software Development for Data Acquisition.....	95
Appendix B	96
Permissions and Approvals.....	96
Curriculum Vitae	102

List of Tables

Table 2.1	Review of wrist tremor suppression devices
Table 2.2	Review of elbow tremor suppression devices
Table 3.1	Sign definition of the raw measurement
Table 3.2	Values of the calibration matrices for 5 accelerometers
Table 3.3	RMS magnitudes of PD tremor
Table 4.1	Parameters for simulated tremor
Table 4.2	Parameters of the KF
Table 4.3	Parameters of the WFLC-KF
Table 5.1	Component specifications for the first concept
Table 5.2	Component specification for the second concept
Table 5.3	Power motor specifications
Table 5.4	Prototype cost
Table 5.5	Parameters of the double-closed loop
Table 5.6	Parameters of the double-closed loop

List of Figures

Figure 1.1	Pill rolling movement of the parkinsonian tremor
Figure 3.1	Sensor placement
Figure 3.2	Six stationary positions for calibration of an accelerometer
Figure 3.3	Accelerometer calibration result
Figure 3.4	Gravity compensation result
Figure 3.5	Representation of parkinsonian tremor in time series
Figure 3.6	Frequency distribution of parkinsonian tremor
Figure 3.7	Representation of the Parkinsonian tremor's harmonics in time series
Figure 3.8	Tremor power distribution across patients
Figure 4.1	Simulated tremor using monoharmonic model
Figure 4.2	Simulated tremor using two harmonics model
Figure 4.3	Block diagram of the Fourier Linear Combiner
Figure 4.4	Time series of the simulated tremor and the WFLC estimated tremor
Figure 4.5	Short time Fourier transform of the simulated tremor and the WFLC estimated tremor
Figure 4.6	Signal flow diagram of a WFLC–KF tremor estimator
Figure 4.7	Time series of the simulated tremor and the estimated tremors from both WFLC and WFLC–KF
Figure 4.8	Short time Fourier transform of the simulated tremor and the WFLC–KF estimated tremor
Figure 4.9	Performance comparison between the WFLC estimator and the WFLC–KF estimator
Figure 4.10	Signal flow diagram of a modified WFLC–KF tremor estimator

Figure 4.11	Time series of the WFLC–KF estimators with different tremor models
Figure 4.12	Performance comparison between the WFLC–KF estimators with different tremor models
Figure 5.1	Diagram of a belt–pulley CVT system
Figure 5.2	Diagram of a direction control mechanism
Figure 5.3	Diagram of a frictional variable speed drive
Figure 5.4	Diagram of the Cobot’s CVT model
Figure 5.5	Signal flow between the power source and output application
Figure 5.6	Signal flow of a total of n MMS units in a serial network
Figure 5.7	Signal flow of a total of n MMS unites in a parallel network
Figure 5.8	Schematic of a hand tremor suppression glove
Figure 5.9	Conceptual model of the first-generation MMS
Figure 5.10	The CAD model of the first-generation MMS
Figure 5.11	An example of a failed linear guide rail
Figure 5.12	The second configuration of the frictional cylinder
Figure 5.13	Configuration of the linear actuation
Figure 5.14	The prototype of the first version of the MMS
Figure 5.15	Configuration of the second-generation MMS
Figure 5.16	Configuration of the gear–spool–cable mechanism
Figure 5.17	Prototype of the gear–spool–cable mechanism with installation sequence
Figure 5.18	A nonlinearity model of the gear–spool–cable mechanism
Figure 5.19	The prototype of the second version of the MMS
Figure 5.20	Experimental setup for MMS evaluation

- Figure 5.21 Friction comparison between different materials for the disc and the cylinder
- Figure 5.22 The cylinder's speed range vs. the miniature motor's revolution
- Figure 5.23 The position control flow graph for the miniature motor
- Figure 5.24 Step response of the MMS
- Figure 5.25 Diagram of the excessive contacting surface area
- Figure 5.26 Continuous motion of the MMS
- Figure A.1 Graphical user interface for hand tremor data acquisition

Nomenclature and Acronyms

Acronyms

ADL	Activities of Daily Living
API	Application Program Interface
AR	Auto-Regressive
BLDC	Brushless DC Motor
CVT	Continuously Variable Transmission
DAQ	Data Acquisition
DOF	Degree of Freedom
DRIFT	Dynamically Responsive Intervention for Tremor Suppression
EM	Electromagnetic
EMG	Electromyography
FES	Functional Electrical Stimulation
FLC	Fourier Linear Combiner
FVSD	Frictional Variable Speed Drive
FXLMS	Filtered-X Least Mean Square
GUI	Graphical User Interface
IF	Index Finger
IMU	Inertial Measurement Units
KF	Kalman Filter
LMS	Least Mean Square
MCU	Microcontroller Unit
MMS	Multi-Channel Mechanical Splitter
MRF	Magnetorheological Fluids
PC	Personal Computer
PD	Parkinson's Disease
PEA	Percentage Estimation Accuracy
PFE	Percentage Fit Error
RMS	Root Mean Square

SD	Standard Deviation
T	Thumb
W	Wrist
WOTAS	Wearable Orthosis for Tremor Assessment and Suppression
WFLC	Weighted-Frequency Fourier Linear Combiner

Variables

A	Coefficient of the harmonic model
A	Raw acceleration measurement
A_v	Amplitude of the voluntary motion
A_c	Calibrated acceleration
A_L	Linear acceleration
B	Coefficient of the harmonic model
C	Coefficient of the harmonic model
F	Pushing force of a lead screw
F_d	Lateral pushing force
F_t	State transition matrix of a tremor model
G	Process noise covariance matrix of the KF
H	Measurement matrix of the KF
K	Kalman gain
M	Number of harmonics in the dynamic truncated Fourier series
M_i	Calibration matrix of the i^{th} accelerometer
N	Number of harmonics
N_m	Small motor revolution
N_t	Order of the harmonic model
\tilde{P}	Prediction error covariance of the KF
\hat{P}	Estimation error covariance of the KF
R	Measurement noise covariance matrix of the KF
S	Innovation covariance of the KF
S_M	Magnitude series of the tremor movement

S_{rms}	RMS value of the tremor magnitude series
S_t	Modelled tremor series
W	Adaptive filter weight of the FLC and WFLC
\tilde{X}	Prediction state of the KF
\hat{X}	Estimation state of the KF
a_n	Time varying coefficient of the tremor model
a_r	Coefficient of the dynamic truncated Fourier series
b_n	Time varying coefficient of the tremor model
b_r	Coefficient of the dynamic truncated Fourier series
e_t	White noise in AR model
f_v	Frequency of the voluntary motion
f_t	Frequency of the tremor
g	Filtered gravity component
s	Input signal of the FLC and WFLC
u	transmission ratio
x_r	frequency component of the FLC and WFLC
y	Dynamic truncated Fourier series
z_m	Measured value
θ	Steering angle
α	Filter convergence coefficient
σ_{st}	Standard deviation of the white Gaussian noise
v_{st}	White noise in harmonic model
ε	Estimation error of the FLC and WFLC
μ	Adaptive gain of the FLC and WFLC
μ_0	Adaptive gain of the WFLC
\mathcal{g}	Innovation of the KF
ω	Tremor frequency
ω_{in}	Input speed
ω_m	Miniature motor rotary speed
ω_0	Tremor's fundamental frequency
$\omega_0(k)$	Estimated frequency series

ω_{out}	Output speed
ω_s	Shaft pivoting speed
τ	Driving torque of a lead screw
τ_{in}	Input torque
τ_{out}	Output torque
η	Velocity transmission efficiency of a CVT
ζ	Torque transmission efficiency of a CVT
γ	Transmission ratio
φ	Pivot angle of the universal joint

Units

mm	Millimetre
g	Gram
m/s	Meter per second
m/s ²	Meter per second squared
Hz	Hertz
dps	Degree per second
N	Newton
Nm	Newton meter
W	Watt
°	Degree
rpm	Revolutions per minute

Chapter 1

1 INTRODUCTION

Parkinson's disease (PD) is considered to be the second most prevalent chronic neurological disease after Alzheimer's disease among the elderly. According to recent epidemiological studies [1–5], the estimated incidences of PD in Canada, USA, UK, Australia and China range from 16 to 450 per 100,000 persons. Higher incidences of PD were found among elderly people. The overall numbers are growing each year and are estimated to double in the next 15 years in both developing and developed countries [5–8]. As worldwide life span has increased, the progressive and chronic nature of PD has led to a substantial economic burden on health care systems and individual patients [7, 9–12]. Understanding and finding an optimal treatment for PD are crucial to both the individual patients and society. The most obvious symptoms of PD are motor related. These include tremor, rigidity, slowness of movement and difficulty with walking and gait [13]. Tremor, among all of these symptoms, significantly affects patients' daily life, creating difficulty in many tasks such as eating and writing. More importantly, it causes social embarrassment so severe that most patients avoid company other than family or friends.

1.1 Motivation

In general, tremor is described as unintentional, rhythmic, oscillatory movements with particular amplitude and frequency. Parkinsonian tremor is often seen as a pill-rolling action of the hand (Fig. 1.1), and may also affect other parts of the body. The pill-rolling action is defined as a circular movement of the opposed tips of the thumb and index finger.

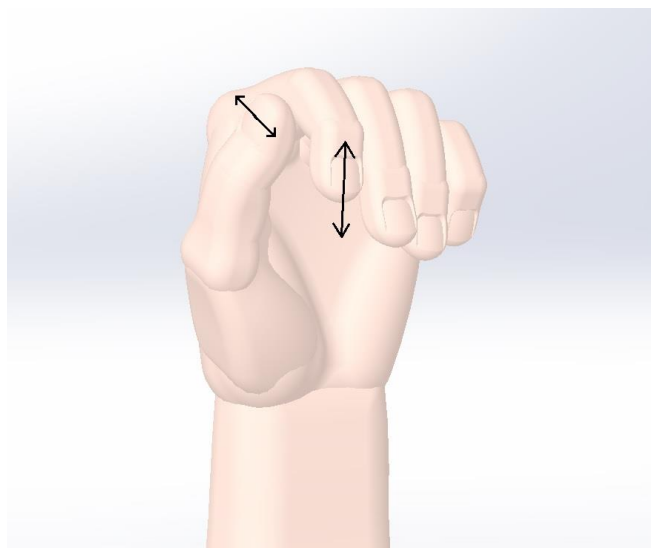


Figure 1.1: Pill rolling movement of the parkinsonian tremor. The arrows indicate the direction of movements of the fingers.

Traditional treatments for pathological tremor include medication and neurosurgery. For the past few decades, amantadine, apomorphine and L-dopa, among others [14–18], were used for the treatment of PD; however, these drugs may cause patients to suffer excessive drowsiness, nausea, ataxia, confusion, blurred vision, fatigue, hallucination, depression and even muscle paralysis [14, 19]. In addition to medication, many researchers have investigated the effects of surgical interventions on PD, including deep brain stimulation and stereotactic thalamotomy [20, 21]. These procedures may ease certain tremors, but they have been connected with permanent complications, paresthesia, dysarthria, speech impediments and even stroke and hemiparesis [22, 23].

Given the complications and adverse effects of the traditional treatments, a less invasive approach with fewer side effects is needed. Rosen, *et al.* have demonstrated experimentally that people with pathological tremor are unable to accomplish the activities of daily living (ADL) because the magnitudes of the superimposed pathological oscillations approach the magnitudes of the ADL [24]. This work inspired the development of mechanical tremor suppression orthoses. However, most of the devices that have been developed [25–39] are either too bulky or too heavy for patient use.

Furthermore, their limited performance indicates the need for a better tremor suppression system.

Most of the studies to date [25–39, 40–42] have focused on only elbow tremor and wrist tremor—finger tremor has not yet been well studied despite the fact that finger tremor is also present. Moreover, devices that provide finger tremor suppression device do not exist. Thus, this research is focused on the investigation of finger tremor and the development of a noninvasive device that can suppress human hand tremors while allowing voluntary movements to occur.

1.2 General Problem Statement

Tremor is an undesired presence, with up to 75% of individuals afflicted with PD suffering from it [19]. Although medication remains the mainstay treatment for PD, it is much less effective for tremor management and often carries significant side effects [16]. Brain surgery is often performed for cases of severe tremor. While this treatment is often very effective, it carries a significant risk for the patient. Thus, the externally worn exoskeleton-type therapy devices become a promising alternative. Although current exoskeletal devices have been shown to suppress tremor, many of them cannot be used directly on patients because of issues associated with their size, weight, power source, and overall effectiveness. Furthermore, tremor of the hand has been neglected by most researchers. Thus, there is a need to study the nature of hand tremor and to develop a lightweight and compact exoskeletal device that is suitable for suppression of involuntary hand tremor.

This work proposes to study the characteristics of hand tremor and to develop a novel mechanism to reduce the size, weight and cost of an actuation system suitable for incorporation into an exoskeletal device.

1.3 Research Objectives

The overall objective of this thesis is to develop a novel mechanism that is capable of suppressing PD hand tremor according to the actual tremor characteristics of PD patients.

The specific objectives are:

- To acquire and analyze tremor data from a set of PD patients.
- To design and simulate a tremor estimator.
- To design, implement and test a novel mechanism that allows splitting a single degree of freedom (DOF) input into multiple DOF independent outputs.
- To test the control system using real patient data and a prototype mechanism.

1.4 Thesis Outline

The structure of the thesis is as follow:

- | | |
|------------|---|
| Chapter 2 | Presents a literature review of Parkinsonian tremor, the state of art in tremor suppression devices and tremor estimation technology. |
| Chapter 3 | Describes the experimental setup for patient data acquisition, and the analysis of the data acquired. |
| Chapter 4 | Describes the tremor model used for simulation modeling and tremor estimators, and the evaluation of the estimator using real patient data. |
| Chapter 5 | Presents the design and implementation of the proposed single-input-multiple-output mechanism. An evaluation of the device is presented at the end of this chapter. |
| Chapter 6 | Gives the conclusions of the work and suggestions for future work. |
| Appendix A | Software Development: Describes the development of the tremor acquisition software interface |
| Appendix B | Permissions and Approvals: Presents the approval notice of ethics for tremor data acquisition trials that involved patient with Parkinson's disease. |

Chapter 2

2 LITERATURE REVIEW AND BACKGROUND INFORMATION

In order to establish the design requirements for a PD hand tremor suppression mechanism, the characteristics of Parkinsonian tremor, existing tremor suppression devices and tremor estimation technology were reviewed. A comprehensive literature review was performed from January to Nov 2015 using Google Scholar using the following keywords: Parkinson's disease, tremor, Parkinsonian tremor, hand tremor, pathological tremor, finger tremor, tremor treatment, tremor model, tremor estimation, noise cancellation, filter, adaptive filter, Kalman filter, tremor suppression device, continuously variable transmission, frictional drive, differential mechanism. A total of 103 papers were reviewed and included as reference in the database. The priority was given to papers published in the last 15 years for tremor suppression devices. A longer time span was adopted for the review of tremor pathology and tremor characteristics.

The remainder of this chapter is organized as follows: Section 2.1 reviews the characteristics of Parkinsonian tremor. Section 2.2 reviews the prior art of tremor suppression devices. It is divided into two categories according to the target joints. The last section reviews tremor estimation algorithms, which can be used to extract tremor signals from overall motion signals.

2.1 Parkinsonian Tremor

Clinically, Parkinsonian tremor can be divided into two categories of movement disorders: resting and postural tremor [43–45]. Resting tremor appears when muscles are relaxed, such as when a hand rests on a table. The typical frequency range of resting tremor in the hand is 3–7 Hz. Postural tremor can be found when muscles are contracted, such as when maintaining a part of the body at a fixed position against gravity. The frequency range of postural tremor is 5–12 Hz [43–46]. Some studies [29, 35, 40, 47] have reported and considered PD tremor as a monoharmonic signal. Other studies [42, 48] have reported that PD tremor has multiple harmonics. The frequency of the k^{th} harmonic is roughly k

times the frequency of the 1st harmonic. The amplitude of tremor varies from person to person. Previous research has found that the acceleration amplitude for tremor is under one unit of gravitational acceleration [46, 47, 49].

2.2 Tremor Suppression Devices: State of the Art

Since Rosen's experiment suggested that a mechanical loading orthosis could be used to selectively suppress tremorous motion [24], a number of studies have been conducted on developing tremor suppression devices. Due to the side effects of the traditional treatments and facilitated by the development of mechatronic technology, mechanical orthoses have become a promising and popular treatment. A review of tremor suppression devices is presented below.

2.2.1 Wrist Tremor Suppression Devices

Several research groups have developed tremor suppression devices for wrist tremor (see Table 1). Rosen, *et al.* [25] designed a tremor suppression wheelchair using a magnetic particle brake. The brake is mounted onto a wheelchair and is connected to a cuff that attaches to the patient's wrist. This device works by applying resistive loads to the user's hand, and therefore, reducing the severity of tremor. Considering the passive operation of the brake, it is safe to use. However, the researchers could not find a damping parameter that was suitable for all of the patients tested. In addition, the resistive loads also impeded the voluntary motion.

Portability and battery life are important to health care related devices, especially for tremor suppression. A ground-based device has sufficient space to carry a large battery and can effectively suppress the tremor of a certain part of the body without impacting other parts of the body. However, the applicability of ground-based devices is highly limited compared to wearable devices as the user is constrained to the base of the device. Related to progress towards portable devices, Kotovsky, *et al.* [26] designed a wearable wrist suppression orthosis using a viscous beam that applies viscous resistance against the user's motion. The viscous beam can be custom made according to different tremor severities. This orthosis is fairly compact and ergonomic, however, the damping level of

the device is 88% lower than the theoretical values. Besides, the invariable damping rate results in an inconsistency in the suppression level for all patients.

An actuator with controllable viscous rate was designed by Loureiro, *et al.* [27]. This actuator employed Magnetorheological fluids (MRF), the viscosity of which can be controlled in the presence of a magnetic field. The controllability of the MRF is the main advantage over the previous two devices. However, it is not possible to suppress tremor without impeding voluntary motion using this passive actuator. Also, the suppression power of this device is relatively low due to the poor performance of the actuator. Another application of MRF in tremor suppression was investigated by Case, *et al.* [50]. This actuator was designed using the configuration of a damper. The performance of the actuator was greatly improved, but the issue of suppressing both voluntary and tremorous motion is still unsolved.

Although passive technology is safer when applied to orthoses, active technology can achieve better performance. Lavu, *et al.* [28] used an electrical vibration exciter to counterbalance the tremor at wrist. The vibration exciter was fixed on a table and connected to an artificial arm. The author claimed that this system can reduce tremor by 55% on an artificial arm and 93.3% on an aluminum beam. However, it is too bulky and heavy for patient use. Besides, the results obtained are likely to be dramatically affected once carried by the patient because additional perturbations will act on the actuator.

A compact smart glove was designed by Kazi, *et al.* [29]. It incorporates a piezoelectric bimorph actuator, which can flex and extend according to different excitation voltages. The bimorph piezoelectric actuator was configured to vibrate constantly at 7, 8 and 9 Hz. The results showed that this glove is best for reducing tremor with a fundamental frequency of 8 Hz or 9 Hz. However, the high excitation voltage for the piezoelectric actuator is not safe for the user. Furthermore, constant shaking from the actuator could result in numbness in the user's hand. A similar approach was adopted by Yu [30]. The proposed glove used two piezoelectric materials to harvest tremor energy and in the meantime suppress tremor. Unfortunately, the harvested energy was too weak to excite

the actuator and the high excitation voltage for the piezoelectric actuator may be a potential safety issue for the user.

Table 2.1: Review of wrist tremor suppression devices

Ref.	Description	Limitation	Type
T1	A wheelchair-mounted device was designed to apply resistive loads to the patient's wrist.	The damping parameters of the device are not adaptive for all patients.	Ground based
T2	A wearable wrist tremor suppression device was designed using viscous resistance beam.	The damping rate of the viscous beam is constant; therefore, the performance of the device is inconsistent between patients. The voluntary motion is impeded by the viscous resistance.	Wearable
T3	A wrist tremor suppression device was designed using controllable double viscous beam actuator.	The voluntary motion is impeded by the viscous resistance, and the suppression power is limited due to the actuator.	Wearable
T4	A vibration exciter was used to counterbalance the tremor at a simulated wrist.	It is not appropriate to simulate wrist tremor as simple vibration; therefore, the use of a vibration exciter to counterbalance the real tremor would be insufficient.	Ground based
T5	A piezoelectric actuator embedded glove was developed to suppress tremor at the wrist.	Constant vibration could result in numbness in the user's hand. The high excitation voltage of piezoelectric actuator is a potential safety issue for the user.	Wearable
T6	A piezoelectric material based glove was designed to harvest wrist tremor energy and suppress tremor.	The piezoelectric material requires extremely high excitation voltage. The harvested energy from the tremor is not sufficient to suppress it. The high voltage is not safe for the user.	Wearable
T7	A wrist tremor suppression device was designed using two pneumatic cylinders.	The installation of the air source is not feasible for the user. The user may be embarrassed by the noise from either the cylinder or the air source. More importantly, air leak and valve failure pose a serious safety risk to the user.	Wearable

A recent study has shown the success of using pneumatic actuators for suppressing tremor [31]. The force generated by the actuator is sufficient to suppress tremor to a great extent. The proposed device is compact and efficient. However, it is not realistic for the user to carry the air source. In addition, the noise from either the cylinder or the air source may cause embarrassment to the user. More importantly, air leak and valve failure of the pneumatic actuator may result in a serious injury to the user.

2.2.2 Elbow Tremor Suppression Devices

The importance of suppressing elbow tremor was also considered by a number of research groups [32, 33, 34–39, 51–61]. Rocon, *et al.* [32] developed an elbow brace for tremor suppression. An ultrasonic motor was chosen as the only actuator in this device because it generates much higher torque than a DC motor. The experimental results show that the range of controllable velocity, from 0 to 3 rad/s, is sufficient for suppressing tremor. However, a large distortion occurs in the motor's output velocity when the frequency of operation is greater than 5 Hz, and this device has a poor response to motions with low velocity.

A 3 DOF Wearable Orthosis for Tremor Assessment and Suppression (WOTAS) was the final product of a five-year European project called Dynamically Responsive Intervention for Tremor Suppression (DRIFT) [33–35]. This device was developed to monitor and suppress tremor with minimal restriction to the voluntary movement and employs both active and passive strategies. The results from the studies showed a superior performance of the active strategy (up to 90% reduction rate in tremor amplitude) over the passive. However, this device is very bulky and cosmetically limited. These disadvantages make it not feasible for constant wear.

Stone *et al.* [36] tested the performance of a voice coil actuator for tremor suppression of an artificial arm. The artificial arm was made of an aluminum beam fixed to a rotary joint. The linear voice coil actuator was constantly moving opposite to the simulated tremor motion. The results showed that tremor amplitude was reduced 20–60% for a 6–13 Hz frequency band. However, the constant vibration from the actuator could result in numbness in the user's hand. Also, the fact that this is a ground-based device means that

it cannot be used for constant wear.

Ando *et al.* [37] developed a myoelectric-controlled elbow robot to suppress elbow tremor. The electromyography (EMG) signal from the user's upper arm was collected and interpreted to control the movement of a DC motor. The DC motor follows the intentional movement of the user while suppressing tremor movement. The device is relatively light and compact. However, the user's elbow range of motion was limited by the device. Also, a 3 degree clearance between the user's arm and the device was reported. This clearance would certainly impact the performance of the device.

Another elbow tremor oriented device was developed by Herrnsstadt and Menon [39]. This device employed an electromagnetic brake to semi-actively suppress tremor in the elbow. The electromagnetic brake is able to generate relatively high torque while keeping the system light and compact. However, the limitation of this brake is that it has poor repeatability and accuracy.

A successful demonstration of the application of a pneumatic cylinder for suppressing wrist tremor [31] was extended to elbow tremor [38]. Two more DOF were added to the device to control the flexion–extension of the elbow and pronation–supination of the forearm. The tremor's fundamental frequency was suppressed to a large degree (96.8–98.8%), but the reduction in tremor's second harmonic was only 52.7–82%. This may be caused by the poor response of the pneumatic cylinder. Although the reduction in tremor magnitude is good, the issues related to a pneumatic actuator make this device infeasible for patient application.

An exoskeleton elbow tremor suppression brace was designed to suppress the elbow tremor [54]. The device was mounted onto the user's forearm and upper arm through two rigid cuffs. Although the use of two cuffs can reduce the measurement error by confining the movement of the user's arm, the poor alignment of the device with the user's elbow joint may generate a significant measurement error. The actuation system of this design incorporated two gearboxes and two motors. Although the use of two actuators distributes the actuation requirements, it largely increases the size of the device and complexity of the control system.

All of the devices reported above use mechanical loading to compensate for tremor. Although the devices are relatively bulky and heavy, they are noninvasive and relatively safe for the user. Some of them have even achieved good performance when suppressing tremor. An alternative option is a technique called Functional Electrical Stimulation (FES), which has also been studied along with mechanical loading devices. This technique uses electrical currents to activate nerves and induce co-contraction of the muscles [61]. It is commonly used to improve motor function in people with disabilities. A number of studies have been conducted to investigate the use of FES in tremor suppression [51–60]. The developed devices are lighter and more compact than exoskeletal devices, but the use of FES can cause muscular fatigue, discomfort and painful sensations while muscles are being stimulated. Besides, the use of FES may interfere with the real tremor signal resulting in a huge distortion of the measured tremor signal [53]. More importantly, there is a significant time delay observed between the electrical stimulation and the actuation of muscle bundles, which impacts the tremor suppression performance [58].

Table 2.2: Review of elbow tremor suppression devices

Ref.	Description	Limitation	Type
E1	An elbow brace was developed using an ultrasonic motor.	Poor response to motions with low velocity and a large distortion on the motor velocity for frequencies greater than 5 Hz.	Wearable
E2–E5	A forearm exoskeletal device (WOTAS) was developed by the DRIFT project. This device was designed for the purposed of assessing and suppressing tremor in the forearm.	This device is bulky and not cosmetic. The size and weight of the device made it unfeasible for patient use.	Wearable
E6	A linear voice coil actuator was adopted in this device to counterbalance the tremor at the elbow.	Constant vibration from the actuator could result in numbness in the user's hand. The movement of a patient is limited to the base of the device.	Ground based
E7	An elbow exoskeletal robot was developed to suppress tremor at elbow. The EMG signal from the user's upper arm was translated into elbow	The user's elbow range of motion was limited by the device. A 3 degree clearance between the user's arm and the device was reported. This clearance would	Wearable

	angle. Elbow motion was controlled by a DC motor.	certainly impact the performance of the device.	
E8	A 4 DOF device was developed for elbow and wrist tremor. Four pneumatic actuators were employed in this device.	The use of a pneumatic cylinder requires an air source, however, it is not realistic for the user to carry the air source. Also, the noise from either the cylinder or the air source may embarrass the user. More importantly, an air leak or valve failure would pose a serious safety risk to the user.	Wearable
E9	An elbow brace was designed to suppress elbow tremor using an electromagnetic brake.	This study demonstrated the feasibility of using an electromagnetic brake to suppress elbow tremor. But the limitation of the brake is its low repeatability and accuracy.	Wearable
E13	An exoskeleton for essential tremor and Parkinsonian tremor	The suppression performance may be impacted by the poor alignment of the device with the user's elbow joint. Also, the device is too bulky for constantly wearing.	Wearable
E10, E11	A compact tremor suppression neuroprosthesis was developed employing functional electrical stimulation (FES).	Although the device is more compact than exoskeletal devices, the use of FES often cause muscular fatigue, discomfort and painful sensations.	Wearable
E12	A multichannel electrical stimulator was incorporated to suppress tremor in both elbow and wrist.	The use of FES may interference the real tremor signal.	Wearable
E14–E17	A FES-based prosthesis was developed for pathological tremor compensation.	Time delay between the electrical stimulation and the muscle activation. Although the application of FES reduces the size of the device, muscular fatigue and painful sensations are still issues that cannot be solved. It is very difficult to suppress tremor in fingers using FES.	Wearable

2.3 Tremor Estimation

“If you know the enemy and know yourself, you need not fear the result of a hundred battles,” said SUN TZU [62]. In order to suppress tremor, it is important to extract the

tremor from a combined signal. Filters are commonly used in this process. A few studies have been conducted on the use of signal filtering for tremor estimation [59, 63, 64]. However, the time delay introduced by the filter is a drawback for tremor control because an actuator cannot generate an estimated tremor with zero-phase delay to oppose the vibration.

The drawback of the common filter prevents its use for tremor suppression. However, adaptive filtering is well suited for tremor estimation as it is constantly adapting its parameters to the input signal based on a learning algorithm [65]. A Fourier linear combiner (FLC) was proposed by Vaz *et al.* [66, 67] based on the assumption that tremor can be simplified to a roughly periodic signal. This suggests that tremor can be modeled by a sinusoidal or Fourier series. The FLC estimates tremor based on a known frequency. The least mean square algorithm was incorporated to update the parameters. It doesn't involve much computational workload [67], and surpasses any common filter with its zero phase feature [66]. However, tremor is not a periodic signal. In order to effectively suppress tremor, both frequency and amplitude are required to adapt to changes.

Not long after the establishment of FLC, Riviere *et al.* [68] proposed a new tremor estimator based on FLC, called the Weighted-Frequency Fourier Linear Combiner (WFLC). The WFLC adapts both the frequency and amplitude parameters of the Fourier series to the input signal. The implementation of frequency estimation greatly improves the performance of the tremor estimator. However, applying a pure sinusoidal estimation of tremor motion seems insufficient to represent real tremor.

In addition, the Kalman filter and its derivative algorithms have also been used as tremor estimators [69–72]. In most of the applications, tremor was modeled as a sinusoidal signal, there are also other studies suggested that tremor is best described by a nonlinear stochastic process [73, 74]. A great effort has been given to designing new KF derivatives. However, the assessment of applying different tremor models has not been well studied.

Other than the three widely adopted tremor estimators presented above, a number of other estimators have been proposed and adopted as well [30, 38, 75–76]. Taheri [38] designed an adaptive control system for tremor estimation and suppression. In this system, tremor

was considered as an unknown harmonic disturbance. Although the author claimed that the reduction in the tremor's peak amplitude is substantial, the use of a sinusoidal function as the simulated tremor is still questionable. [75] and [76] designed two tremor estimation algorithms based on WFLC and FLC, respectively. Both of these estimators track tremor within a band of frequencies. However, similar to the WFLC, applying a pure sinusoidal estimation of tremor motion seems insufficient to represent real tremor. In [30], a filtered-X least mean square (FXLMS) algorithm was adopted to estimate and suppress tremor. The author concluded that the FXLMS algorithm works well on simulated tremor signals, especially in the case of a tremor with a single frequency. However, the performance of FXLMS algorithm on real tremors was not investigated. Therefore, further evaluation is required for this algorithm.

2.4 Conclusion

Traditional treatments for PD often come with side effects. These side effects greatly impact the patient's daily life. The development of mechatronics-enabled exoskeletal devices is becoming a promising solution for tremor management. A number of research groups have developed tremor suppression devices for the wrist and the elbow [25–31, 32–39, 50–58]. Both active and semi-active technologies have been adopted in these devices, but only a limited number of devices were designed to meet the basic requirements for patient use. Tremor reduction rate was the only measurement criteria accepted by most research groups, however, the criteria for patient use was often neglected. That is why most of the devices are too bulky and heavy to use.

Furthermore, tremor in the fingers has been neglected by most of the researchers. This is very limiting as one of the most distinguishing features of PD tremor is the pill-rolling motion of the patient's hand, which involves the wrist and fingers. In order to provide a better life quality to the patients who are suffering from tremor, it is important to suppress tremor in the fingers as well. Thus, to fill this gap in the area of tremor suppression, the focus of current project is to study the characteristics of finger tremor and wrist tremor, and to design a mechatronic device that can be used on a patient's hand. The following chapter presents the acquisition of finger tremor motion characteristics and the results of the data analysis.

Chapter 3

3 TREMOR MOTION ACQUISITION

Given the lack of effectiveness and the side effects of traditional treatments, externally worn exoskeleton-type therapy devices are a promising alternative. Prior to the development of a externally worn exoskeleton-type therapy device, the design specifications are normally determined by the electro-mechanical characteristics of tremor, position, force and EMG signals are the most commonly used forms for tremor characterization. In order to achieve good tremor suppression, it is important to develop a deep understanding of the nature of tremor.

However, most of the studies [33, 40, 41, 46] were conducted based on rather old tremor reports which can trace back to 1980s, besides, the characteristics of tremor were quantified with a very board range which is not very accurate. Therefore, it is necessary to update the knowledge of the nature of tremor. Furthermore, for the past few decades, most of the studies [30, 33, 40–42] have focused on only elbow tremor and wrist tremor—finger tremor has not yet been well studied despite the fact that finger tremor is also present. With the dedicated support from Dr. Mary Jenkins (movement disorders neurologist, University Hospital, London, ON), patients with PD were recruited to have their tremors characterized. The following sections describe the experimental procedure and data analysis.

3.1 Subjects

A total number of 18 subjects with PD participated in this study. All subjects were diagnosed and recruited by a neurologist. The hand that presented the greatest amount of tremor was selected for data collection. Based on the severity of the hand tremor for each subject, 17 subjects' right hands and 1 subject's left hand were recorded. The experimental procedures were approved by the University of Western Ontario's Research Ethics Board.

3.2 Experimental Procedure

Prior to the experiment, each patient was given a consent form and an explanation of the consent from the experimenter. The explanation included the objectives of the study, details of the study, data acquisition instruments, risks, benefits and confidentiality of the patient's data. After the patient agreed and signed the consent form, the experiment was started with an evaluation of the severity of the Parkinson's disease. The movement disorders neurologist administered the MDS-Unified Parkinson's Disease Rating Scale: Part III (Motor Assessment) (1) to quantify the severity of the PD, including the severity of the tremor.

After the evaluation, a custom motion-sensing device was affixed over the patient's hand (Fig. 3.1). The device consists of four 5 degree-of-freedom (DOF) electromagnetic (EM) motion trackers (Aurora, NDI®) and four 9-axis inertial measurement units (IMUs) (STEVAL-MKI108V2, STMicroelectronics®). Two sets of sensors were placed on each side of the index finger (IF) MCP joint, one on the thumb (T) MCP joint, and an additional one on the forearm close to the wrist (W) joint. A magnetic field generator was placed in front of the subject's hand to generate a magnetic field for the EM trackers. In addition, an eight-channel EMG sensing device (Myo, Thalmic Labs®) was placed on the patient's forearm. In order to eliminate the movements generated by other parts of the body, the patient's forearm was securely strapped to the table, permitting only the hand to move freely in space. All sensors were sterilized with alcohol swabs, and affixed to the patient using latex-free medical tape.

During the trial, the patient was asked to perform a total of five tasks. While the patient was performing the tasks, he/she was asked simple distracting questions (e.g., simple math questions) in order to divert their attention away from their desire to suppress the tremor. During all of the tasks, the patient was sitting on a chair while the proctor used custom software (See Appendix A) to record data from the sensing device and video images of the patient's hand. No patient identifiers were collected as part of this study. The tasks are listed below:

1. Rest: the patient was required to keep his/her arm in a rest position with the palm facing up and down on a table. Recording lasted for 60 seconds.
2. Hand outstretched: the patient was required to keep his/her forearm in a rest position on a table, and then he/she had to maintain his/her hand at a tangential position, against gravity, for 60 seconds.
3. Reaching for an object: the patient's forearm was strapped on a table, and then he/she was required to reach to a lightweight pencil, which is placed over his/her hand. This task had to be repeated 5 times. The patient had to perform the movement slowly. The approximate duration of this task was 15 seconds for each trial.
4. Moving an object: the patient's forearm was strapped on a table, and then he/she was required to move a lightweight pencil, which was located above his/her hand, in three steps: reach to the pencil from the rest position, move the pencil to the rest position, and move the pencil back to its original position. The patient had to perform this task slowly 5 times. The approximate duration of this task was 20 seconds for each trial.
5. Drawing a spiral: the patient's forearm was strapped on a table, and then he/she was required to use a pencil to follow an exemplar spiral on a sheet of paper.

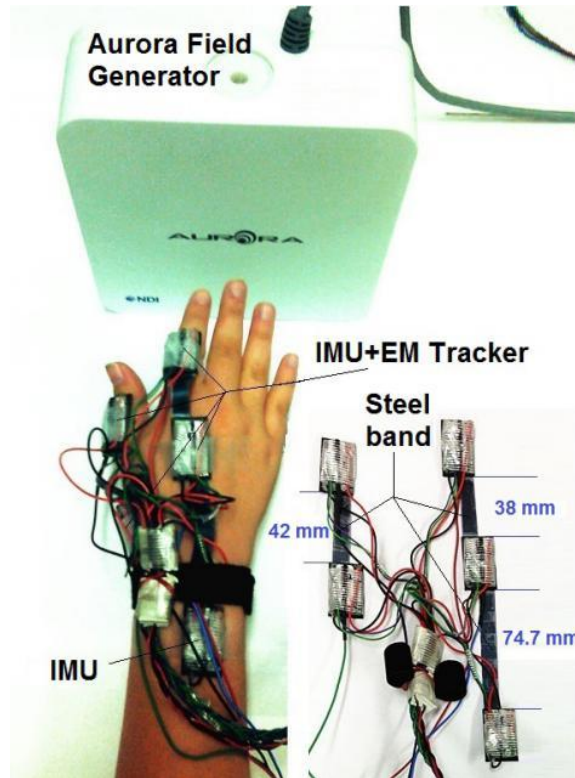


Figure 3.1: Sensor placement on an experimental subject's right hand and Aurora field generator placed in front (left). Sensing system showing each sensing unit connected to other sensing units through thin steel bands (right). The length of each band is shown as reference.

3.3 Data Recording and Processing

All signals were recorded directly onto a personal computer (PC) using a customized graphical user interface (GUI), the development of the GUI is introduced in Appendix A. The GUI was developed in C++ using Visual Studio 2013 to manage data transfer from the different sensing modalities. The IMUs interfaced with an STC89C52RC micro-controller, which sends data at 100 Hz through the I²C protocol. The data were then sent to the PC through the serial port. Each IMU incorporates one 16-bit 3-DOF accelerometer, one 16-bit 3-DOF gyroscope and one 16-bit 3-DOF magnetometer. All accelerometers were calibrated prior to the start of each trial. The data from the Aurora system were collected using the Aurora application program interface (API) at its maximal sampling frequency of 40Hz. The data from the Myo were collected using the Myo API at 200 Hz.

The GUI ensured that all collected data were synchronized to the same timestamp and recorded.

Data processing and analysis were performed offline using Matlab software (Version R2013a, The Mathworks, Inc.). Prior to the data analysis, the data were calibrated and then filtered using a 2nd-order band-pass Butterworth filter using cutoff frequencies at 1 and 30 Hz. The root mean square (RMS) was adopted to quantify the tremor signal.

3.4 Calibration and Gravity Compensation for the Accelerometer

Calibration is an important process to ensure the quality of measurement. Since gravity is a relatively stable force, the gravitational acceleration may be used as a reliable calibration reference for accelerometer. To calibrate the accelerometers to the gravitational reference, the sign of the output of the accelerometer for each axis is defined according to its alignment with the axis of gravity (Table 3.1). The relationship between the calibrated acceleration (A_{cx} , A_{cy} , A_{cz}) and the raw acceleration measurements (A_x , A_y , A_z) is shown below [77],

$$\begin{bmatrix} A_{cx} \\ A_{cy} \\ A_{cz} \end{bmatrix} = \begin{bmatrix} m_{11} & m_{12} & m_{13} \\ m_{21} & m_{22} & m_{23} \\ m_{31} & m_{32} & m_{33} \end{bmatrix} \cdot \begin{bmatrix} A_x \\ A_y \\ A_z \end{bmatrix} + \begin{bmatrix} m_{10} \\ m_{20} \\ m_{30} \end{bmatrix}. \quad (3.1)$$

In order to calibrate the accelerometer at the six stationary positions shown in Table 3.1, Equation (3.1) can be rewritten as:

$$\begin{bmatrix} A_{cx} & A_{cy} & A_{cz} \end{bmatrix} = \begin{bmatrix} A_x & A_y & A_z & 1 \end{bmatrix} \cdot \begin{bmatrix} m_{11} & m_{21} & m_{31} \\ m_{12} & m_{22} & m_{32} \\ m_{13} & m_{23} & m_{33} \\ m_{10} & m_{20} & m_{30} \end{bmatrix} \quad (3.2)$$

or,

$$A_c = A \cdot M, \quad (3.3)$$

where matrix M contains the 12 calibration parameters that need to be determined; matrix A contains the raw data collected at six stationary positions (Fig. 3.2), and matrix A_c contains gravitational acceleration. At X-up position, $A_{c1}=[-9.81 \ 0 \ 0]_{n1 \times 3}$, $A_1=[A_{x1} \ A_{y1} \ A_{z1} \ 1]_{n1 \times 4}$; at X-down position, $A_{c2}=[9.81 \ 0 \ 0]_{n2 \times 3}$, $A_2=[A_{x2} \ A_{y2} \ A_{z2} \ 1]_{n2 \times 4}$; at Y-up position, $A_{c3}=[0 \ -9.81 \ 0]_{n3 \times 3}$, $A_3=[A_{x3} \ A_{y3} \ A_{z3} \ 1]_{n3 \times 4}$; at Y-down position, $A_{c4}=[0 \ 9.81 \ 0]_{n4 \times 3}$, $A_4=[A_{x4} \ A_{y4} \ A_{z4} \ 1]_{n4 \times 4}$; at Z-up position, $A_{c5}=[0 \ 0 \ -9.81]_{n5 \times 3}$, $A_5=[A_{x5} \ A_{y5} \ A_{z5} \ 1]_{n5 \times 4}$; at Z-down position, $A_{c6}=[0 \ 0 \ 9.81]_{n6 \times 3}$, $A_6=[A_{x6} \ A_{y6} \ A_{z6} \ 1]_{n6 \times 4}$, $n_{1,2,3,4,5,6}$ are the lengths of the raw data collected from each position. Combining them together, Equation 3.3 becomes:

$$A_{c_{n \times 3}} = A_{n \times 4} \cdot M_{4 \times 3}, \quad (3.4)$$

where

$$A_c = \begin{bmatrix} A_{c1} \\ A_{c2} \\ A_{c3} \\ A_{c4} \\ A_{c5} \\ A_{c6} \end{bmatrix}_{n \times 3} \quad \text{and} \quad A = \begin{bmatrix} A_1 \\ A_2 \\ A_3 \\ A_4 \\ A_5 \\ A_6 \end{bmatrix}_{n \times 4}.$$

Therefore, the matrix M can be calculated by the least square method as:

$$M = [A^T \cdot A]^{-1} \cdot A^T \cdot A_c. \quad (3.5)$$

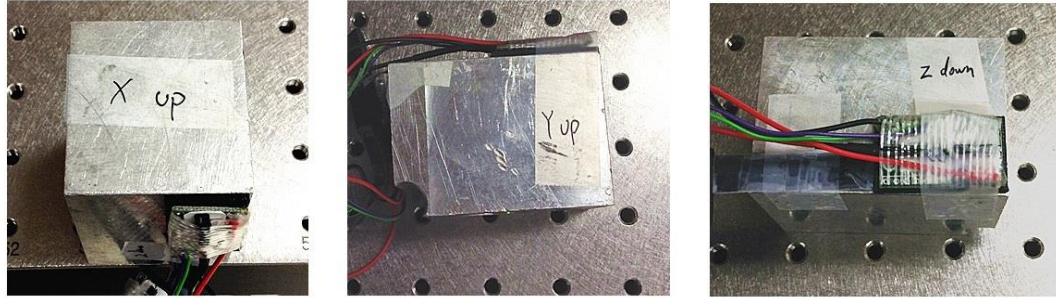


Figure 3.2 : Six stationary positions: X up, X down, Y up, Y down, Z up and Z down. X, Y, Z represent the 3 axes of an accelerometer. Left: X up position. Middle: Y up position. Right: Z down position.

The calculated calibration matrices of 5 accelerometers are given in Table 3.2. Fig. 3.3 shows the result of calibration using the data from one accelerometer. The left panel presents the signals before calibration, and the right panel presents the signals after calibration. The mean RMS error is reduced from 0.33 m/s^2 to 0.07 m/s^2 .

Table 3.1: Sign Definition of the Raw Measurement.

Stationary position	Accelerometer output (m/s^2)		
	X output	Y output	Z output
X up	-9.81	0	0
X down	+9.81	0	0
Y up	0	-9.81	0
Y down	0	+9.81	0
Z up	0	0	-9.81
Z down	0	0	+9.81

Following the calibration process, the linear acceleration caused directly by the tremor

motion was extracted using a high-pass filter [78] given in equation 3.6, and the tremor magnitude is given in equation 3.7:

$$\begin{aligned} g(k) &= \alpha \cdot g(k-1) + (1-\alpha) \cdot A_c(k), \quad g(0) = [0 \ 0 \ 0] \\ A_L(k) &= A_c(k) - g(k), \quad k \in [1, n] \end{aligned} \quad (3.6)$$

$$\begin{aligned} S_M(k) &= \sqrt{s_x^2(k) + s_y^2(k) + s_z^2(k)}, \quad k \in [1, n] \\ S_{\text{rms}} &= \sqrt{\frac{1}{n} (S_M^2(1) + S_M^2(2) + \dots + S_M^2(n))}, \end{aligned} \quad (3.7)$$

where $g(k)$ represents the filtered gravity component, α represents the filter convergence coefficient, A_c represents the calibrated data, A_L represents the linear acceleration caused directly by the tremor motion, s_x , s_y and s_z which represent the amplitudes of the tremor motion on each axis, $S_M(k)$ represents the varying magnitude series of the tremor motion, and S_{rms} represents the RMS value of the magnitude series.

Table 3.2: Values of the calibration matrices for 5 accelerometers.

Parameter	Value	Parameter	Value
M_1	$\begin{bmatrix} 0.98 & -0.03 & 0.00 \\ 0.02 & 0.98 & -0.09 \\ -0.02 & 0.07 & 0.98 \\ 0.05 & -0.01 & 0.05 \end{bmatrix}$	M_4	$\begin{bmatrix} 0.99 & -0.06 & -0.01 \\ 0.04 & 1.01 & 0.01 \\ -0.01 & 0.00 & 0.98 \\ 0.02 & -0.02 & 0.05 \end{bmatrix}$
M_2	$\begin{bmatrix} 0.98 & 0.01 & -0.02 \\ 0.01 & 1.01 & 0.04 \\ 0.02 & -0.02 & 1.01 \\ 0.06 & 0.00 & 0.03 \end{bmatrix}$	M_5	$\begin{bmatrix} 1.01 & 0.01 & -0.01 \\ -0.01 & 0.98 & -0.07 \\ 0.01 & 0.08 & 1.03 \\ 0.04 & 0.01 & 0.05 \end{bmatrix}$
M_3	$\begin{bmatrix} 0.98 & 0.01 & -0.02 \\ 0.00 & 1.00 & -0.02 \\ 0.01 & 0.03 & 0.98 \\ 0.02 & 0.00 & 0.06 \end{bmatrix}$		

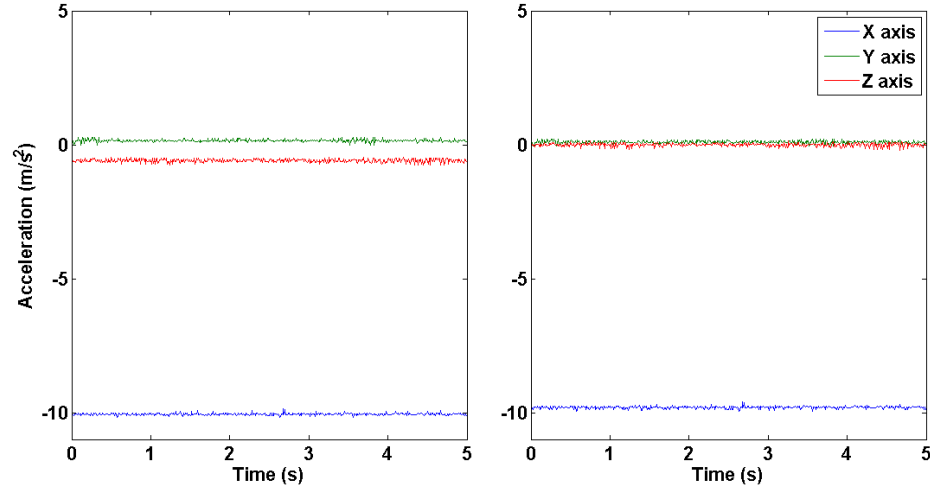


Figure 3.3: Accelerometer calibration. Data before calibration (*Left*). Data after calibration (*Right*).

Fig. 3.4 shows the result of gravity compensation. The data were randomly chosen from the patient data set. The left panel presents the signals before gravity compensation, and the right panel presents the signals after gravity compensation. The mean correlation coefficient calculated from all three axes is 0.96. This result indicates that the introduced low-pass filter is sufficient to extract the tremor signal.

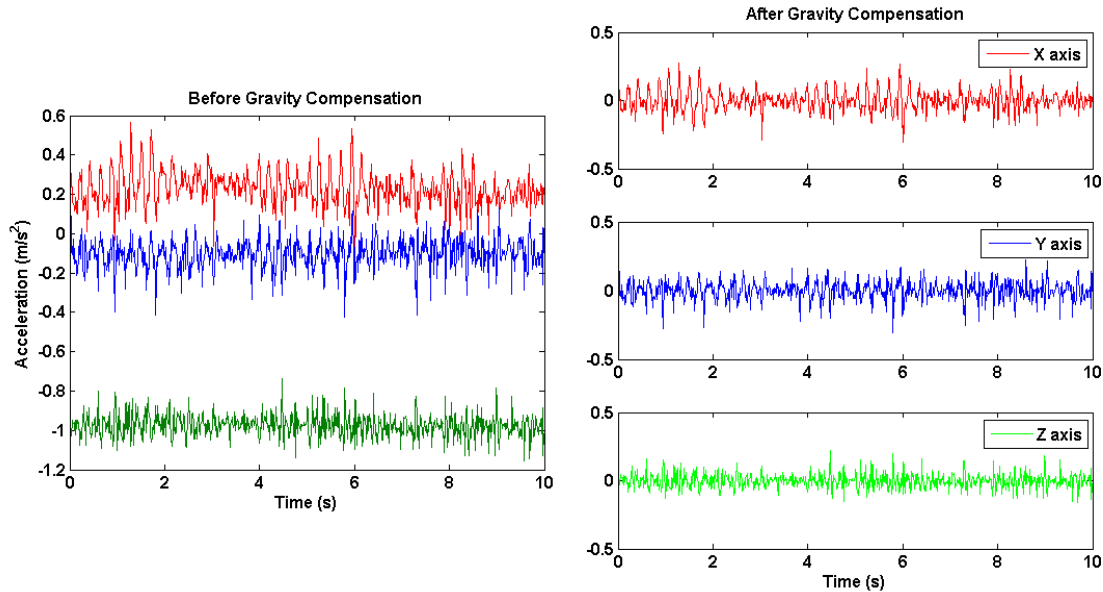


Figure 3.4: Gravity Compensation. Data include gravity (*Left*). Data without gravity (*Right*).

3.5 Results

3.5.1 Time-domain Characteristics of PD Tremor

Fig. 3.5 shows a typical PD tremor represented as a time series. For each joint, both the resting and postural tremor are presented. From these signals, we can see that the tremor magnitude varies with time.

A 1-second long window was used to identify the onset of the tremor. The data after the onset were used to calculate the tremor RMS. The linear acceleration and angular velocity collected from the IMU, and the angular displacement from the Aurora system are reported in Table 3.3. All 18 subjects presented with resting tremor, however, only 13 subjects presented with postural tremor. The other 5 subjects' data were excluded from the analysis of the postural tremor. The RMS angular displacement of the wrist tremor is not reported in this paper, as an additional EM tracker would be required to calculate the wrist angle. The results from both the resting tremor and the postural tremor show that the tremor magnitude increases from the proximal joint to the distal joint in the hand. The tremor from the thumb has a lower magnitude compared to the tremor from the index finger. In comparison with the resting tremor, it is possible to conclude that the postural tremor shows higher magnitude. This conclusion is in line with the results from other studies [46, 79–82]. However, it could be the result of a smaller sample size compared to the resting tremor. Therefore, a statistical analysis with a larger homogeneous PD group is necessary to make a robust conclusion.

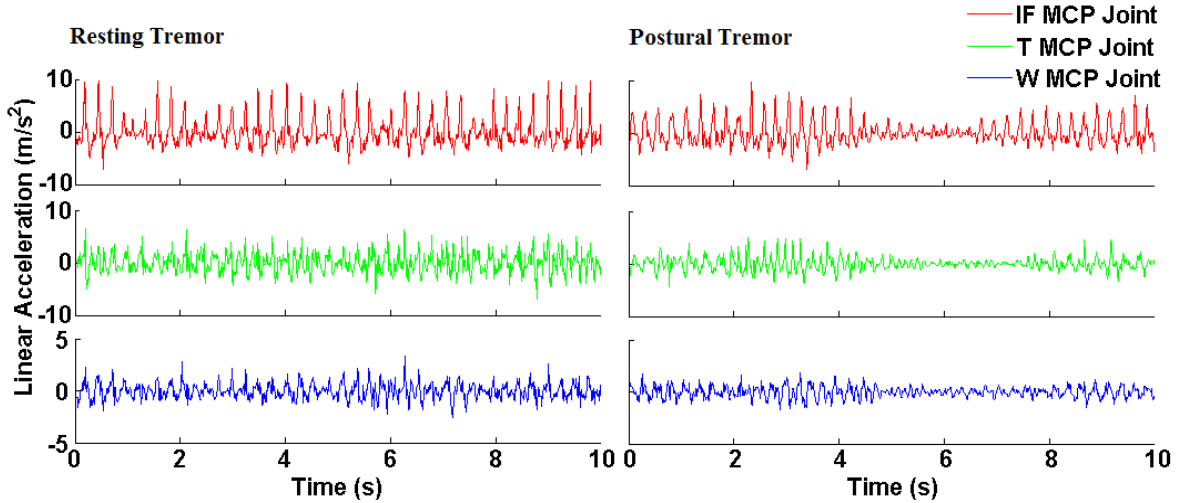


Figure 3.5: Sample time series of the resting tremor (left) and postural tremor (right) from the index finger MCP joint (red), thumb MCP joint (green) and wrist MCP joint (blue).

3.5.2 Frequency Characteristics of PD tremor

The right side of Fig. 3.6 shows the frequency distribution of PD tremor. Multiple harmonics were observed in the resting tremor as a pattern in 94.4% of the subjects, and in the postural tremor in 84.6% of the subjects. Every joint presents the same pattern for both resting tremor and postural tremor. The distribution of the PD tremor frequency of all 18 patients is shown on the left side of Fig. 3.6. The peak frequency of the 1st harmonic, 2nd harmonic and the 3rd harmonic of the resting tremor for all joints were used to determine the PD frequency ranges, which are 3.5 Hz to 5.8 Hz, 6.9 Hz to 11.5 Hz, and 10.4 Hz to 17.3 Hz, respectively. For the postural tremor, the 1st through the 3rd harmonics are within the ranges of 3.9 Hz to 7.7 Hz, 7.7 Hz to 11.2 Hz, and 11.5 to 16.8 Hz, respectively. The fourth and higher harmonics were considered too weak to be included in the results. It is also important to point out that the monoharmonic tremor has a higher fundamental frequency than the multi-harmonics tremor. The frequency lies within the range of 5.3 Hz to 7.7 Hz for the postural tremor and about 5.2 Hz for the resting tremor.

Table 3.3: RMS Amplitudes of PD Tremor

		Resting Tremor (Mean \pm SD)	Postural Tremor (Mean \pm SD)
RMS linear acceleration (m/s ²) from accelerometer	IF MCP Joint	2.1 \pm 1.2	2.7 \pm 1.0
	Thumb MCP Joint	1.8 \pm 1.1	2.5 \pm 1.3
	Wrist	0.9 \pm 0.5	1.5 \pm 0.8
RMS angular velocity (degrees/s) from gyroscope	IF MCP Joint	58.5 \pm 34.0	77.7 \pm 38.2
	Thumb MCP Joint	49.9 \pm 35.5	64.0 \pm 32.5
	Wrist	35.6 \pm 20.9	48.8 \pm 23.2
RMS angular displacement (degrees) from Aurora system	IF MCP Joint	2.9 \pm 1.8	3.1 \pm 1.3
	Thumb MCP Joint	2.2 \pm 1.6	2.4 \pm 1.2
	Wrist	—	—

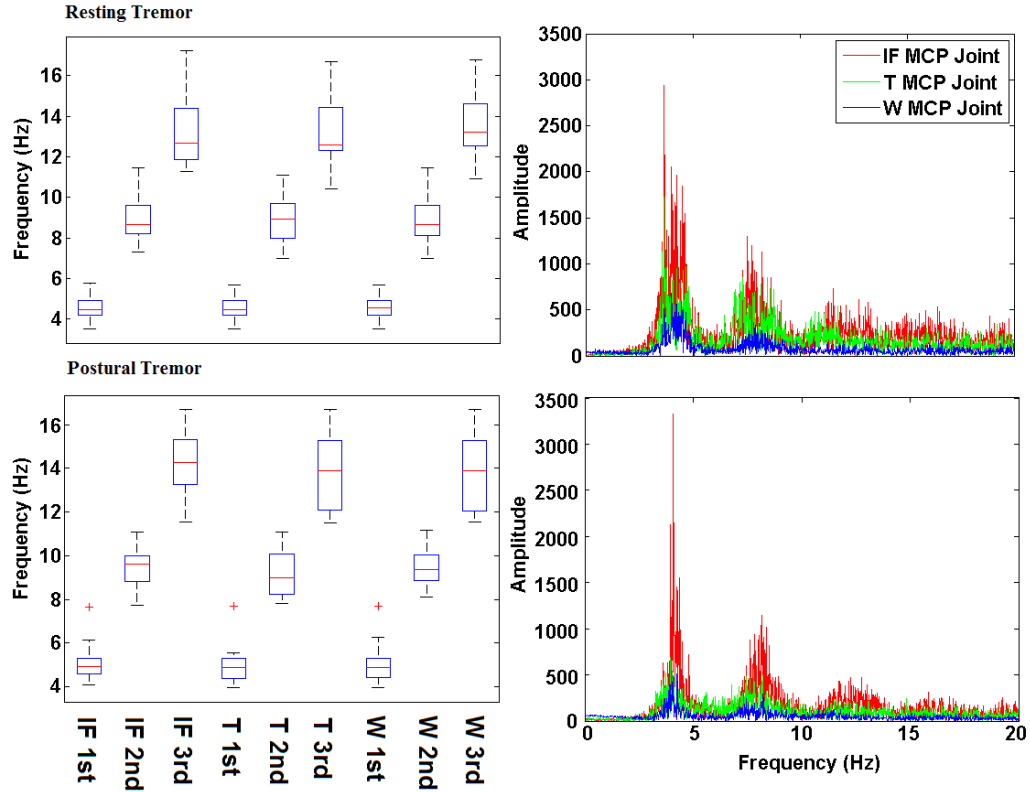


Figure 3.6: Frequency distribution of PD tremor from all 18 patients (left), and frequency analysis of the PD tremor from one patient (right).

The first three harmonics of the tremor signal from Fig. 3.5 were extracted using three 2nd-order band-pass Butterworth filters with cutoff frequencies of 3 to 5.5 Hz, 5.5 to 9.5 Hz, and 9.5 to 13 Hz (Fig. 3.7). The left column shows the time series of the first three harmonics. The right column shows the RMS amplitude of each harmonic calculated over the entire time span with a 1-second window. An analysis of the tremor energy distribution from each joint was conducted in order to evaluate the contribution of each harmonic. The energy proportion of the 2nd and 3rd harmonic to the 1st harmonic is presented in Fig. 3.8. Multiple harmonics were observed in the resting tremor of 17 patients and in the postural tremor of 11 patients. For the resting tremor, the mean values of the 2nd and 3rd harmonics of all joints are 60.9% and 38.9%; for the postural tremor, the mean values of the 2nd and 3rd harmonics of all joints are 50.3% and 20.9%.

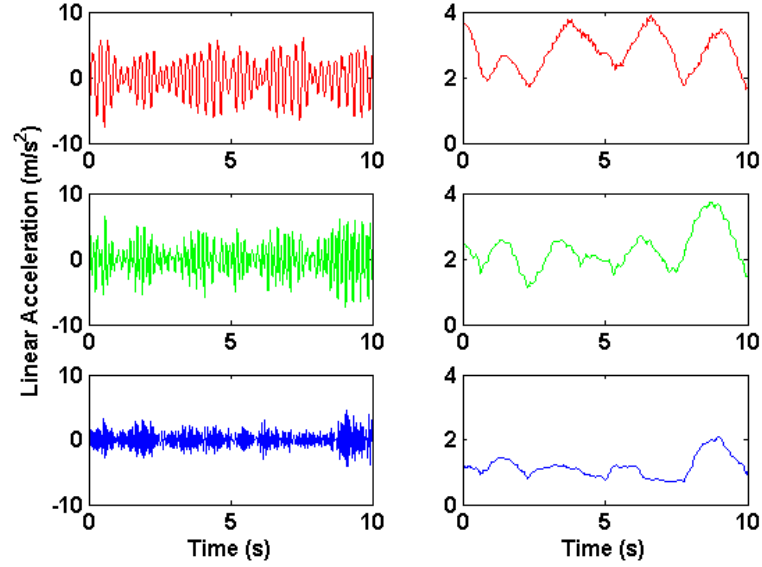


Figure 3.7: Decomposition of the PD resting tremor from the index finger MCP joint. Time series (left) of the 1st harmonic (red), the 2nd harmonic (green), and the 3rd harmonic (blue). RMS amplitude (right) of each harmonic calculated over the entire time span with a 1 second time window. 10 s data segment from one PD subject was used in this analysis.

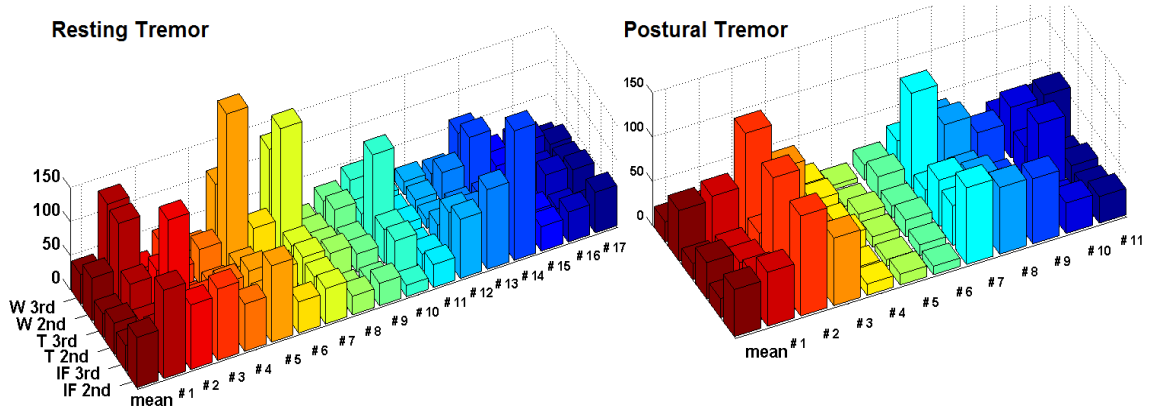


Figure 3.8: Tremor power distribution across patients. The values represent the magnitude percentage of the nth harmonic with respect to the 1st one.

3.6 Discussion

The quantification of tremor not only allows researchers to develop tremor suppression devices, but also to establish mathematical model for the purpose of simulation and

control. The data from the IMUs and Aurora system were analyzed and the quantified results are presented in Table 3.3. Additional data from the Myo and their correlations with the tremor motion data and the level of disease have not been analyzed in this work due to the difficulty of interpreting the finger motions using forearm EMG signals.

In Table 3.3, large deviations of the RMS amplitudes are observed. One possible reason could be the heterogeneity of PD patient. Large heterogeneity would lead to large difference in tremor severity, which would result in a large deviation. Besides, some patients may consciously or subconsciously suppressed tremor during the experiment, even though they were asked math questions. All these factors would result in a large deviation. Therefore, a larger sample size is required in order to achieve more accurate results.

In previous studies [29, 35, 40, 47], PD tremor is considered and reported as a single frequency signal with a fundamental frequency ranging between 4–12 Hz. However, the results presented in Fig. 3.6 show that PD tremor consists of several harmonics. The frequency of the k^{th} harmonic is roughly k times the frequency of the 1st harmonic—this feature is in accordance with the reports from other studies [42, 48]. In both the medical and the engineering fields, the frequency characteristics of the PD tremor have been reported and considered as mono-frequency vibrations. However, 17 out of 18 subjects from our study showed that PD tremor consists of multiple harmonics. The discovery of this pattern may actually facilitate the design of tremor suppression orthoses by improving the PD tremor model.

Some studies [30, 50, 82] have been conducted using a combination of several sinusoidal signals with different frequencies to simulate and control tremor; however, Fig. 3.7 shows that the harmonics of the real tremor are not sinusoidal. The RMS amplitude series shows that the amplitude of each tremor's harmonic varies with time. This approach for combining sinusoidal signals with different frequencies matches the frequency component of real tremors; however, additional mathematical description of the amplitude is necessary.

The tremor energy distribution (Fig. 3.8) shows that the 2nd and the 3rd harmonics are so strong that they cannot be neglected. About 70.6% of the participants have at least one joint in which the power of the 2nd harmonic is higher than 50% of the 1st harmonic. Neglecting the presence of the second tremor harmonic in their model may be the reason why some the tremor suppression devices have not achieved better performance. Based on the results shown above, a more accurate PD tremor model should consist of at least two key characteristics: the first one is time varying amplitude and the second one is multiple harmonics.

3.7 Conclusion

Finger and wrist tremors from 18 PD patients have been studied in both the time and the frequency domains. The RMS tremor magnitudes were presented in the form of linear acceleration, angular velocity and angular displacement; a common multi-frequency pattern has been observed for all patients. Based on the pattern observed, further analysis was conducted and the results showed that the second harmonic (6.9–11.5 Hz) makes a large contribution to the tremor and, therefore, it should not be neglected. In summary, neither the time varying amplitude, nor the multiple harmonics that characterize PD tremor motion can be neglected or simplified.

Chapter 4

4 Tremor Estimation

Offline tremor analysis is often useful in the research and evaluation of a patient's response to treatments. Such analysis requires quantification methods to analyze the data acquired from sensors [71]. As opposed to offline analysis, the purpose of online analysis is to provide tremor information in real time, thereby allowing tremor to be actively suppressed. In order to provide precise tremor information, the online analysis method must be able to track tremor parameters and eliminate noise.

Ideally, there is an algorithm/model that can perfectly extract the tremor behavior without any error. However, it is nearly impossible to find such an algorithm/model. In this chapter, a detailed study of tremor estimators is provided.

4.1 Tremor Model

Tremor modeling is an important step for evaluating a tremor estimator prior to using real patient data. In this section, the two most commonly used tremor models are described.

A tremor signal can be described as a quasi-periodic and nonstationary signal. The amplitude, frequency and phase of the tremor are considered to be changing over time. Two models that have been commonly used to simulate quasi-periodic signals are auto-regressive (AR) and harmonic models [48, 71].

A. Auto-regressive Model

In statistics and signal processing, an AR model is an approximation process that forecasts the current value of a particular parameter using a linear combination of the past values of the parameter. In general, an AR model can be used to model an arbitrary time series. The mathematical model is given below,

$$s_t(k) = u + \sum_{n=1}^N a_n(k) s_t(k-n) + v_{st}, \quad (4.1)$$

where u is a constant, v_{st} is white Gaussian noise, $v_{st} \sim N(0, \sigma_{st}^2)$, N is the model order, and a_n is a time-varying parameter. Changing the value of a_n results in different a signal pattern. The variance of the white noise v_{st} will alter the scale of the signal.

B. Harmonic Model

The harmonic model is also referred to as a Fourier series model. Due to the properties of the Fourier series, every periodic signal may be represented by this model. Although tremor is not defined as a typical periodic signal, its principal frequency only changes slowly over time. This not-approximately periodic feature allows for the use of the harmonic model as an approximation of the real tremor signal. The mathematical model is given below,

$$\begin{aligned}
 s_t(k) &= \sum_{n=1}^{N_t} \left[a_n(k-1) \cdot \sin\left(n \cdot \sum_{t=1}^{k-1} \omega(t)\right) + b_n(k-1) \cdot \cos\left(n \cdot \sum_{t=1}^{k-1} \omega(t)\right) \right] + v_{st}(k-1) \\
 h_n(k) &= A_n(h) \cdot \exp\left(-\frac{(k - B_n(h) \cdot (N_s / 2))^2}{2(C_n(h) \cdot N_s)^2}\right), \quad n \in \{1, 2..N\}, \quad h \in \{a, b\} \\
 \omega(k) &= \omega_0 + \frac{0.75}{1 + \exp(5 - 10 \cdot (k / N_s))},
 \end{aligned} \tag{4.2}$$

where h denotes the time varying Fourier coefficients a and b , A , B and C are parameters of the a and b functions, ω is the estimated tremor frequency, ω_0 is the fundamental frequency, and N_t is the number of harmonics.

As discussed in Chapter 3, frequency analysis has shown that a tremor signal presents as a combination of multiple harmonics. Therefore, the harmonic model may be adapted to this feature. The values of the parameters used are shown in Table 4.1. The values of $a_1(A)$, $b_1(A)$, $a_2(A)$ and $b_2(A)$ were adjusted to match the average RMS magnitude from the real patient data.

Table 4.1 Parameters for Simulated Tremor [71]

Parameter	Value	Parameter	Value
$A_1(a)$	0.3	$A_1(b)$	0.15
$B_1(a)$	1.25	$B_1(b)$	1.25
$C_1(a)$	0.59	$C_1(b)$	0.63
$A_2(a)$	0.1	$A_2(b)$	0.2
$B_2(a)$	1.25	$B_2(b)$	1.25
$C_2(a)$	0.59	$C_2(b)$	0.63
σ_{st}^2	10^{-4}	N_t	1, single harmonic 2, two harmonics
ω_0	4.5 Hz		

From the analysis of real patient data, it was found that a high proportion of PD tremor consists of multiple harmonics. Therefore, two different types of tremors were simulated using the harmonic model (Fig. 4.1 and Fig. 4.2). All signals were simulated using a 0.01 s time step in Matlab.

Fig. 4.1 shows a simulated tremor with a single harmonic ($N_t=1$ for the harmonic model). The frequency analysis shows that the fundamental frequency is approximately 4.5 Hz. The RMS amplitude is 2.19 m/s^2 . A two-harmonics tremor motion is shown in Fig. 4.2 ($N_t=2$ for the harmonic model). The frequencies of the first harmonic and second harmonic are 4.5 and 9 Hz respectively. The RMS amplitude is 2.49 m/s^2 . Although it is not sufficient to claim that the simulated tremor and real tremor are equivalent, the

amplitude and frequency characteristics of the simulated tremor are similar to real tremor. Therefore, in the following sections, the simulated tremor is used for the evaluation of several tremor estimators.

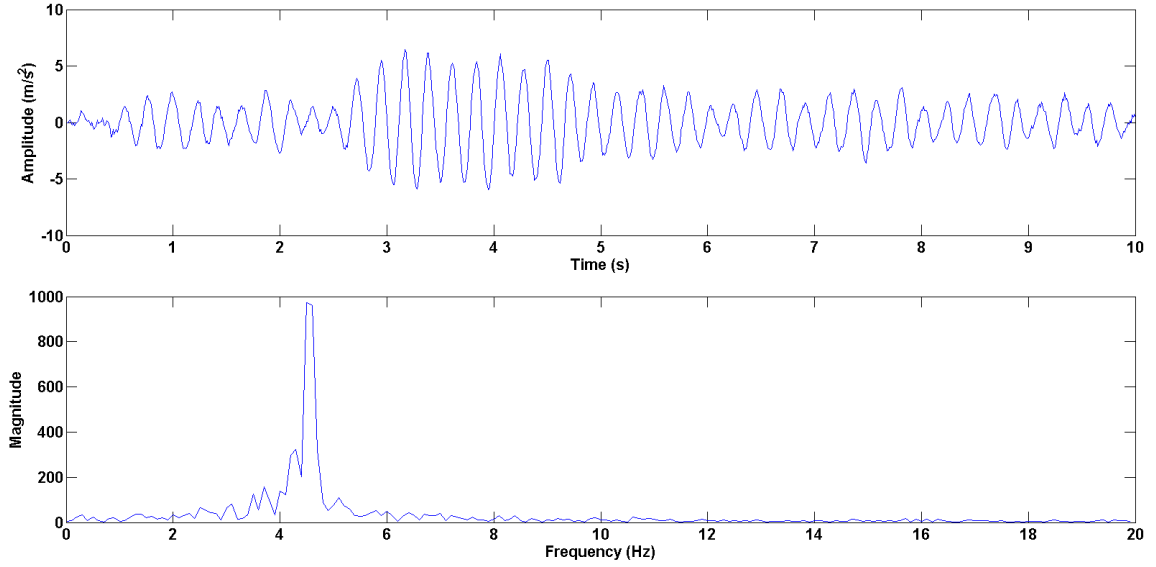


Figure 4.1: Simulated tremor using harmonic model. Top: Tremor manifestation in the time domain. Bottom: Tremor manifestation in the frequency domain. $N_t = 1$.

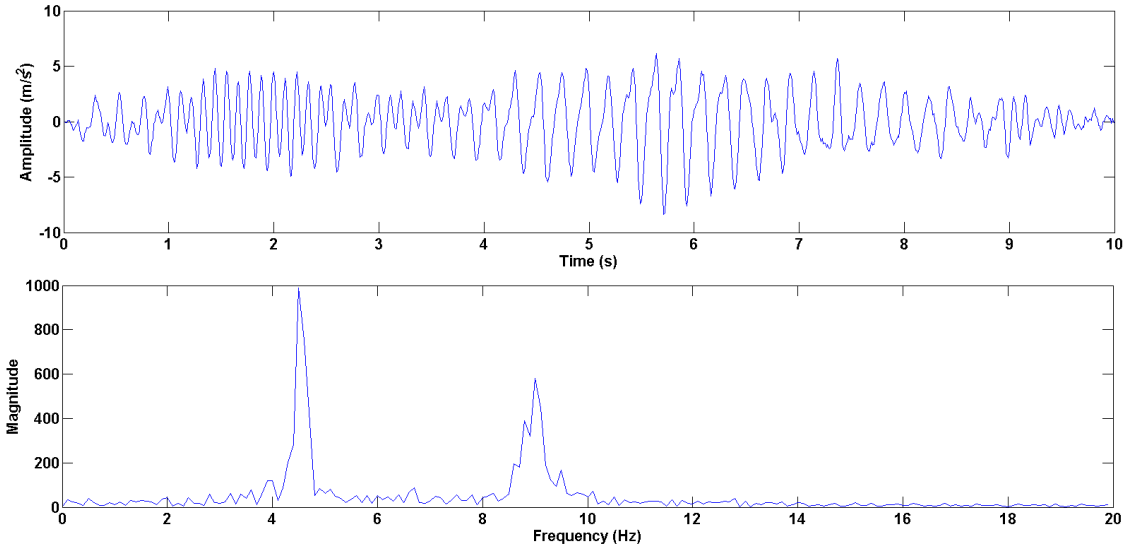


Figure 4.2: Simulated tremor using harmonic model. Top: Tremor manifestation in the time domain. Bottom: Tremor manifestation in the frequency domain. $N_t = 2$.

4.2 Adaptive Tremor Estimator

Due to the nonstationary nature of the tremor, an adaptive algorithm is particularly effective for estimating the tremor signal because it constantly adjusts its parameter to achieve optimal performance. There are several tremor estimation algorithms have been developed. Most of them are derivatives of two basic estimators: the WFLC and the Kalman Filter (KF). In this section, these two basic estimators are compared, and a combined algorithm is studied based on real tremor data.

4.2.1 Weighted Fourier Linear Combiner

Prior to the establishment of the WFLC, the FLC was first introduced in 1994 [67] to decouple the noise that exhibits on the brain evoked response of an anesthetized cat. It filters the input signal in the form of a dynamic truncated Fourier series model as follows:

$$y(k) = \sum_{r=1}^M [a_r \sin(r\omega_0 k) + b_r \cos(r\omega_0 k)], \quad (4.3)$$

where the adaptive filter weights are the Fourier coefficients, a_r and b_r . M is the number of harmonics.

The FLC estimates the Fourier coefficients at a given frequency (ω_0) using the Least Mean Square (LMS) algorithm. The frequency components are given as follows:

$$x_r(k) = \begin{cases} \sin(r\omega_0 k), & 1 \leq r \leq M \\ \cos[(r-M)\omega_0 k], & M+1 \leq r \leq 2M \end{cases} \quad (4.4)$$

The adaptive filter weight is given as, where $W(k) = [w_1(k) \cdots w_{2M}(k)]^T$, $\varepsilon(k) = s(k) - W^T(k) \cdot X(k)$ is the estimation error, μ is the adaptive gain that is inversely proportional to convergence, and $s(k)$ is the input signal. The estimated tremor signal is given as:

$$\hat{y}(k) = X(k) \cdot W(k) \quad (4.5)$$

where $X(k) = [x_1(k) \cdots x_{2M}(k)]^T$.

A block diagram of the FLC is shown in Fig. 4.3. An input signal with a known frequency component can be effectively estimated and cancelled through the FLC. However, it is not optimal for a signal with varying frequency, such as tremor. Therefore, a WFLC, which tracks both frequency and amplitude, was developed subsequent to the FLC [68].

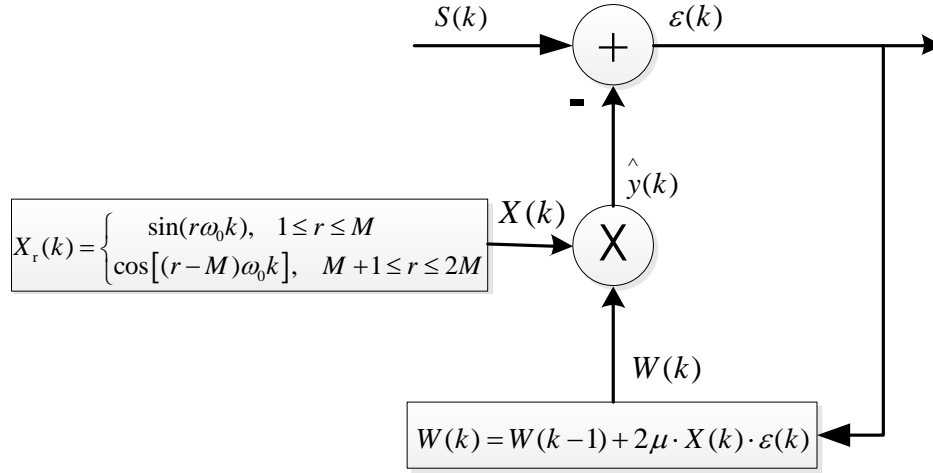


Figure 4.3: Block diagram of the Fourier Linear Combiner.

Similar to the estimation of the Fourier coefficients in the FLC, a second LMS algorithm was applied to estimate the frequency component ω_0 ,

$$\omega_0(k+1) = \omega_0(k) + 2\mu_0 \varepsilon_k \sum_{r=1}^M (w_r x_{M+r} - w_{M+r} x_r) \quad (4.5)$$

accordingly,

$$X_r(k) = \begin{cases} \sin(r \sum_{i=0}^k \omega_0(i)), & 1 \leq r \leq M \\ \cos\left[(r-M) \sum_{i=0}^k \omega_0(i)\right], & M+1 \leq r \leq 2M \end{cases} \quad (4.6)$$

where μ_0 is the adaptive gain that is inversely proportional to convergence.

The values of μ_0 and μ are crucial to the convergence of the system. They were chosen based on the method used in [67, 68]. To determine the optimal values for μ_0 and μ , the following value ranges were considered:

$$\begin{aligned} u &= 0.01 + 0.025i \quad i = 1, 2, 3, \dots, 20 \\ u_0 &= [10^{-9}, 5 \times 10^{-9}, 10^{-8}, 5 \times 10^{-8}, \dots, 10^{-4}, 5 \times 10^{-4}, 10^{-3}]. \end{aligned}$$

To test the performance of the WFLC and identify the optimal values for its parameters, a simulated tremor with a 4.5 Hz fundamental frequency was generated using the harmonic model introduced in Section 4.1. The percentage fit error (PFE) value (Equation 4.7) and the correlation coefficient were used to test each value combination. A total number of 20 trials were performed.

$$PFE = \frac{\|S - \hat{y}\|}{\|S\|} \times 100\% \quad (4.7)$$

The minimal PFE and maximal correlation coefficient were achieved when $\mu_0 = 1e^{-7}$ and $\mu = 0.21$. The time series of the simulated tremor and estimated tremor signal is shown in Fig. 4.4. The PFE and the correlation coefficient obtained from 20 trials are $34.55\% \pm 1.82\%$ and 0.94 ± 0.01 , respectively. Fig. 4.5 shows the tremor motion in the frequency–time domain, the colour bar indicates the magnitude of the tremor motion. These results demonstrate that the WFLC can track the frequency of the tremor well; however, there is a relatively large error in the amplitude of the estimated tremor. This large error may be caused by a limitation of the gradient-based estimation algorithm of the WFLC. To improve the performance of the amplitude estimation, a KF is introduced for tremor amplitude estimation.

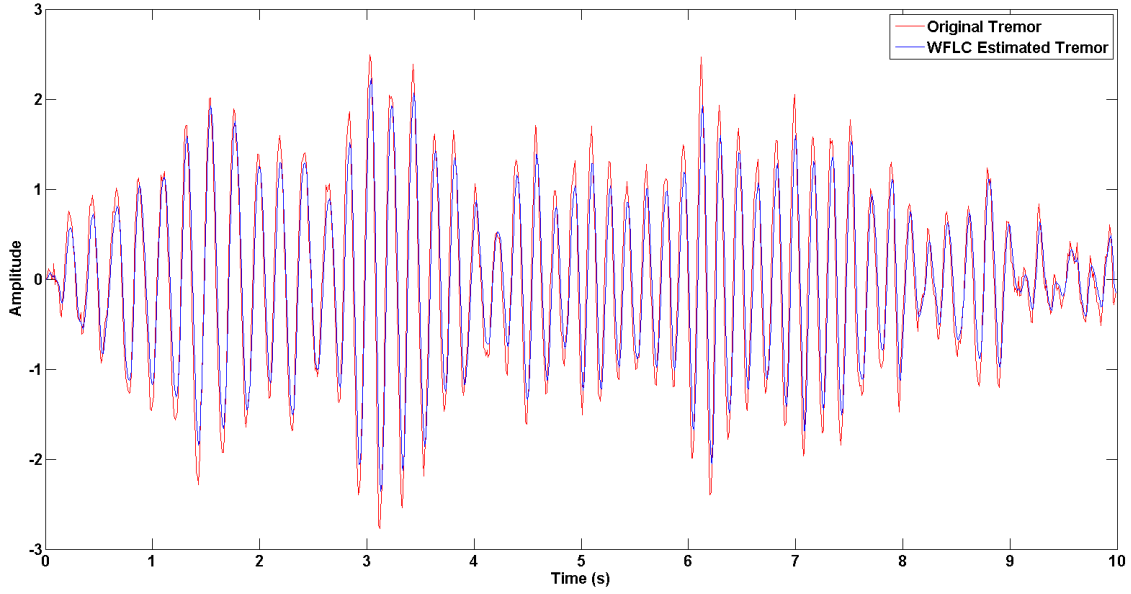


Figure 4.4: Time series of the simulated tremor and the estimated tremor from one randomly selected trial. The simulated tremor signal is shown in red and the estimated tremor is shown in blue.

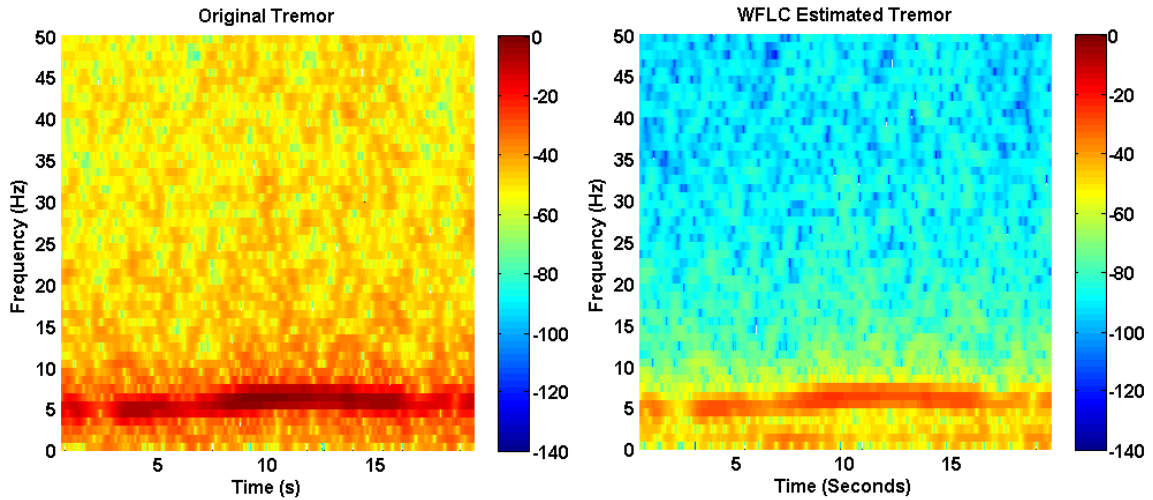


Figure 4.5: Short time Fourier transform of the simulated tremor and the estimated tremor from one randomly selected trial.

4.2.2 WFLC-based Kalman Filter

Different from the WFLC, a KF estimates the optimal solution by minimizing the covariance of a posteriori estimation error [83]. Therefore, the adoption of a KF makes it

possible to enhance the accuracy of tremor estimation. Since the development of the KF [84], it has become a widely used approach for tracking estimation. A standard KF model is given below,

$$\begin{aligned}
\tilde{X}(k|k-1) &= F_t \hat{X}(k-1|k-1) \\
\tilde{P}(k|k-1) &= F_t \hat{P}(k-1|k-1) F_t^T + G Q G^T \\
\mathcal{G} &= z_m(k) - H \tilde{X}(k|k-1) \\
S &= H \tilde{P}(k|k-1) H^T + R \\
K &= \tilde{P}(k|k-1) H^T S^{-1} \\
\hat{X}(k|k) &= \tilde{X}(k|k-1) + K \mathcal{G} \\
\hat{P}(k|k) &= (1 - KH) \tilde{P}(k|k-1)
\end{aligned} \tag{4.8}$$

where \tilde{X} is the prediction state, \tilde{P} is the prediction error covariance, \mathcal{G} is the innovation, which integrates the input signal to the estimator, S is the innovation covariance, K is the Kalman gain, \hat{X} is the estimation state, which represents the estimated tremor, \hat{P} is the estimation error covariance, F_t is the state transition matrix of a tremor model, G and R are the process and measurement noise covariance matrices, z_m is the measured value, and H is the measurement matrix of the input signals.

In order to adopt a KF for tremor estimation, PD tremor is modeled as a quasi-sinusoidal motion in the absence of a complete PD tremor model:

$$S_t(k) = a_n(k) \sin(2\pi f_t k T_s) + b_n(k) \cos(2\pi f_t k T_s), \tag{4.9}$$

where a_n and b_n are the Fourier coefficients, f_t is the frequency of the tremor, and T_s is the sampling time. Therefore, the state transition matrix can be calculated as follows:

$$\begin{aligned}
\begin{bmatrix} S_t(k+1) \\ \dot{S}_t(k+1) \end{bmatrix} &= F_t \cdot \begin{bmatrix} S_t(k) \\ \dot{S}_t(k) \end{bmatrix} \\
F_t &= \begin{bmatrix} \cos(2\pi f_t T_s) & \sin(2\pi f_t T_s) / (2\pi f_t T_s) \\ -2\pi f_t T_s \sin(2\pi f_t T_s) & \cos(2\pi f_t T_s) \end{bmatrix}
\end{aligned} \tag{4.10}$$

notice that

$$\begin{aligned} S_t(k+1) &= \cos(2\pi f_t T_s) S_t(k) + \sin(2\pi f_t T_s) \dot{S}_t(k) / (2\pi f_t T_s) \\ \dot{S}_t(k+1) &= \cos(2\pi f_t T_s) \dot{S}_t(k) - 2\pi f_t T_s S_t(k) \sin(2\pi f_t T_s) \end{aligned} \quad (4.11)$$

The frequency (f_t) of the PD tremor is estimated by a WFLC, the signal flow diagram is shown in Fig. 4.6. The values of the parameters of the KF are given in Table 4.2.

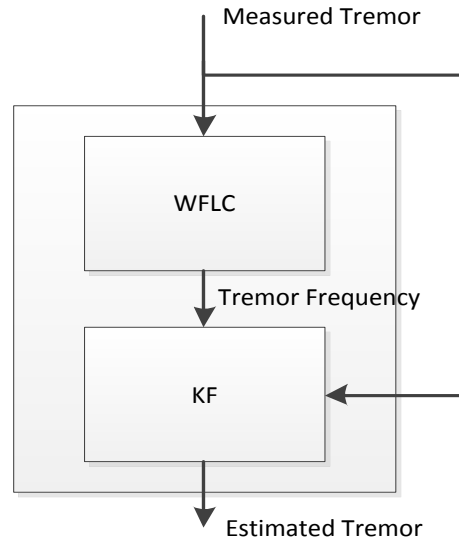


Figure 4.6: Signal flow diagram of a WFLC–KF tremor estimator

Fig. 4.7 shows the time series of the simulated tremor, the WFLC estimated tremor and the WFLC–KF estimated tremor. From the figure, it can be observed that the WFLC–KF estimator has better performance on amplitude tracking over the WFLC estimator. A time–frequency analysis was performed to investigate the performance of frequency tracking of the WFLC–KF estimator. Fig 4.8 shows that the frequency curve of the estimated tremor matches the frequency curve of the simulated tremor. These preliminary results indicate that the WFLC–KF estimator may achieve a better performance for tremor estimation.

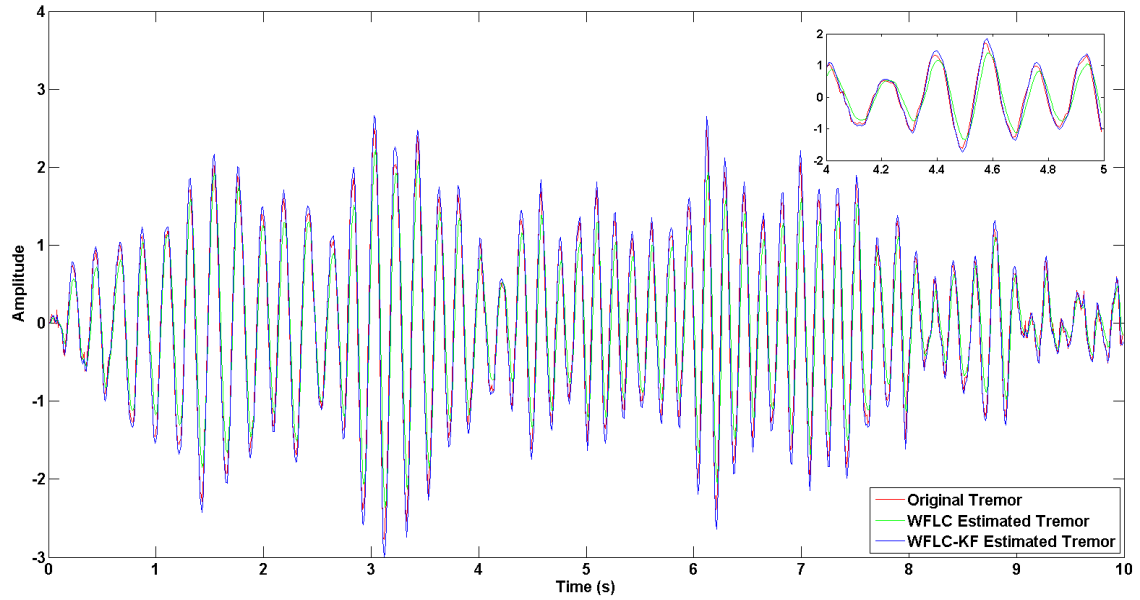


Figure 4.7: Time series of the simulated tremor and the estimated tremors from both WFLC and KF. The simulated tremor signal is shown in red, the WFLC estimated tremor is shown in green, and the KF estimated tremor is shown in blue.

Table 4.2 Parameters of the KF

Parameter	Value	Parameter	Value
R	400	G	$\begin{bmatrix} 0.1 & 10^{-4} \\ 10^{-4} & 0.1 \end{bmatrix}$
Q	0.9	H	[1, 0]
T_s	0.01 s		

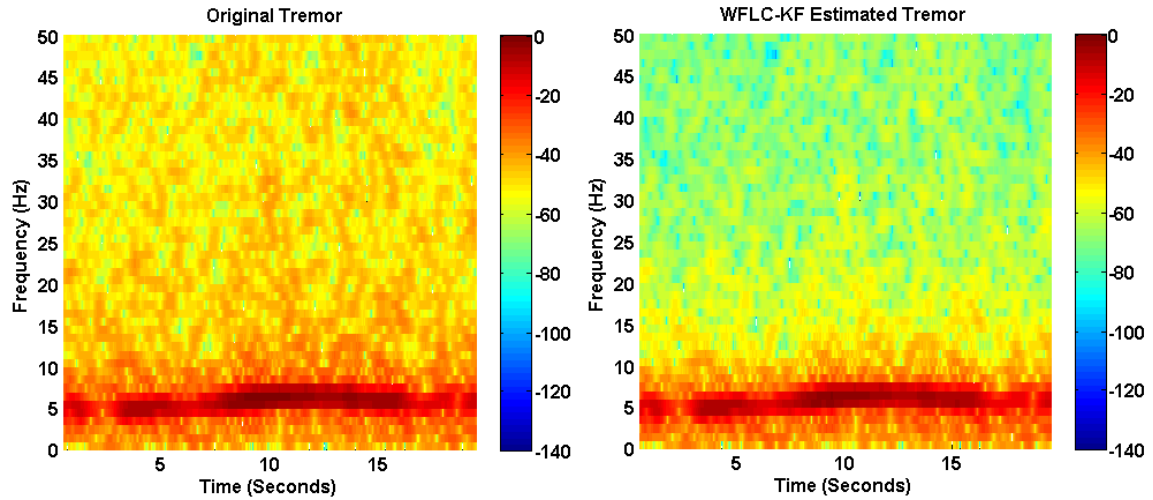


Figure 4.8: Short time Fourier transform of the simulated tremor and the WFLC–KF estimated tremor from one randomly selected trial.

A total of 20 trials were conducted to compare the performance of the WFLC and the WFLC–KF estimator, and to generate a more robust conclusion (Fig. 4.9). Prior to each trial, a different simulated tremor signal was generated for both estimators. In comparison with the WFLC estimator, the WFLC–KF estimator has a lower fit error ($7.08\% \pm 1.01\%$) and higher correlation (0.9980 ± 0.0007). This supports the conclusion that the WFLC–KF tremor estimator provides better tremor estimation performance than the WFLC estimator.

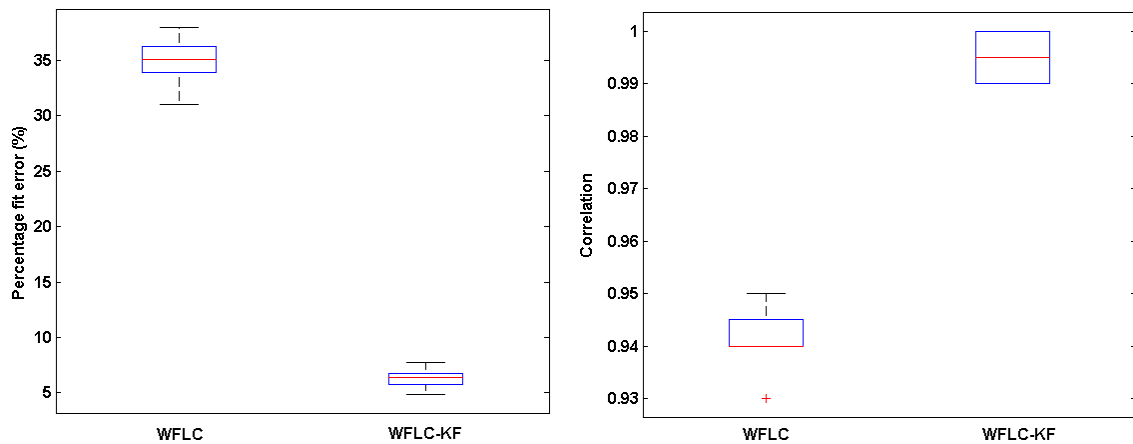


Figure 4.9: Performance comparison between the WFLC estimator and the WFLC–KF estimator. A total of 20 trials were performed.

4.3 The Effect of the PD Tremor Model's Harmonics on Tremor Estimation

The analysis of real patient data in Chapter 3 shows that the PD tremor consists of multiple harmonics. The frequency of the k^{th} harmonic is roughly k times the fundamental frequency. In most previous studies [68, 70, 71, 75, 85], the tremor estimators use only a single harmonic model; however, this is insufficient to achieve a good estimation result. Therefore, in this section, the effect of the PD tremor model's harmonics on the performance of the estimator is investigated. A PD tremor model with two harmonics is adopted in the WFLC–KF, as follows:

$$\begin{aligned} S_t(k) &= S_{t1}(k) + S_{t2}(k) \\ S_{t1}(k) &= a_{n1}(k) \sin(2\pi f_{t1} k T_s) + b_{n1}(k) \cos(2\pi f_{t1} k T_s) \\ S_{t2}(k) &= a_{n2}(k) \sin(4\pi f_{t2} k T_s) + b_{n2}(k) \cos(4\pi f_{t2} k T_s) \end{aligned} \quad (4.12)$$

where S_{t1} and S_{t2} represent the models of the first and second harmonic. f_{t1} and f_{t2} are the estimated frequencies of the first and second harmonic using two WFLCs. Correspondingly, the state transition matrix is modified as follows:

$$\begin{aligned} \begin{bmatrix} S_{t1}(k+1) \\ \dot{S}_{t1}(k+1) \\ S_{t2}(k+1) \\ \dot{S}_{t2}(k+1) \end{bmatrix} &= F_t \cdot \begin{bmatrix} S_{t1}(k) \\ \dot{S}_{t1}(k) \\ S_{t2}(k) \\ \dot{S}_{t2}(k) \end{bmatrix} \\ F_t &= \begin{bmatrix} \cos(2\pi f_{t1} T_s) & \sin(2\pi f_{t1} T_s) / (2\pi f_{t1} T_s) & 0 & 0 \\ -2\pi f_{t1} T_s \sin(2\pi f_{t1} T_s) & \cos(2\pi f_{t1} T_s) & 0 & 0 \\ 0 & 0 & \cos(2\pi f_{t2} T_s) & \sin(2\pi f_{t2} T_s) / (2\pi f_{t2} T_s) \\ 0 & 0 & -2\pi f_{t2} T_s \sin(2\pi f_{t2} T_s) & \cos(2\pi f_{t2} T_s) \end{bmatrix} \end{aligned} \quad (4.13)$$

The signal flow diagram is shown in Fig. 4.10. Prior to the frequency estimation, the measured tremor is decomposed into two harmonics using two 1st-order band-pass Butterworth filters with cutoff frequencies of 3 to 6 Hz, and 6 to 30 Hz. The values of the parameters of the modified WFLC–KF estimator are given in Table 4.3.

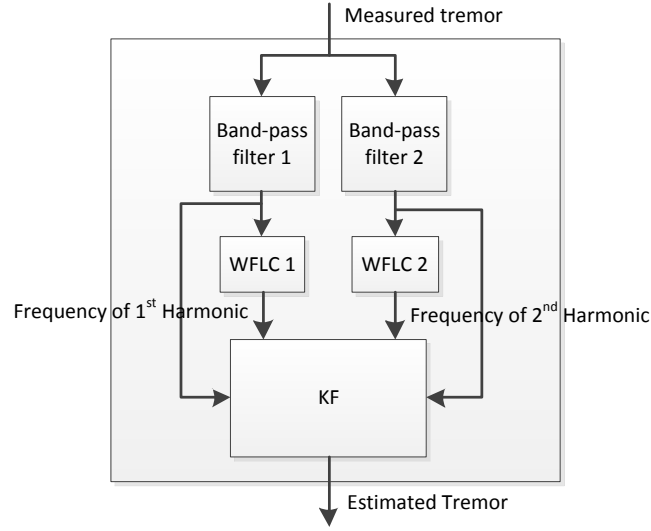


Figure 4.10: Signal flow diagram of a modified WFLC–KF tremor estimator

In order to compare the estimated tremor with a reference tremor signal, a 1st-order band-pass Butterworth filter with cutoff frequencies of 3 to 30 Hz was used to acquire the reference tremor signal after sampling.

Table 4.2 Parameters of the WFLC–KF

Parameter	Value	Parameter	Value
R	diag(400, 800)	T_s	0.01 s
Q	diag(0.9, 0.9, 2, 2)	H	$\begin{bmatrix} 1 & 0 & 0 & 0 \\ 0 & 0 & 1 & 0 \end{bmatrix}$
G	$\begin{bmatrix} 10^2 & 10^{-1} & 0 & 0 \\ 10^{-1} & 10^2 & 0 & 0 \\ 0 & 0 & 10^8 & 10^5 \\ 0 & 0 & 10^5 & 10^8 \end{bmatrix}$		

Fig. 4.11 shows a preliminary estimation result using real PD tremor data. The top figure shows the estimated tremor generated by the WFLC-KF estimator using the single harmonic model. The bottom figure shows the estimated tremor generated by the WFLC–

KF estimator using the two-harmonics model. In comparison with the former estimator, the estimator adopting a two-harmonics model appears to produce a better estimation result. In order to draw a more robust conclusion, both of the estimators were tested on a total of 18 real PD tremor signals.

The percentage estimation accuracy (PEA) is adopted for the evaluation,

$$PEA = 100 - \frac{\|\text{true value} - \text{estimated value}\|}{\|\text{true value}\|} \cdot 100\% \quad (4.14)$$

Fig. 4.12 *Left* shows that the adoption of a two-harmonics model results in better estimation performance than the single harmonic model. The average increase in accuracy is about 13%. This increase is probably facilitated by the fact that most of the PD tremors consist of multiple harmonics. Furthermore, the increased correlation (Fig. 4.12 *Right*) also indicates that the two-harmonic tremor model surpasses its counterpart.

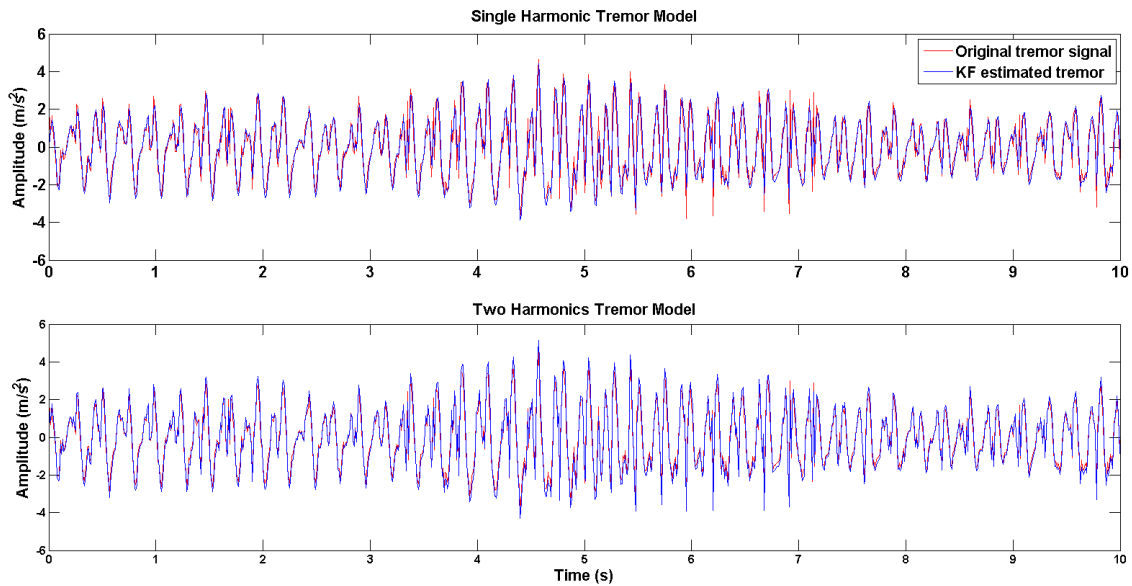


Figure 4.11: Time series of the WFLC–KF estimators with different tremor models. The top figure shows the result from the estimator using the single harmonic model. The bottom figure shows the result from the estimator using the two-harmonics model.

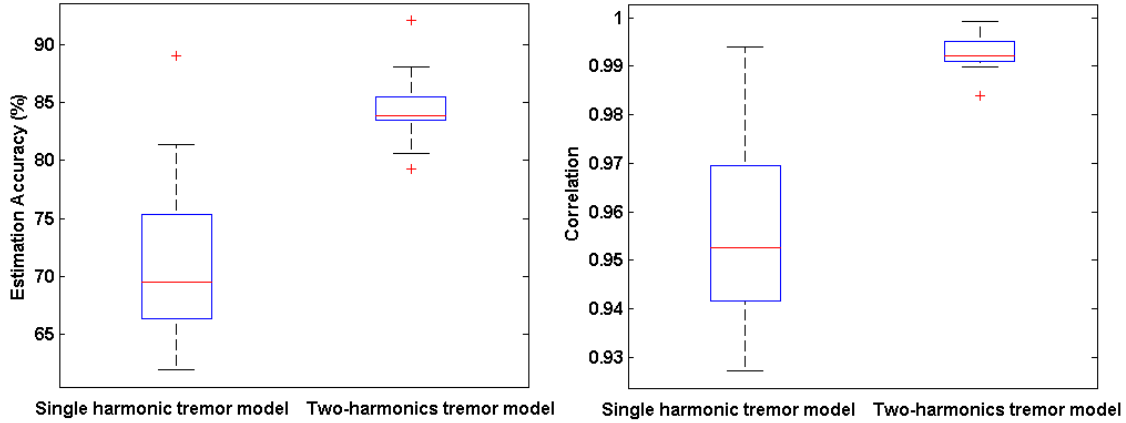


Figure 4.12: Performance comparison between the WFLC–KF estimators with different tremor models. A total of 18 trials were performed.

4.4 Conclusion

This chapter presented two motion-tracking algorithms (WFLC and KF) and their combination (WFLC–KF). The results showed that the WFLC–KF utilizes the frequency tracking capabilities of the WFLC, complemented by the KF for better amplitude estimation. Finally, the effect of the PD tremor model’s harmonics on estimation performance was investigated. A two-harmonics tremor model was introduced in the WFLC–KF. The results showed a 13% increase in the estimation accuracy and the correlation was increased from 0.96 to 0.99.

In a tremor suppression system, the tremor estimator sends the estimated tremor signal to the actuation system to conduct suppression on tremor. The actuation systems of many current exoskeleton devices have issues associated with their size, weight, power source, and overall effectiveness. In the next chapter, a novel multi-channel mechanical splitter (MMS) for tremor suppression device is introduced as a possible solution.

Chapter 5

5 DESIGN OF A MULTI-CHANNEL MECHANICAL SPLITTER FOR TREMOR SUPPRESSION

As mentioned in Chapter 2, most of the tremor suppression devices designed within the last 15 years are either too bulky or too heavy, mostly due to the fact that these devices need one heavy actuator for each DOF. Other problems are also associated with their actuation systems, such as pneumatic cylinders or vibration exciters. Although some devices achieved good suppression performance, widespread adoption by patients is still further down the road because of the issues presented above. Therefore, we need a novel solution to facilitate the transition of wearable devices from the lab environment to patient use. In this chapter, a possible solution is introduced: to split one powerful input into multiple independent outputs using a novel mechanism.

5.1 Literature Review

A continuously variable transmission (CVT), also known as a gearless transmission, can consecutively change the effective gear ratio between a minimum and a maximum value. In comparison with other mechanical transmissions, this feature allows the input speed to maintain a constant value while modifying the output speed. Therefore, a CVT could be used as the core of a single-input-multiple-output mechanism. A variety of continuously variable transmissions have been introduced and used in manufacturing, vehicles, and robotics, among others. [86–92]. These CVTs use friction, belts, and chains to change the transmission ratio.

A belt–pulley CVT system is the most commonly used CVT system. It contains two pulleys that are split axially into two halves. Each half has an inclined surface that supports a belt. The edge of the belt slides on the inclined surfaces of the pulleys as each half moves along the axis of rotation. The gear ratio is determined by the locations of the belt on the driving pulley and the driven pulley. A diagram of a belt–pulley CVT system is shown in Fig. 5.1. One disadvantage of this belt–pulley CVT system is that it requires high friction at the belt–pulley interface to transmit force from one to the other, while

simultaneously requiring low friction in order to allow the belt to slide along the surface of the pulley. These requirements dictate the use of a high power actuator to move each half of the pulley along the axis of rotation. Another disadvantage is that the system is rather complex. Therefore, it is difficult to minimize the size of the device for use in wearable devices.

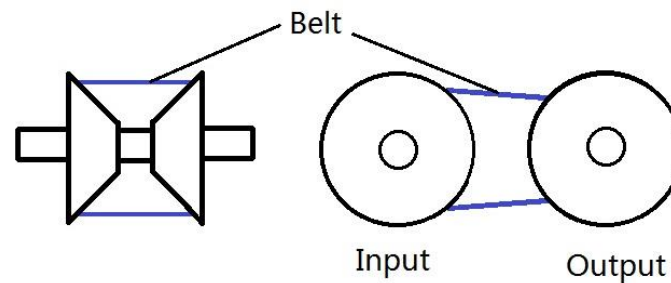


Figure 5.1: Diagram of a belt–pulley CVT system

In addition to the CVT, a direction control mechanism is required in a transmission system to change the direction of motion of the output of a CVT. An example of a direction control mechanism is shown in Fig. 5.2. The internal gear A and pinion B are connected concentrically, and are driven by the one-way input. The pinion C is connected concentrically, and are driven by the one-way input. The pinion C is controlled by an actuator to engage with either the internal gear A or the pinion B. Hence, the direction of rotation of the pinion C can be changed accordingly. The use of a direction control mechanism allows the transmission system's output to have a controllable direction and speed. However, this additional mechanism not only increases the complexity of the device, but also its size and weight. Besides, an additional actuator is needed. Therefore, to be suitable for a wearable device, the transmission system must incorporate both direction control and speed control with a minimal number of components.

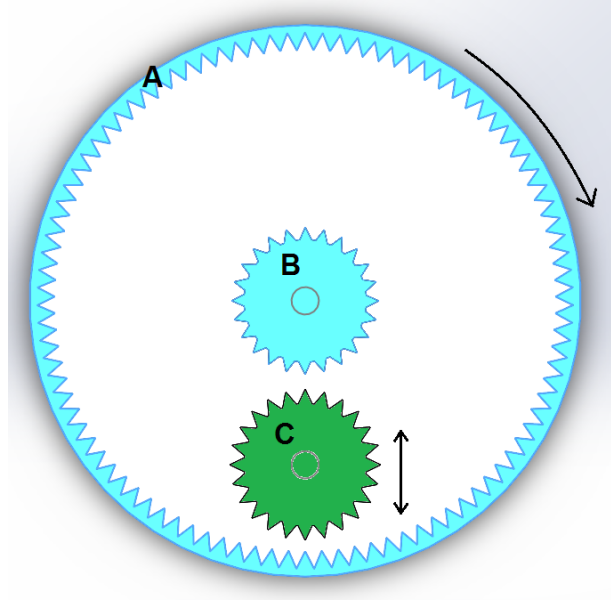


Figure 5.2: Diagram of a direction control mechanism. A is an internal gear, B and C are pinion gears. The black arrows represent the direction of motion.

A frictional variable speed drive (FVSD) is a CVT system that transmits speed from one side to another using contact friction. A simple example of FVSD [93] is shown in Fig 5.3. The driving plate rotates at a constant speed ω_{in} , while the speed of the driven plate varies with its relative position to the centre of rotation of the driving plate. The gear ratio is given as follows:

$$u = \frac{r_{out}}{r_{in}} \quad (5.1)$$

The disadvantage of this system, similar to the belt–pulley CVT system, is that it requires high friction in order to transmit enough force from one side to the other, but at the same time, it must have low friction for the driven plate to slide smoothly along the surface of the driving plate. The advantage is that the direction of rotation can be switched simply by sliding the driven plate from one side of the driving plate to the other. In comparison with the belt–pulley CVT system, this design has significantly reduced complexity, size and weight.

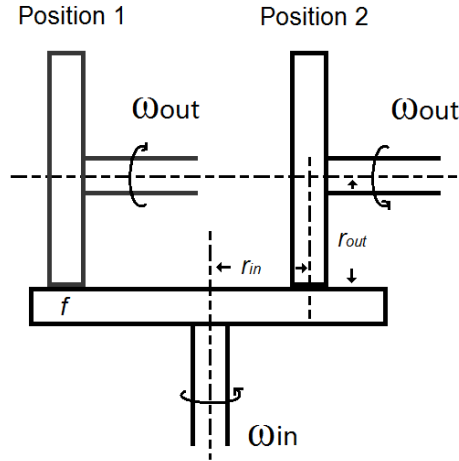


Figure 5.3: Diagram of a frictional variable speed drive. f is the friction coefficient of the materials of two plates. r_{in} is the distance between the driven plate and the rotation axis of the driving plate; r_{out} is the radius of the driven plate.

As mentioned above, the friction issue of the FVSD makes it difficult to use in a wearable device because a high power steering actuator is required to slide the driven plate. In order to design a power efficient MMS, the design of the Cobot was considered for generating a new concept [94–96]. A diagram of the Cobot's CVT is shown in Fig. 5.4. The Cobot's CVT includes two driven rollers, one steering/driving roller, two following rollers and one sphere. All rollers are pressed against the sphere in order to provide continuous transmission. The two driven rollers are placed perpendicular to each other. The output velocities are controlled by the steering angle and driving velocity.

The adoption of a sphere as the transmission medium reduces the static friction generated by the rotation of the steering roller, therefore, it reduces the torque requirement for the steering actuator. However, a number of drawbacks are identified, as follows:

- The speed range of a driven roller corresponds to the range of the steering angle (0–180°). This large range of rotation significantly increases the response time of the CVT.
- The output velocities of the driven rollers are coupled.
- The size is too bulky to allow for a network with multiple independent outputs.

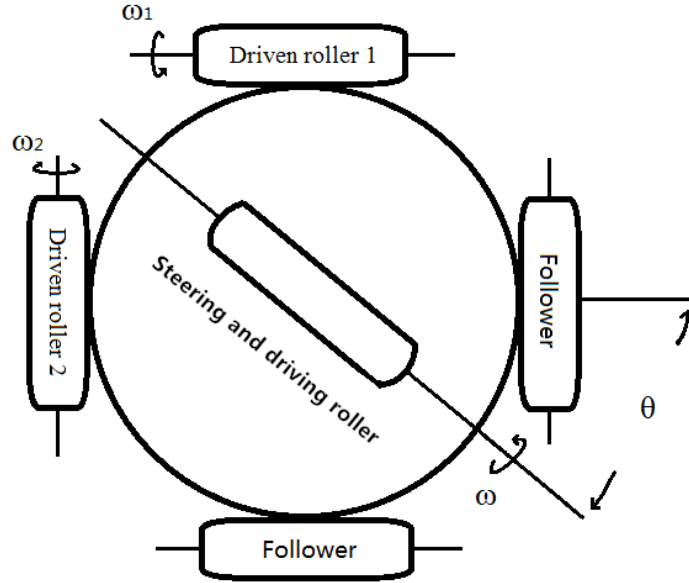


Figure 5.4: Diagram of the Cobot's CVT model. The transmission ratio from the driving roller to the 1st and 2nd driven rollers are defined as $\omega_1/\omega = \cos(\theta)$ and $\omega_2/\omega = \sin(\theta)$, where θ is the steering angle. In the drawing, ω , ω_1 and ω_2 are the angular velocities of the rollers.

Based on the advantages and drawbacks of the Cobot's CVT and FVSD, the first-generation MMS was developed. The detailed design is given in the following section.

5.2 Concept Generation

The purpose of a MMS is to couple a single input power source to multiple output applications. It also allows each output to operate with a required direction of motion, velocity and torque. The signal flow between the power source and the output is shown in Fig. 5.5. The power source supports the unit with a stable speed and torque, while the speed control unit and the direction control unit change the transmission ratio (γ) and direction of motion (σ) according to the control signal.

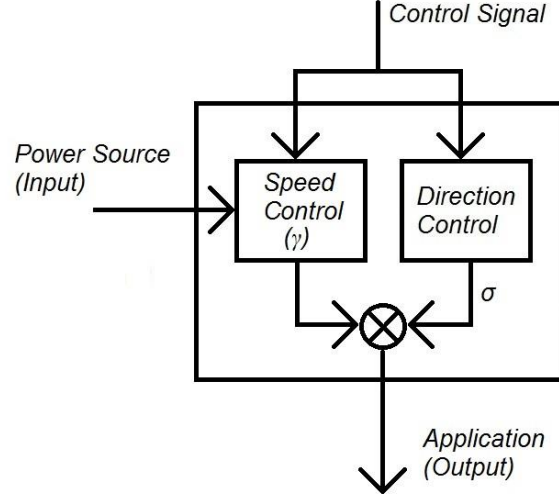


Figure 5.5: Signal flow between the power source and the output.

Denoting the input speed and torque as w_{in} and τ_{in} respectively, the output speed (w_{out}) and torque (τ_{out}) are given as follows:

$$\begin{aligned} w_{out} &= \sigma \cdot \eta \cdot \gamma \cdot w_{in} \\ \tau_{out} &= \sigma \cdot \xi \cdot \tau_{in} / \gamma, \end{aligned} \quad (5.2)$$

where η and ξ are the efficiency coefficients of the CVT for velocity and torque transmission, γ is the transmission ratio, and σ is a sign function:

$$\sigma = \begin{cases} +1 & x > 0 \\ 0 & x = 0 \\ -1 & x < 0 \end{cases}, \quad (5.3)$$

where $x > 0$ means that the output and input motions have the same direction, $x < 0$ means that the output and input motions have opposite directions, and $x = 0$ means that the output speed is zero.

Since the control signal of the MMS is separate from the input, the MMS can be used as a unit in either a serial network (Fig. 5.6) or in a parallel network (Fig. 5.7).

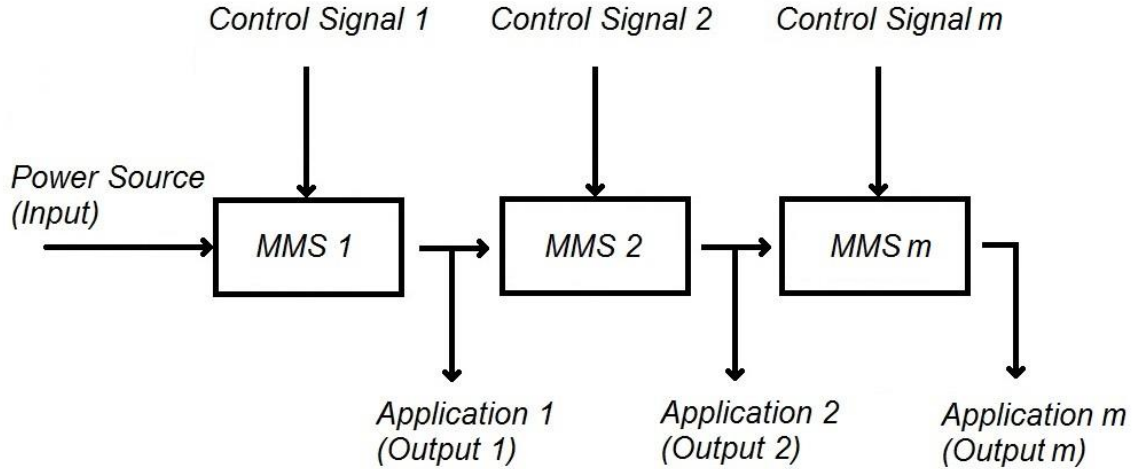


Figure 5.6: Signal flow of a total of n MMS units in a serial network.

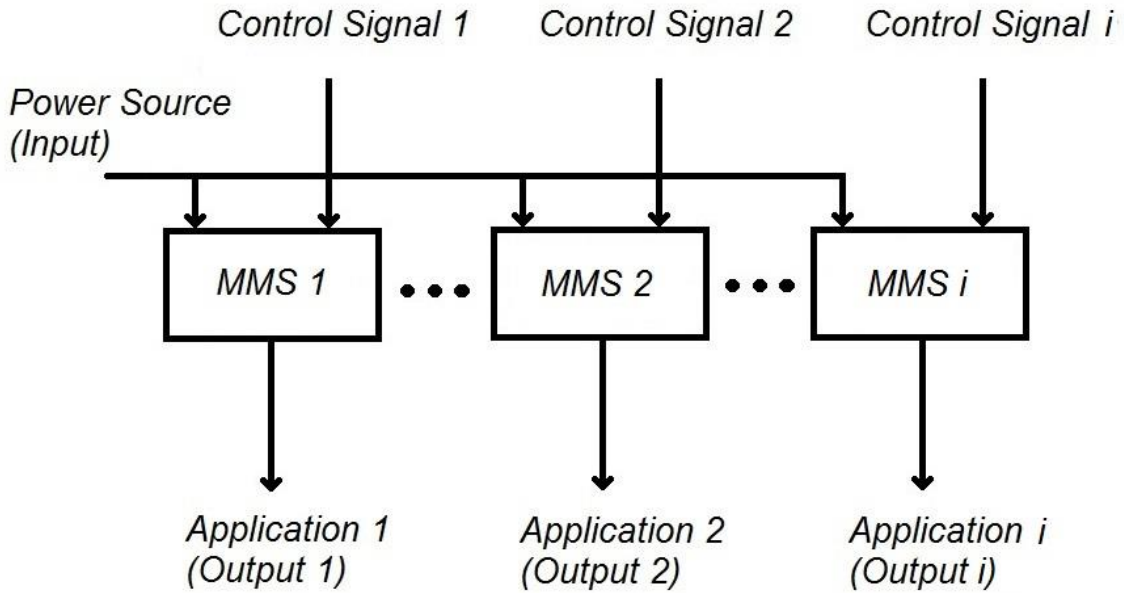


Figure 5.7: Signal flow of a total of n MMS units in a parallel network

In the serial configuration, each MMS unit transmits power from the previous unit to the next. Based on the application requirements, the output speed and torque of each unit can be controlled by the user's control command. Suppose the transmission ratio, speed efficiency and torque efficiency of the i^{th} MMS are γ_i , η_i and ξ_i respectively. The direction sign function of each unit is denoted as σ_i . Therefore, the output speed and torque of the last unit (m^{th}) are given as follows,

$$\begin{aligned}
w_m &= w_{in} \cdot \prod_{i=1}^m (\sigma_i \cdot \eta_i \cdot \gamma_i) \\
\tau_m &= \tau_{in} \cdot \prod_{i=1}^m (\sigma_i \cdot \xi_i / \gamma_i)
\end{aligned} \tag{5.4}$$

With this configuration, the output velocity of the m^{th} unit can be promptly reduced/raised to any value compared with a single MMS unit. Besides, it offers a wider range of transmission ratios. This feature is achieved by linking the input and the output through a series of MMS. Hence, the output of each MMS is highly dependent on the others. By changing the transmission ratio of each MMS at the same time, the output velocity of the terminal MMS can be changed rapidly.

In the parallel configuration, each MMS unit shares the same power source, while controlled separately by different control signals. Supposing that the impact of the internal power consumption of all MMS on the power source can be neglected and the power source can provide sufficient power for all units, then the output speed and torque of the i^{th} unit can be given as follows:

$$\begin{aligned}
w_i &= w_{in} \cdot \sigma_i \cdot \xi_i \cdot \gamma_i \\
\tau_i &= \tau_{in} \cdot \sigma_i \cdot \xi_i / \gamma_i
\end{aligned} \tag{5.5}$$

With this configuration, all outputs are independent of each other. This feature allows the use of one power source to supply different applications. Moreover, each MMS unit can be customized according to different application requirements. The flexibility of this configuration is much higher than the serial configuration. However, this configuration requires a longer time to achieve the target speed in comparison with the serial configuration. The simultaneous responses of multiple MMSs in the serial configuration result in an exponential change to the total transmission ratio. Therefore, the parallel configuration has a slower response compared to the serial configuration.

Based on the proposed concept of the MMS, the design process is described in the following sections.

5.3 Design Specifications

The goal of this work was to design and develop a MMS that can be used in a wearable tremor suppression glove. A schematic of the concept of the wearable tremor suppression glove is shown in Fig. 5.8. It consists of a sensing glove and an actuation box. These two sections are connected through non-stretchable cables. The sensing glove contains IMUs, tubes that guide the cables and insertion points for all cables to transfer force from the actuation box to the hand. The core component of the actuation box is the MMS.

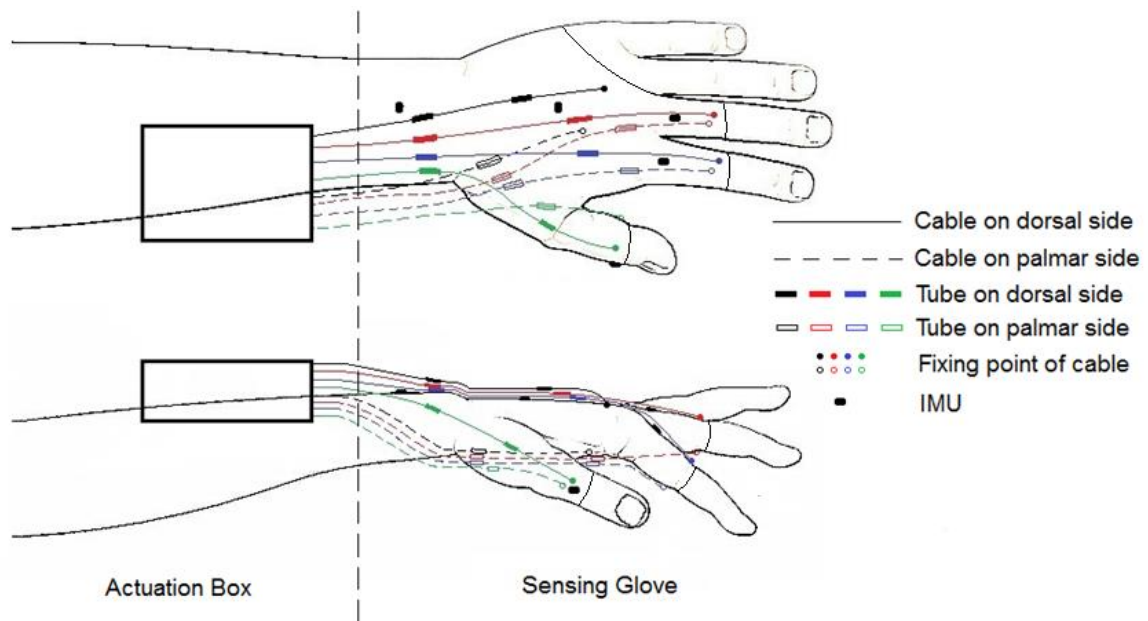


Figure 5.8: Schematic of a hand tremor suppression glove. The actuation box section and the sensing glove section are separated by the dashed line.

The MMS should have the following functions:

- 1) It can suppress the tremor movement while allowing the voluntary movement to occur,
- 2) Its size and weight can be scaled according to different applications. The weight of the MMS should be less than 100 g in order to be suitable for use in a tremor suppression device.
- 3) It can generate at least 0.2 Nm torque, which is the wrist flexion/extension torque generated by tremor [97]

4) The efficiency of the MMS should be close to 60% (as compared with a motor–gearhead combination with an efficiency of 60–70%).

A detailed discussion of the design of MMS is presented below.

5.4 First-Generation MMS

5.4.1 MMS Conceptual Model

The conceptual model of the first-generation MMS and a schematic of its operation are shown in Fig. 5.9. It incorporates a universal joint, which links a hemispherical disc and a power source. A cylinder (output shaft) is held against the disc so that the power can be transmitted to the cylinder. The position of the cylinder is a control variable that determines the transmission ratio. The hemispherical disc passively pivots with the movement of the cylinder. The use of the universal joint allows the disc to pivot in the same plane as the axis of the output shaft, while transmitting rotational movement. The transmission ratio, which depends on the operating radius of the disc, is given as follows:

$$u = \eta \cdot \frac{r_{\text{out}}}{r_{\text{in}}} = \eta \cdot \frac{r_{\text{out}}}{R \cdot \sin \frac{p}{R}} \quad (5.6)$$

$$r_{\text{in.max}} = R \cdot \sin(\varphi_{\text{max}})$$

where r_{in} is the distance between the contact point and the rotation axis of the hemispherical disc, r_{out} is the radius of the output shaft, R is the radius of the hemispherical disc, η is the efficiency coefficient, p is the surface distance from the centre of the disc to the contact point of the output shaft and the hemispherical disc, $r_{\text{in.max}}$ is the maximal operating radius for r_{in} , and φ_{max} is the maximal operating angle of the universal joint.

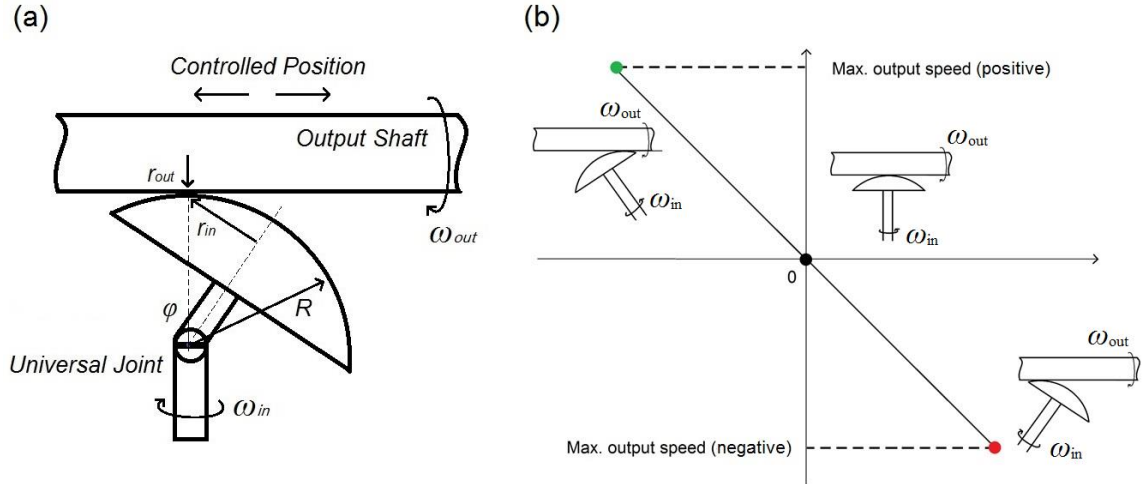


Figure 5.9: (a) Conceptual model of the first-generation MMS. R represents the radius of the hemispherical disc. r_{in} represents the distance between the contacting point and the rotation axis of the hemispherical disc. r_{out} is the radius of the output shaft. ω_{in} and ω_{out} represent the input speed and output speed respectively. φ represents the pivot angle. (b) Relation of the pivot angle of the hemispherical disc with the output shaft speed.

In comparison with the Cobot's CVT system, this first-generation MMS has a much lower contact friction between the input medium and the output medium because the static friction is converted to rolling friction by the pivoting motion of the disc. No additional transmission medium is required in this design. Furthermore, the size of the MMS can be scaled without affecting the transmission ratio.

5.4.2 MMS CAD Model

Based on the conceptual model introduced above, a CAD model was created (Fig. 5.10). The rotational motion of the output shaft (#3) is transmitted through the surface of the hemispherical disc (#16) while the translational motion is permitted by two sets of ball bearing carriages and rail guides (#13 and #15) mounted on the inside platforms of the output shaft. Two shaft collars (#1 and #12) are used to hold the rail guide support (#14) in position, therefore, allowing only the output shaft to move along the steel shaft (#11). A universal joint (#6) is used to transmit power from the power source (#10, a DC motor) to the hemispherical disc, while allowing the disc to pivot with the movement of the

output shaft. The specifications of the components used in Fig. 5.10 are given in Table 5.1.

In some cases, the application requires the MMS to have a high stall torque, i.e., the output shaft approaches the centre of the hemispherical disc. In order to provide a sufficient amount of torque when the output speed reduces to zero, a series of grooved sections were added along the mid-line of the output shaft (Fig. 5.10 #3). As the output shaft approaches the centre of the disc, a pin–spring combination (#4 and #5), which is assembled inside of the hemispherical disc, locates within one of the grooved sections preventing the output shaft from rotating further.

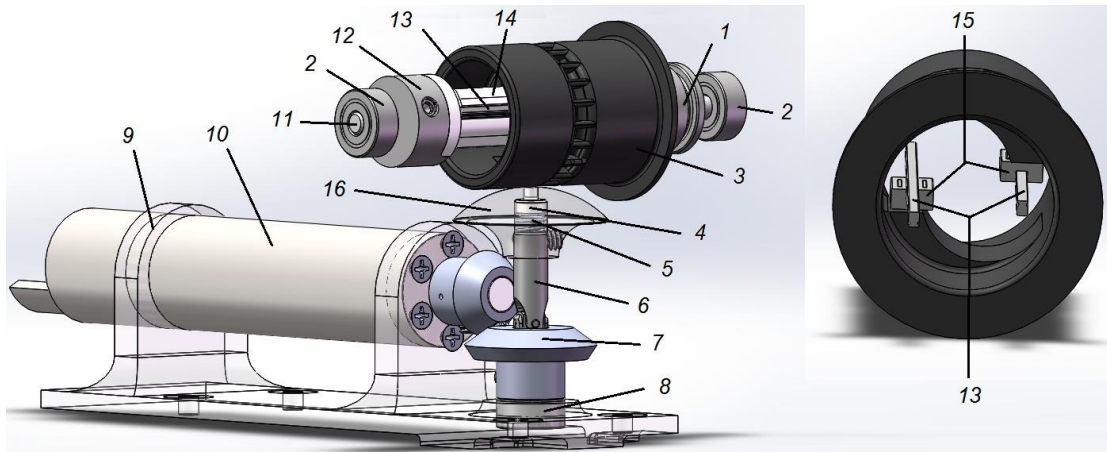


Figure 5.10: The CAD model of the first-generation MMS. 1 and 12. shaft collar, 2 and 8. ball bearings, 3. output shaft, 4. holding pin, 5. compression spring, 6. universal joint, 7. bevel gear set, 9. supporting base, 10. brushless DC motor (BLDC), 11. Steel shaft, 13. linear rail guide, 14. rail guide support, 15. ball bearing carriage, and 16. hemispherical disc.

Table 5.1: Component specifications for the first concept.

Part No.	Part Name	Specification
1, 12	Shaft collar	OD: 10 mm, ID: 3.18 mm, Width: 9 mm, M3 set screw
2, 8	Ball bearings	OD: 9.53 mm, ID: 3.18 mm, Width: 3.97 mm, dynamic load: 64 lbs.
3	Output shaft	OD: 20mm, ID: 16 mm, flange OD: 25 mm, flange width: 1 mm, groove dimension: $2.55 \times 2 \times 1.25$ mm, inside platform: 7.1×2.84 mm
4	Holding pin	Base diameter: 4.16 mm, base height: 2 mm, pin diameter: 1.8 mm, pin length: 4 mm
5	Compression spring	OD: 4.57 mm, wire diameter: 0.46 mm, length: 3.2 mm, max. Load: 1 lbs.
6	Universal joint	OD: 4.78, bore diameter: 3.18 mm, length: 25.4 mm, max. op. Angle: 30 °, static torque: 1.792 Nm
7	Bevel gear set	Pitch diameter: 19.05 mm, face width: 4.06 mm, overall width: 10.31 mm, bore: 4.76 mm, teeth: 32/48 (pinion/gear)
11	Steel shaft	Diameter: 3.18 mm, length: 67.35 mm
13, 15	Linear rail guide with carriage	Rail width: 1 mm, rail length: 42 mm, carriage width: 4 mm, carriage length: 6.5 mm, over all height: 2.5 mm, max. dynamic load: 15 lbs.
16	Hemispherical disc	Radius R : 15 mm, Max. r_{in} : 10 mm, overall height: 10 mm

The advantages of using a linear guide rail with the carriage in this design are that it allows the translational movement of the cylinder to coexist with the rotational movement and that it is relatively lightweight. However, the contact area of the carriage is not large enough to dissipate the force applied by the cylinder, causing the parts to break when force is applied to the edge of the cylinder. A picture of a failed linear carriage is shown in Fig. 5.11.

In order to support higher forces applied by the cylinder, another design was proposed to solve this problem (Fig. 5.12). In this second design, there are four linear ball bearings (#5), and two guide shafts (#3). Two linear bearings were placed on each shaft to keep the guide shafts aligned with the steel shaft (#1). A 0.5 mm clearance between the cylinder and the steel shaft was created to reduce unwanted friction. All three shafts are press fitted into two shaft collars (#2 and #4) to transmit the rotational movement from the cylinder to the two shaft collars. This design solved the force issue from the first

version. Furthermore, the use of four bearings guaranteed that the applied force was distributed evenly on the guide shafts, hence improving the linearity of the translational movement.

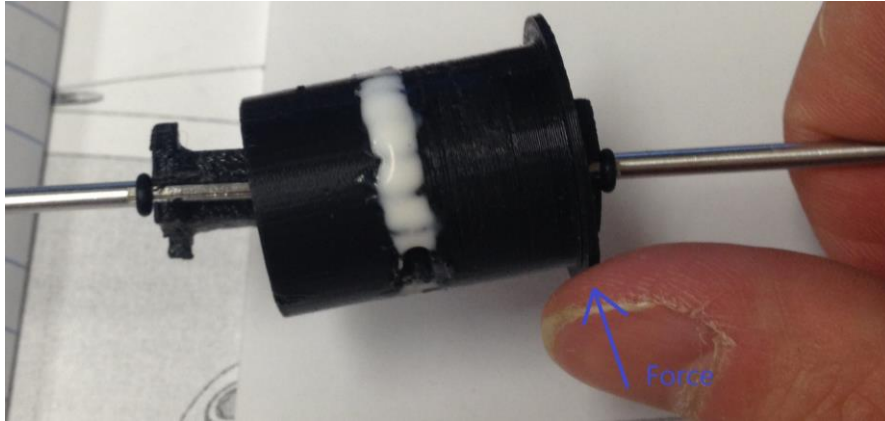


Figure 5.11: An example of a failed linear guide rail. The force was applied on one side of the cylinder causing the cylinder to lose alignment with the axis of the shaft. Hence, the failure of the linear guide rail is present due to the lack of concentricity.

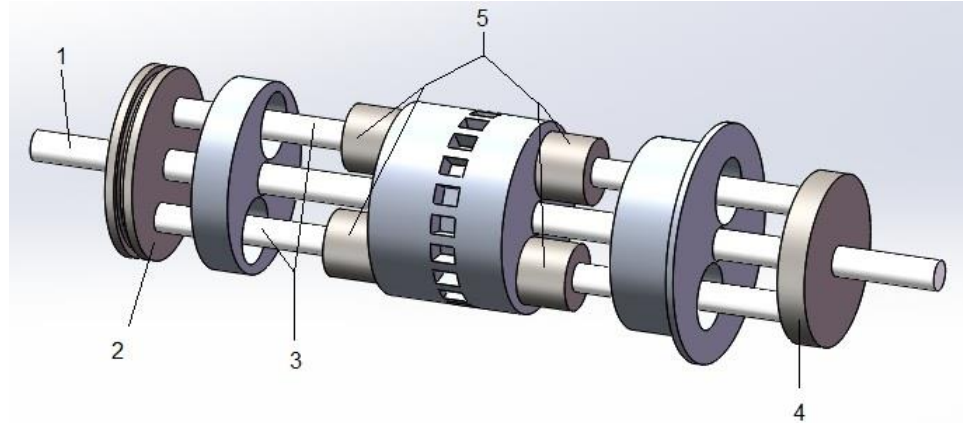


Figure 5.12: The second configuration of the frictional cylinder. 1. Steel shaft, 2. shaft collar with groove, 3. guide shaft, 4. shaft collar, and 5. linear ball bearing.

In order to control the position of the cylinder along its axis, additional actuation is required. The configuration of the linear actuation section is shown in Fig. 5.13. A miniature brushless DC (BLDC) motor (# 1) is incorporated in this section to serve as the power source. The power is transmitted to a nut (#5) through a set of bevel gears (#2) and

a lead screw (#3). The flange of the cylinder is held by two miniature bearings (#7) mounted on a carriage. With this configuration, the translational movement of the cylinder can be controlled by the motor's rotation. Since the universal joint can move in space, two stainless steel bars (#8) are fixed in parallel on both sides of the universal joint. These two bars constrain the movement of the universal joint to only one plane. The specifications of the components used in Fig. 5.13 are given in Table 5.2.

Table 5.2: Component specifications for the second concept.

Part No.	Part Name	Specification
1	Miniature BLDC motor	OD: 6 mm, length: 26.7 mm
2	Bevel gear set	OD: 10.16 mm, ID: 3.18 mm, pitch diameter: 9.53 mm, hub diameter: 8.33 mm, overall width: 7.14 mm, ratio: 1:1
3	Lead screw	Thread: 3.56 mm, length: 64.65 mm, travel distance per turn: 1.22 mm
4	Aluminum rod	Diameter: 2.38 mm, length: 49 mm
5	Wear compensating nut	Length: 12.7 mm, travel distance per turn: 1.22 mm, load capacity: 5 lbs.
6	Machine screw	Length: 4.76 mm, thread: 00-90
7	Ball bearings	OD: 3.97 mm, ID: 1.19 mm, width: 1.59 mm, dynamic load: 14 lbs.
8	Stainless steel bar	Diameter: 3.18 mm, length: 64.65 mm

The selection of the steering motor and lead screw depends on the application of the MMS. Normally, the voluntary human motion has frequencies of less than 3 Hz. In order to keep the output of the MMS following the voluntary motion while suppressing tremor motion, the frequency of movement for the cylinder should be greater than 3 Hz. The travel distance of the cylinder is 26 mm, therefore, the minimal speed for the nut is 78 mm/s, which is the product of the travel distance of the cylinder (26 mm) and the frequency of movement (3 Hz).

A lead screw is used to increase the pushing force of the nut and to convert rotary motion to linear motion. A 1.22 mm travel distance per turn lead screw was adopted; the pushing force generated by this lead screw is calculated below. With this lead screw, the minimal rotary speed for the steering motor becomes 3,836 rpm. A number of miniature motors

were compared, and eventually, a miniature BLDC motor (Maxon, EC 6 brushless DC motor, 2 watt, 41,000 rpm nominal speed, 0.49 mNm nominal torque) with 3.9:1 reduction ratio gearbox was chosen as the steering actuator. Based on this motor, the pushing force of the nut can be calculated using the equation below,

$$F = \frac{2\pi \cdot \tau \cdot \eta_l}{L} \quad (5.7)$$

where τ is the steering motor nominal torque, η_l is the efficiency, and L is the travel distance per turn of the lead screw. Choosing $\eta_l = 0.8$, the minimal pushing force is 6.93 N. In the presence of linear ball bearings, this pushing force is enough for the current configuration.

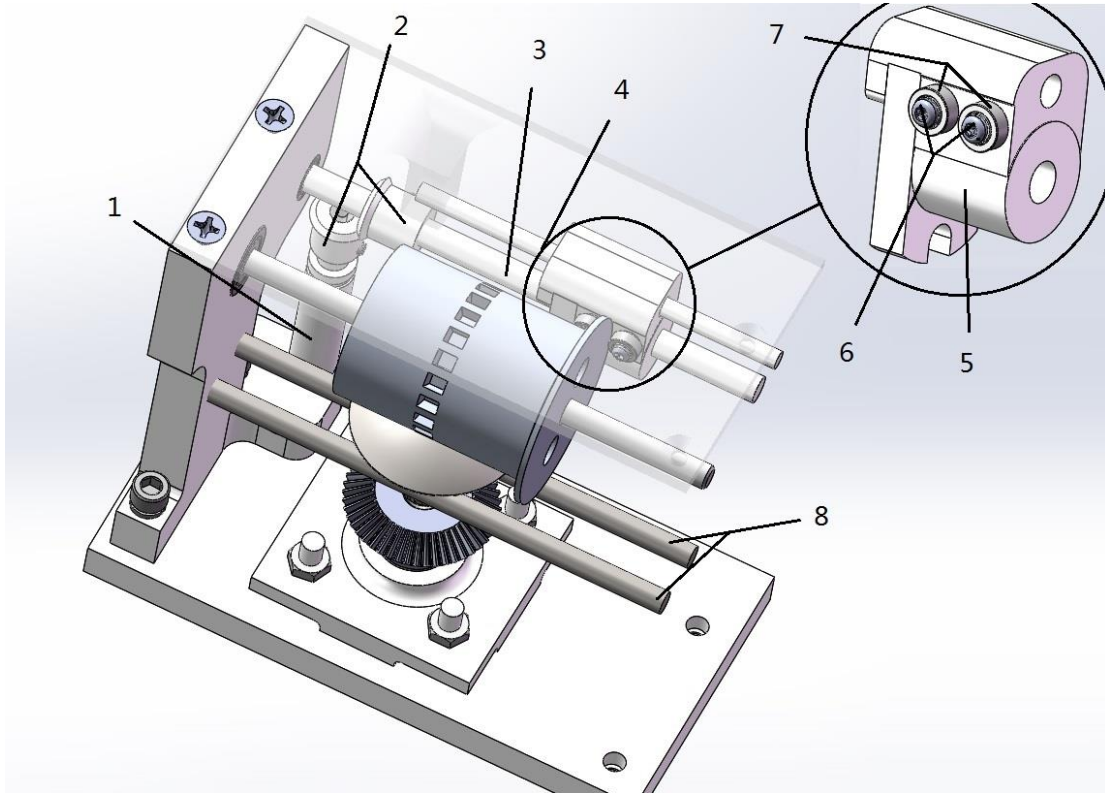


Figure 5.13: Configuration of the linear actuation. 1. Miniature BLDC motor, 2. bevel gear set, 3. lead screw, 4. aluminum rod, 5. wear compensating nut, 6. machine screw, 7. miniature ball bearings, and 8. stainless steel bars.

5.4.3 MMS Prototype

A prototype of the first version MMS is shown in the Fig. 5.14. Both the cylinder and the disc are covered with thin natural rubber to increase the friction coefficient. In theory, by changing the position of the cylinder, the output power can be changed. However, the experiment result showed that the hemispherical disc is not able to stay at a demanded angle once it starts to rotate. One possible reason is that when the disc rotates, the component force of the friction at the contacting point pushes the disc to the pivoting side. Since there is no external force applied to counterbalance this force, the disc will keep pivoting until it is stopped by the bars. Without the use of an additional mechanism, the performance is significantly affected by this drawback. In order to solve this issue, a second-generation MMS was proposed.

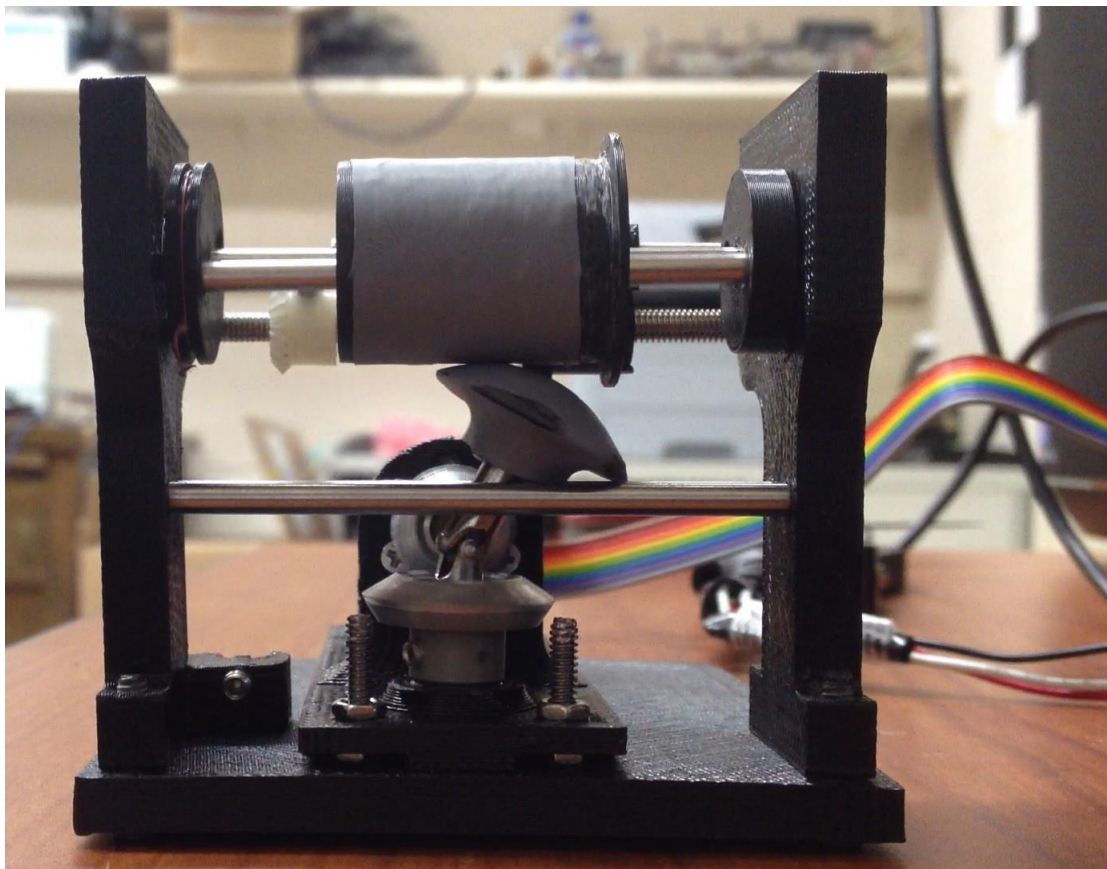


Figure 5.14: The prototype of the first version of the MMS.

5.5 Second-Generation MMS

5.5.1 MMS Model

In the previous design, the output of the MMS is controlled by the position of the frictional cylinder. Adding more components to solve the slippage issue would lead to increased complexity and size of the MMS. In order to achieve the expected function with minimal complexity, a second version of the MMS was envisioned, and is introduced in this section.

Different from the first generation, the controlled component was changed from a cylinder to a hemispherical disc (Fig. 5.15). In this version, the hemispherical disc (#12), a ball bearing (#4) and a disc support (#13) are connected through a steel shaft (#14). There are two ball bearings placed on each side of the disc support, allowing the hemispherical disc to pivot along the major axis of the disc support.

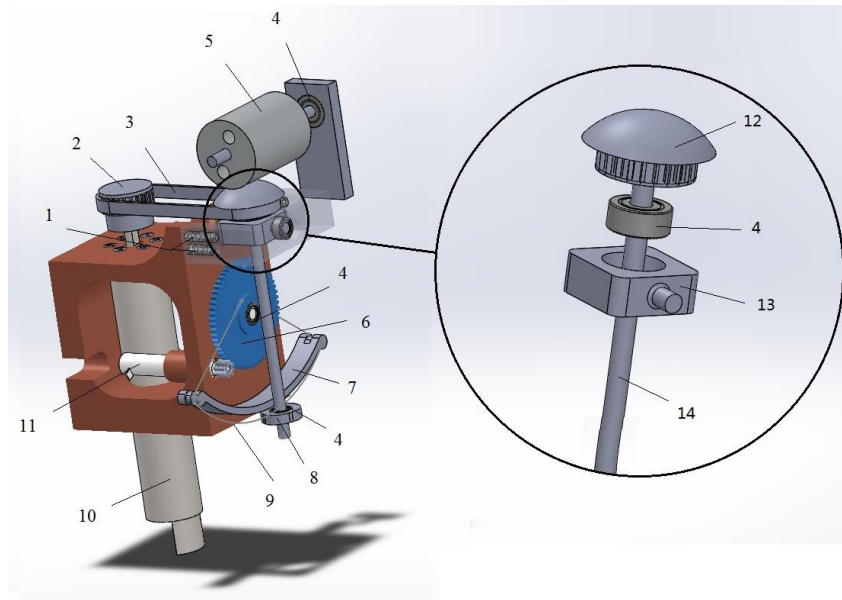


Figure 5.15: Configuration of the second-generation MMS. 1. Machine screw, 2. pulley, 3. timing belt, 4. ball bearings, 5. frictional cylinder with embedded linear bearings, 6. gear set, 7. arc guide rail, 8. shaft carriage, 9. nonstretchable cable, 10. BLDC motor, 11. miniature BLDC motor, 12. hemispherical frictional disc, 13. Disc support, and 14. steel shaft.

A gear–spool–cable mechanism is used to control the pivot angle of the hemispherical disc (Fig. 5.16). There are two circular grooves that function as a spool on either side of the larger gear. A nonstretchable cable (#4) is wound on the spools with both ends fixed to the gear. The midpoint of the cable is fixed inside of the carriage (#3) to transmit the motion to the hemispherical disc. The angle range of the arc guide rail (#2) determines the pivot angle range of the hemispherical disc.

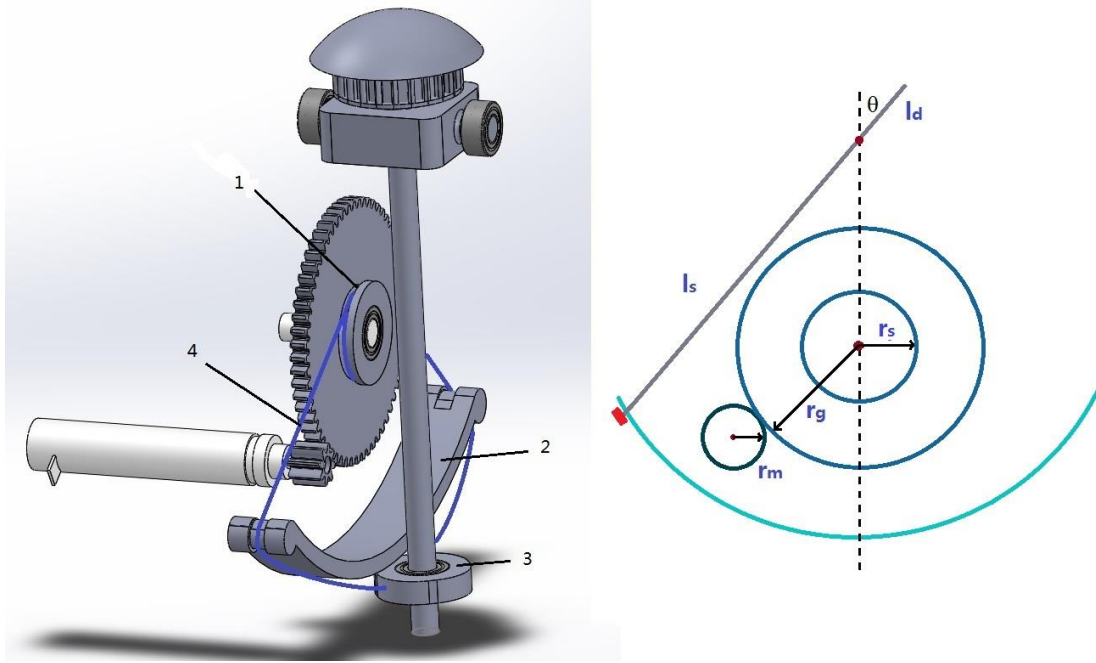


Figure 5.16: Left: Configuration of the gear–spool–cable mechanism. 1. Circular groove, 2. arc guide rail, 3. shaft carriage, 4. nonstretchable cable. Right: Diagram of the gear–spool–cable mechanism. r_m is the radius of the minimal motor gear, r_s is the radius of the spool on the bigger gear, r_g is the radius of the bigger gear, l_d is the short length of the disc shaft from the pivot centre to the surface of the hemispherical disc, l_s is the length of the disc shaft from the pivot centre to the point where the nonstretchable cable and the shaft intersect, and θ is the pivot angle.

The advantage of this design over the other frictional speed drive is the reduced friction requirement between the cylinder and the disc. Similar to the operation of steering a vehicle that requires less torque to steer when the vehicle is moving, this mechanism requires less torque to steer when the hemispherical disc is rotating. Once power is

transmitted from the power motor to the disc, only a small amount of torque is required to pivot the disc. The designs of the hemispherical disc, elongated disc shaft, the gear set and the linear bearings contribute to reducing the power requirement of the miniature BLDC motor. A diagram of the power reduction mechanism is shown in Fig. 5.16, and the reduction ratio is given below,

$$\mu = \frac{\omega_s}{\omega_m} = \frac{r_m \cdot r_s}{r_g \cdot l_s} \quad (5.8)$$

where ω_s and ω_m are the shaft pivoting speed and miniature motor rotary speed, respectively. The relationship between the pivoting angle and the small motor rotation can be defined as follows:

$$\theta = \frac{2 \cdot \pi \cdot r_s \cdot r_m}{r_g \cdot l_s} \cdot N_m \quad (5.9)$$

where N_m is the small motor rotation. The lateral pushing force generated on the disc can be defined as follows:

$$F_d = \frac{\tau_m}{\mu \cdot l_d}, \quad (5.10)$$

where τ_m is the miniature motor nominal torque. Using the same steering motor as was used for the first version of the MMS, the maximal lateral pushing force is 8.1 N. Here, $r_m = 2.5$ mm, $r_s = 5.25$ mm, $r_g = 15.5$ mm, $l_s = 53$ mm, $l_d = 13$ mm, and $\tau_m = 1.68$ mNm (with a gearbox efficiency of 0.88). This pushing force is sufficient to move the cylinder with a maximal load of 162 N (0.025 rolling friction coefficient and a 0.5 efficiency). Accordingly, the maximal speed of the cylinder is 229 mm/s. Therefore, this configuration is sufficient to be used in the tremor suppression application.

In comparison with the previous designs, another difference is the method of power transmission. Since the hemispherical disc is constantly pivoting, the transmission mechanism should be able to adapt to the relative movement between the power source (input) and the disc (output). The use of a gear set has high efficiency in a transmission

system. However, it is not ideal to use it in the MMS because an additional differential mechanism is required to eliminate the effect of the time-varying movement between the input and output of the gear set. This not only increases the complexity of the MMS, but also increases its size and weight. Therefore, in this version, a timing belt (Fig. 5.15, #3) was used as the medium to transfer power from the BLDC motor (#10) to the hemispherical disc (#12).

5.5.2 Cable Installation

The use of a nonstretchable cable provides good power transmission. In order to minimize the effect of backlash, appropriate tension was applied to the cable [98]. In order to attach the cable (Spectra® fiber with breaking strength 10 lb, diameter 0.2 mm) to the gear, two 0.8-mm diameter bores were drilled into the aluminum gear (Fig. 5.17.a). The cable was first glued onto the bore ① on the back of the gear, then wound through the shaft carriage ② (Fig. 5.17.b) in order to provide enough force to the disc shaft, and then glued to the bore ③.

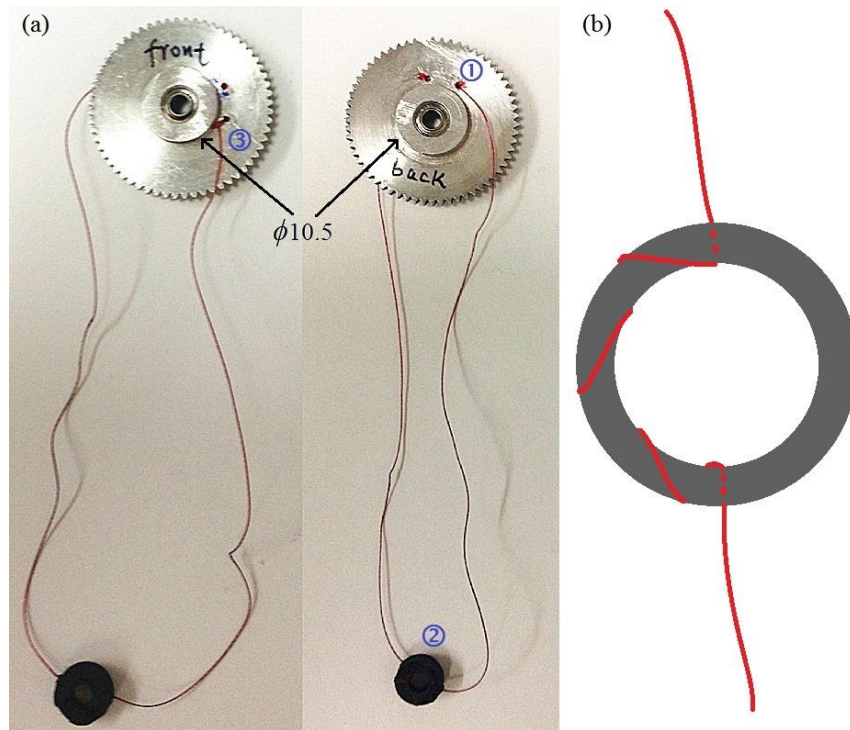


Figure 5.17: (a) Prototype of the gear-spool-cable mechanism with installation sequence. (b) Cable winding method for the shaft carriage.

With appropriate cable tension and a suitable installation method, the cable is able to provide good power transmission with no backlash. However, a small nonlinearity is caused by the height of the shaft carriage (Fig. 5.18). The nonlinearity can be modeled as follows:

$$\Delta = \frac{d'+r}{d} = \frac{\sqrt{(R+\frac{h}{2})^2 + r^2} - R^2 + r}{d} \times 100 - 100\% . \quad (5.11)$$

The height of the carriage is $h = 3.1$ mm, the radius of the carriage is $r = 4.7$ mm, the radius of the arc guide rail is $R = 49.4$ mm, the arc length between the two contacting points (green dots in Fig. 5.18) is $d = 17.2$ mm, and d' is the cable length between the contacting point (the left green dot in Fig. 5.18) and the edge of the carriage. Therefore, the nonlinearity was calculated as 4.83%.

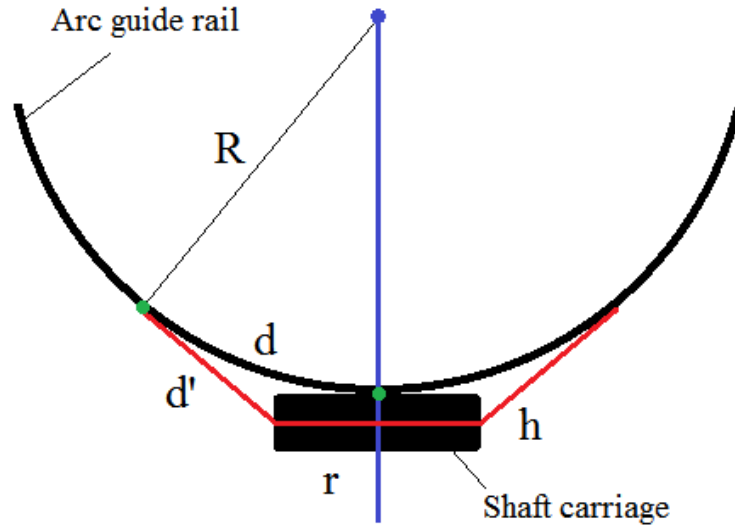


Figure 5.18: Model of the nonlinearity present in the gear–spool–cable mechanism. R represents the radius of the arc guide rail, d represents arc length between the two contacting points (green spots), d' represents the cable length between the contacting point (left) and the edge of the carriage, r represents the radius of the carriage, and h represents the height of the carriage.

5.5.3 Power Motor Selection

The DRIFT project measured the torque value of pathological tremor from a total of 33 patients [97]. The reported wrist flexion/extension torque is 0.2 Nm. Even though the research team did not clarify whether this value belongs to the Parkinsonian tremor or other kinds of tremor, it provides a reference for the selection of the power motor for the MMS.

Voluntary human motion is 3 Hz, and the angular range of motion for the index finger is from -30 °to +90 °[99] for flexion and extension and -71 °to 73 °[100] for adduction and abduction. Therefore, the minimal speed requirement for the power motor can be calculated as follows:

$$\omega_{\min} = \text{MAX} \left[d \left(A_v \cdot \sin(2\pi ft) + \psi \right) / dt \right], \quad (5.12)$$

where $A_v = 72^\circ$ represents the amplitude of the voluntary motion, $f = 3$ Hz represents the frequency of the voluntary motion, and ψ represents the bias. The calculated minimal speed for the power motor is 226 rpm.

The minimal requirements for the power motor are therefore 0.2 Nm nominal torque and 226 rpm nominal speed. According to this requirement, a combination of a BLDC motor and a gearbox was selected, the details of which are shown in Table 5.3. The adoption of this combination guarantees a sufficient and stable power supply for a system with multiple MMS.

Table 5.3: Power motor specifications.

Part	Specification
Maxon EC 16 motor	Diameter: 16 mm, nominal speed: 39400 rpm, nominal torque: 17 mNm, stall torque: 221 mNm, weight: 58 g
Planetary gearhead GP 16	Reduction ratio: 84:1, efficiency: 73%, weight: 29 g

5.5.4 MMS Prototype

Based on the CAD model, a prototype was created as shown in Fig. 5.19. For the current project, the power motor was connected to only one MMS. The frictional cylinder was installed on a cylindrical base that can be connected to a torque sensor for experimental

evaluation. The dimensions of the MMS prototype are given in the Fig. 5.19. The total weight of the MMS is 128.7 g. This weight does not include the weight of the power motor support. The majority of the weight is from the steel support that confines the motion of the disc support to only 1 DOF. The weight can be reduced to 112.4 g if the disc support is machined using aluminum.

Apart from the weight and size, none of the tremor suppression devices reviewed in the literature have reported the cost. However, the cost of the device is an important index that influences whether the device is suitable for use in consumer products. Therefore, the detailed cost of this prototype is given in Table 5.4.

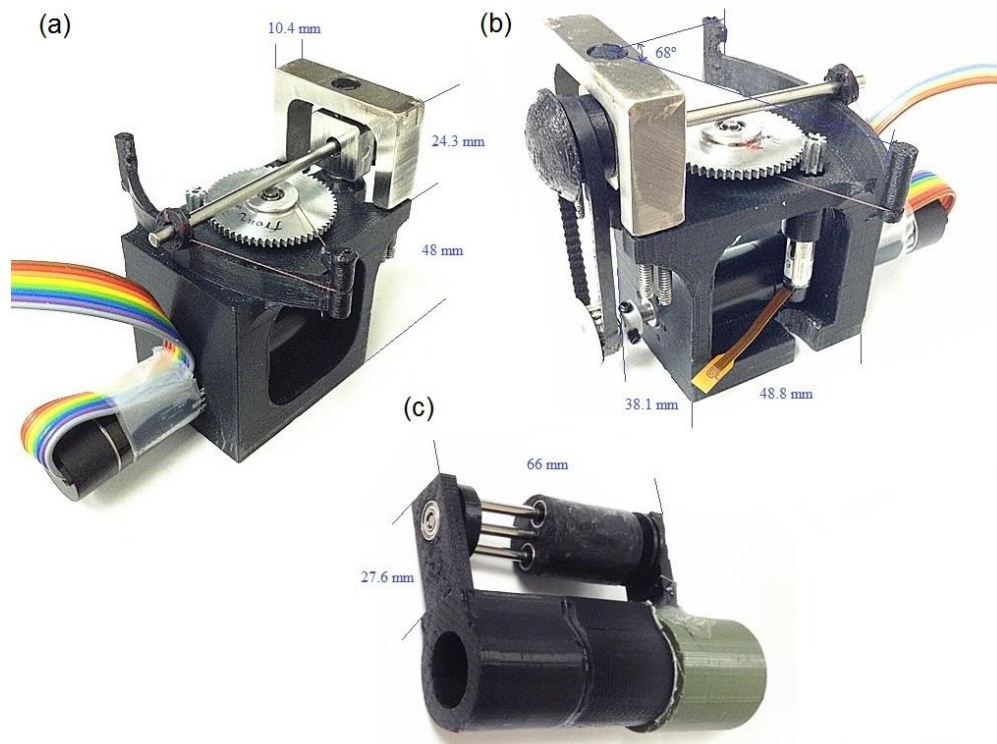


Figure 5.19: Second prototype of the MMS. (a) and (b): side views of the MMS actuation system. (c): side view of the passive cylinder, the cylinder is fixed on a base that can be connected to a torque sensor for experimental evaluation.

The total price shown Table 5.4 includes the power motor. The total price of the MMS is 1589 CAD. From the chart, we can see that the machining fee counts for a large amount of the total cost. This cost can be reduced when the MMS is produced in large quantities.

Table 5.4: Prototype cost.

Part	Cost (CAD)
	\$143
	Approx. \$13
	Material: \$13 Machining fee: \$390
	\$1030
Total	\$1589

5.6 Experimental Evaluation

5.6.1 Experimental Setup

In order to evaluate the performance of the MMS, an evaluation platform was designed (Fig. 5.20). It contains two motion controllers (EPOS 24/1 and ESCON 36/3 EC, Maxon Motors®), an incremental rotary encoder (E6C3-CWZ, OMRON®), a rotary torque sensor (FSH02056, FUTEK®), a data acquisition (DAQ) card (USB-6002, NI®), one microcontroller unit (MCU) (STC89C52RC, STC MCU®), and a power supply (BK PRECISION®). A USB–Serial adapter was used to connect the EPOS motion controller to a PC. The ESCON motion controller and the DAQ card communicate with the PC through USB directly. The motion controllers are supplied with 24 V, the torque sensor is supplied with 12 V, and the DAQ card and the MCU are supplied with 5 V.

5.6.2 Data Recording and Processing

The purpose of the DAQ card is to record the torque signal, the velocity of the miniature motor and the velocity of the cylinder, and to transfer the processed data to the PC. Since the DAQ card has only one counter, an additional MCU is introduced to calculate the cylinder's direction of rotation from the encoder's output. The direction of rotation is signaled to the DAQ card with digital 0 and 1. The DAQ's analog input one is connected to the torque sensor's output, and the analog input two is connected to the ESCON's analog output one, which exports the speed of the miniature motor.

All signals were recorded directly by a PC using LabView software (Version 2014, NI®). The sampling frequency was configured to 1 kHz. Data processing and analysis were performed offline using MATLAB software (Version R2013a, The Mathworks, Inc.). Prior to data analysis, each signal was filtered through a low-pass filter with a cutoff frequency of 30 Hz.

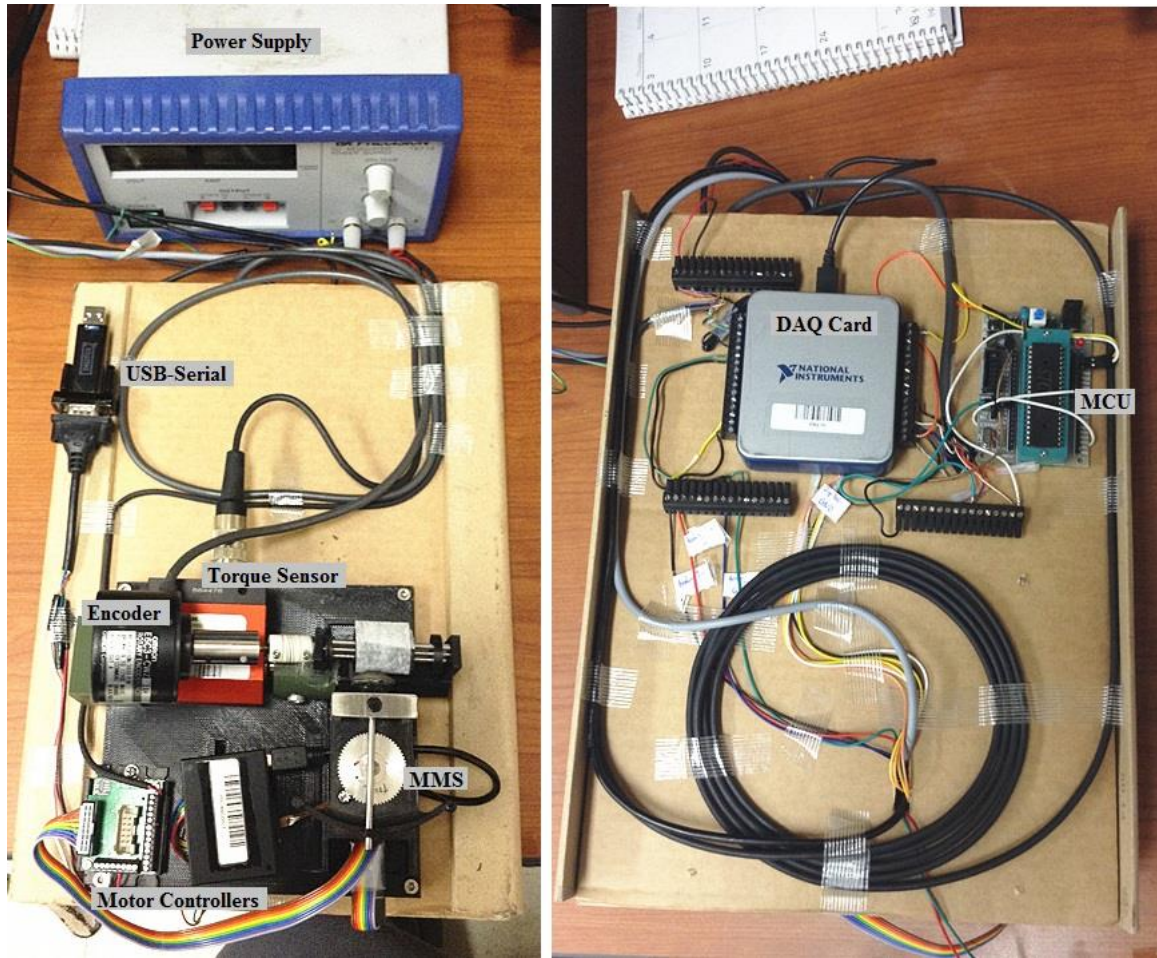


Figure 5.20: Experimental setup for MMS evaluation. Left: front view of the evaluation platform. It contains a torque sensor, an encoder, one MMS, two motion controllers and one USB–serial adapter. Right: bottom view of the evaluation platform. It contains one DAQ card and one MCU.

5.6.3 Coating Material for the Disc and Cylinder

Friction plays an important role in the MMS. In order to achieve good transmission efficiency, high friction must exist between the disc and the cylinder. It is known that the magnitude of the friction is determined by both the friction coefficient and the normal force. Considering the small size of the MMS and the materials used to manufacture its components, it is important to choose a proper coating material for the frictional disc and the cylinder. An experiment was designed to select the proper coating material for the disc and cylinder. The experimental setup includes a weight hanger and weight set which

includes 50 and 100 gram weights. The weight hanger (99.8 g) was connected to the grooved shaft collar (10 mm radius) through a nonstretchable cable. Three different materials were tested on the disc and two materials on the cylinder, consequently, 6 material combinations were tested. A total of 20 trials were performed for each material combination. The contact force was held at 11.52 N for all trials, calculated using the torque information measured from the torque sensor and considering a moment arm of 34.75 mm. The three materials tested on the disc were Ecoflex 00-30 silicone, natural rubber and a commercial mounting tape. The two materials tested on the cylinder were neoprene rubber and mounting tape.

The disc shaft was first fixed at the midpoint of the arc guide rail to guarantee the cylinder's speed remaining at zero. Weights were then mounted on the hanger until the cylinder started to rotate. The mean \pm standard deviation (SD) of the maximal applied weights for the different materials are given in Fig. 5.21.

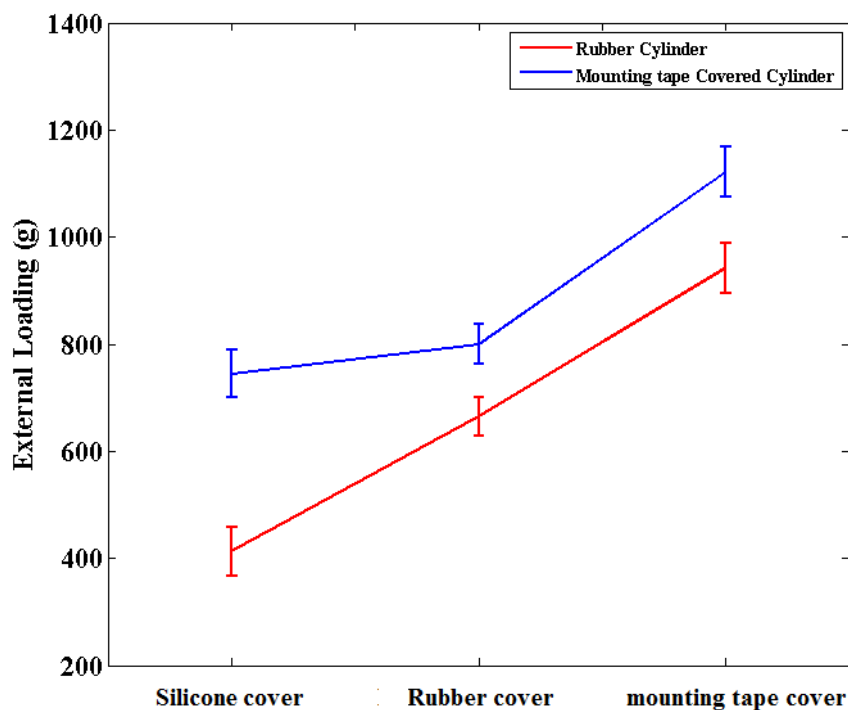


Figure 5.21: Friction comparison between different materials for the disc and the cylinder. The total trial number for each material combination was 20.

The results show that the mounting tape has the highest friction coefficient and that the silicone has the lowest. Therefore, the mounting tape was chosen as the coating material for the current study.

However, it was found during the evaluation process that the mounting tape has a few limitations that generate the need to select better materials. These limitations are listed below:

- Due to the high compliance property, the deformation of the mounting tape generates high nonlinearity at the output.
- The thickness of the mounting tape has a large impact on the effective radius of the disc.
- The friction coefficient of the mounting tape is not enough for high torque transmission.

To further increase the friction between the disc and the cylinder, the adoption of high friction material is required, for example, microfiber array based stiff polymers [101], gecko tape [102], or fibrillar interfaces [103]. In addition, compliance is another metric that must be considered when selecting a proper coating material.

5.6.4 Performance Evaluation

The results from the previous section showed that the mounting tape is the best option among the other tested materials. In this section, a number of indices of the MMS were investigated based on the chosen coating material. The performance evaluation is described in the following sequence: 1. the range of motion, 2. step response and 3. dynamic output torque of the MMS.

As shown in Fig. 5.19, the maximal angular range of the arc guide rail is 68°. Since each side of the shaft carriage is confined by the end of the arc guide rail, the actual operating range of motion for the disc shaft along the arc guide rail was measured as 62.8°. Prior to testing the output speed range of the MMS, the EPOS motion controller was used to control the speed of the power motor to 20,000 rpm. The disc shaft was initially moved

from one end of the arc guide rail to the other. The speed range of the cylinder is given in Fig. 5.22.

The bottom figure in Fig. 5.22 shows the rotation of the miniature motor in time series (three cycles are shown). The maximal rotation is 5.5 revolutions, which corresponds to 31.46° for the disc shaft. With respect to the peak value of the rotation, the cylinder speed range was calculated as $[-123 \pm 7, 122 \pm 6]$ rpm with a sample size of 10. Since the cylinder speed is proportional to the speed of the power motor at a given position, the cylinder speed of the current configuration can reach up to 241 rpm when the power motor operates at its nominal speed, which is 39,400 rpm.

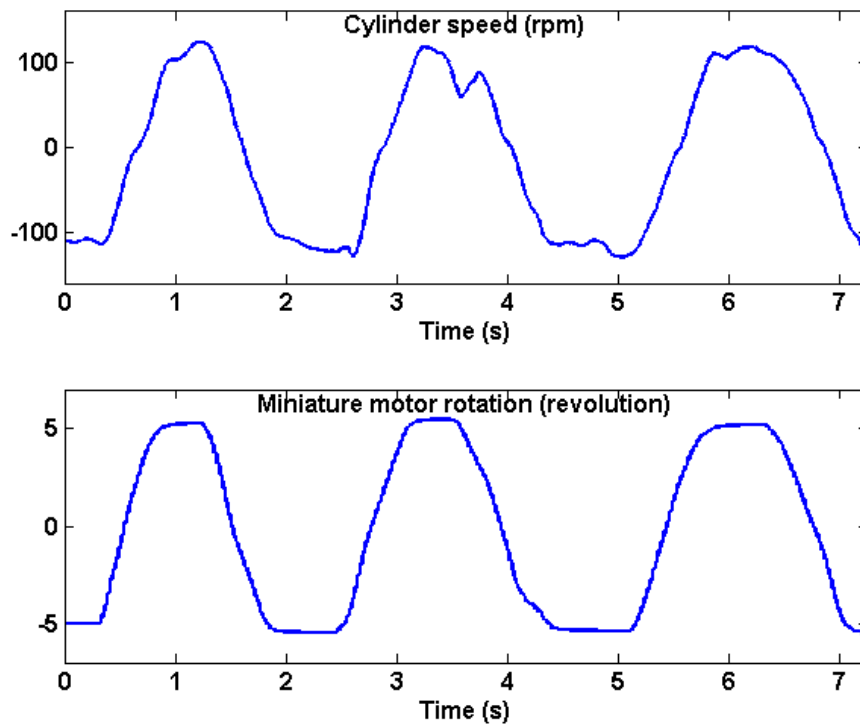


Figure 5.22: Speed of the cylinder corresponding to the rotation of the miniature motor.

It is worth noting that the cylinder speed should reach up to 238 rpm when the edge of the disc contacts the cylinder (with the power motor operating at 20,000 rpm). However, the current design only reaches 122 rpm. This is because the maximal pivot angle of the disc shaft is limited by the arc guide rail. Therefore, the effective contact radius of the disc is

only 68% of the cylinder's radius. Furthermore, the precision of the 3D printed disc and the thickness of the coating material also affect the effective contact radius. Therefore, the maximal effective transmission ratio is restricted to 0.51, i.e., the efficiency of the MMS motion transmission is 75%.

The advantage of using a smaller angular range for the arc guide rail is the reduced size of the MMS, The response time of the MMS is also shorter. However, the maximal transmission ratio is restricted because the effective radius of the disc (r_{in}) is limited to a smaller value.

In addition to the range of motion, the response time of the MMS was also tested. Since different positions of the disc shaft correspond to different cylinder speeds, a double closed loop control system was implemented to control the miniature motor, which includes both position control and speed control (Fig. 5.23).

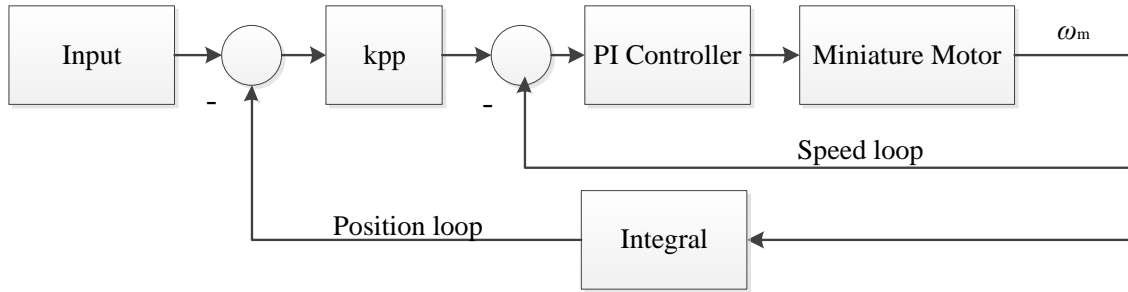


Figure 5.23: The position control flow graph for the miniature motor. ω_m is the miniature motor's speed. kpp is the velocity gain.

For the inner loop, a PI controller was used to control the speed of the motor. The position of the motor shaft is calculated as the integral of its speed. The amplitude of the step input was given as 4.69 revolutions, which corresponds to the cylinder speed of 80 rpm. The parameters used in this control system are given in Table 5.5.

Table 5.5: Parameters of the double-closed loop.

Parameter	Value
Velocity gain, k_{pp}	70
Proportional gain, k_c	0.004
Integral time, T_i	0.05
Derivative gain, I_d	0
Sampling frequency	1 kHz
Time step	1 ms

The step response of the cylinder speed, motor rotation and motor speed are shown in Fig. 5.24. The response time is measured as the time span before 95% of the actual value is reached after the input is applied. Using the current parameters, the response time of the motor rotation is 206 ms. Ideally, the cylinder speed should reach its maximum value at the same time that the miniature motor rotation reaches its maximum value. However, comparing the top figure with the middle figure in Fig. 5.24, it was found that there is a 53.3 ms time delay in the transmission, i.e., the cylinder reaches the target value 53.3 ms after the miniature motor reaches its target value. This delay may be caused by the inertia of the cylinder and the compliance of the coating materials (Fig. 5.25).

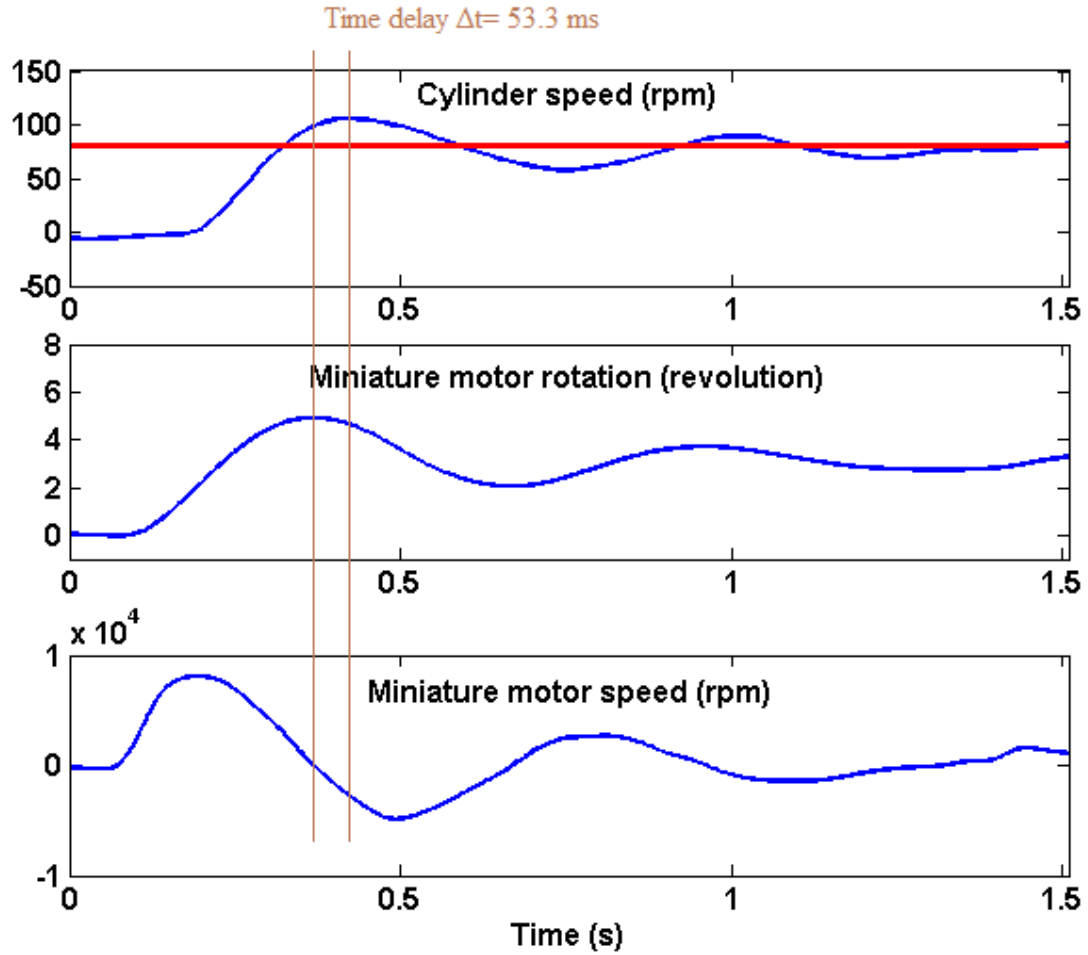


Figure 5. 24: Step response of the MMS. The input (red line) was given as 80 rpm.

Ideally, the contact area between the cylinder and the disc is merely a line. However, different coating materials have different compliance. Therefore, the resultant contact area is different. For the current configuration, mounting tape was adopted as the coating material, as described earlier. The compliance of this material is relatively high compared to the other solid materials. This generates a large contact area between the cylinder and the disc. Therefore, the existence of the time delay may be caused by the material compliance.

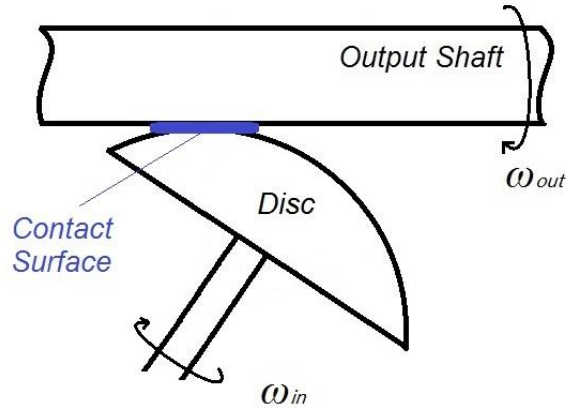


Figure 5.25: Diagram of the excessive contact surface area.

Finally, the dynamic output torque of the MMS was tested. The disc was positioned at its maximal pivot angle. A weight set hanger was connected to the grooved shaft collar through a Spectra® fiber. A 700 g weight was first added to the hanger followed by 100 g and 50 g weights until the cylinder started to slip. The contact force between the disc and cylinder was held at 12 N for all trials. A total of 20 trials were performed. The maximal lifting force of the MMS was found to be 1024.5 ± 59.6 g. The corresponding torque was 0.1 ± 0.01 Nm.

According to the specifications of the power motor, the maximal dynamic torque is 0.4 Nm. With the current configuration, the output of the MMS only reaches 25% of the dynamic torque of the power motor. One feasible solution to increasing the torque transmission efficiency is to increase the contacting force between the disc and the cylinder. However, too much force would impact the performance of the miniature motor, and it may also reduce the robustness of the MMS system. Therefore, the importance of finding a material with a high friction coefficient for the disc and cylinder is crucial to the performance of the MMS.

5.6.5 Motion Tracking

In this section, the continuous motion performance of the MMS was tested. The same position control algorithm (Fig. 5.23) was adopted for this test. The only difference was

that instead of giving a constant value to the input, a sinusoidal signal was used. The parameters of the control system are given in Table 5.6.

Table 5.6: Parameters of the double-closed loop.

Parameter	Value
Input signal frequency	2 Hz
Input signal amplitude	3 revolutions
kpp	70
kc	0.004
Ti	0.05
Id	0
Sampling frequency	1 kHz
Time step	1 ms

Fig. 5.26 shows the motion results for the cylinder and the miniature motor. With the current parameters, the maximum amplitude of the miniature motor rotation is measured as 3.27 revolutions, which corresponds to the maximum cylinder speed from the middle figure (76 rpm). The cylinder position was calculated as the integral of the cylinder speed. The corresponding maximum cylinder position amplitude was 32.1 °

Theoretically, the amplitude of the cylinder position is 43.9 ° for the demanded input amplitude (3 revolutions). However, the experimental results show that only 73.2% of the theoretical value is achieved. This result is consistent with the efficiency of the MMS motion transmission achieved in the previous section.

This section shows that the MMS is able to trace the demanded trajectory. However, due to the precision of the disc surface and the thickness of the coating material, the motion transmission efficiency of the MMS is about 75%.

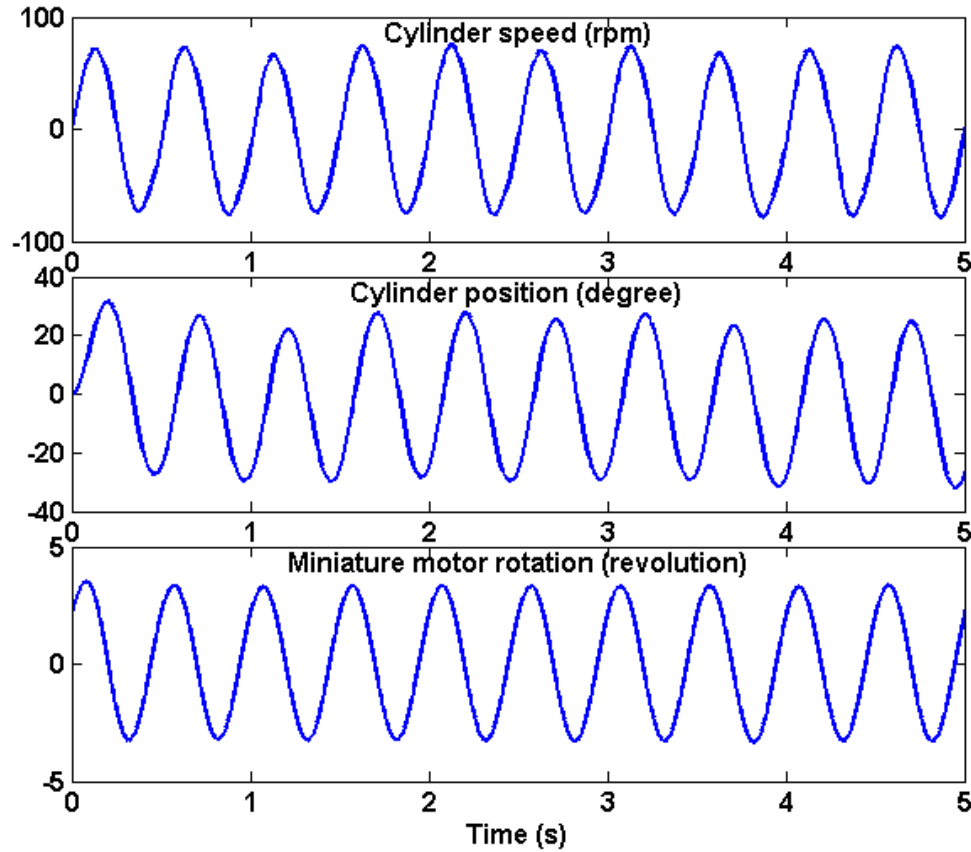


Figure 5.26: Continuous motion of the MMS.

5.7 Conclusions

A MMS was designed and a prototype was built. The total weight of the MMS is 128 g. Since the core of the MMS is a frictional drive system, the transmission ratio would remain nearly constant if the size of the MSS is scaled up or down. This feature allows the size and the weight of the MMS to be reduced in the future depending on the application.

In addition to the size and weight, another benefit of the MMS is the power consumption. The MMS is controlled by a 2 W miniature motor and the power source is a 60 W motor. The adoption of two MMS's would significantly reduce the total power consumption compared to an application that uses two 60 W motors. This feature is especially important for wearable devices because battery life is always a significant constraint.

Longer working times require a larger battery. Therefore, the weight of the device would increase by a large amount. The invention of the MMS may provide a promising solution for this issue.

There are currently two issues regarding the efficiency of the MMS. First, the motion transmission efficiency is affected by the precision of the disc and the thickness and compliance of the coating material. An imprecise disc surface increases the nonlinearity of the output, which affects the robustness of the control system. A thick material reduces the transmission ratio, and the compliance of the material prolongs the response time of the MMS. Second, the torque transmission efficiency is relatively low because the coating material used cannot provide sufficient friction.

The following chapter summarizes the current work and makes suggestions for the issues that have been identified and related future work.

Chapter 6

6 CONCLUSIONS AND FUTURE RESEARCH

The work presented in this thesis was focused on studying the nature of PD tremor and investigating tremor suppression technology for PD hand tremor. A comprehensive literature review was performed to identify the existing gap in the study of tremor and tremor suppression devices. A large amount of effort has been given to elbow and wrist tremor; however, hand tremor has not received the same amount of attention. Furthermore, there are currently no commercially available wearable tremor suppression devices for patient use.

The analysis of PD hand tremor presented in Chapter 3 provides the characteristics of PD finger tremor and wrist tremor. Based on this tremor data and the characteristics of tremor, a two-harmonics-model-based WFLC–KF tremor estimator was introduced and proven to have better performance than the estimators that use a single harmonic model.

The MMS presented herein is an alternative to the costly and heavy actuators available for use in wearable devices. It combines the concepts of CVT and differential mechanisms, and adopts the principle of a frictional drive to achieve continuous speed and direction change with minimal components. Based on the concept, a prototype was designed and tested. The experimental evaluation has shown that the MMS prototype presents good performance on motion transmission. However, limitations on the coating material affect the torque transmission. Nevertheless, the feasibility of the concept of the MMS was proven. The specific contributions of this work are detailed in the following section.

6.1 Contributions

This work studied the characteristics of PD hand tremor based on real patient data, investigated the impact of the tremor model on the tremor estimation algorithm, and described the design of a MMS for a wearable tremor suppression glove. The specific contributions of this work are given below:

- The characteristics of hand tremor from a total of 18 PD patients were analyzed. The frequencies of the 1st, 2nd and 3rd harmonics for the resting tremor of all joints lie within the range of 3.5 Hz to 5.8 Hz, 6.9 Hz to 11.5 Hz, and 10.4 Hz to 17.3 Hz, respectively. For the postural tremor, the 1st through the 3rd harmonics are within the ranges of 3.9 Hz to 7.7 Hz, 7.7 Hz to 11.2 Hz, and 11.5 Hz to 16.8 Hz, respectively.
- The results of tremor data analysis showed that a large amount of PD tremor motion consists of multiple harmonics, and the second and third harmonics are of considerable significance, therefore, they should not be neglected. These findings supplement a gap in the study of tremor.
- The effect that the number of the harmonics within a PD tremor model has on a tremor estimation algorithm was investigated. A WFLC–KF tremor estimator was tested using real tremor data. The result indicates that the use of multiple harmonics in a tremor model provides better estimation performance than using a monoharmonic tremor model. There was a 13% increase in the estimation accuracy and the correlation was increased from 0.96 to 0.99.
- Finally, a novel mechanism, i.e., an MMS, was developed for potential use in a wearable tremor suppression glove. The MMS uses a low-power miniature motor to control the transmission ratio. The size of the MMS can be scaled up and down for different applications. Furthermore, it doesn't require high power to actuate; therefore, its use for a wearable device may extend the battery life of the device.

6.2 Future Research

Although significant progress towards the development of a wearable tremor suppression glove was achieved, a significant amount of work can be foreseen. The future work regarding the development of the glove is as follows:

- *PD tremor modelling*: The widely used tremor model is developed based on a harmonic model that consists of only pure sinusoidal components. However, real tremor signals are not a combination of pure sinusoidal signals. In order to improve

the performance of tremor suppression, it is necessary to develop a more advanced PD tremor model.

- *Tremor estimation:* The current tremor estimators have satisfactory performance on estimating the tremor signal. However, issues regarding phase lag, tremor amplitude tracking and tremor frequency tracking still have a huge impact on the overall performance of the estimator. In addition, most of the estimators use a simplified tremor model as a reference. Although this approach is not computationally expensive, the accuracy of the estimator is compromised. Therefore, the importance of developing a more intelligent tremor estimator in the future work is identified.
- *Interpretation of forearm EMG signal to finger motion:* The forearm EMG signals collected from the patient trials have not been studied yet. However, the EMG-to-finger-motion map may be beneficial for a wearable tremor suppression glove, because the size of the glove can be minimized by moving the sensing system from the hand to the forearm. In addition, unlike an IMU, the orientation of the electrode does not change the output data. Therefore, the calibration process of the glove could be simpler for the user if EMG sensor is adopted.
- *Friction material for the MMS:* The torque transmission performance of the MMS is highly dependent on the coating material of the cylinder and the disc. In order to increase the efficiency of the torque transmission, an in-depth study of the friction material selection and installation is required. The material selection must consider not only the friction coefficient, but also the durability of the material to ensure predictable and robust operation.
- *Configuration of the MMS:* Although the size of the MMS can be scaled down, further configuration optimization should be conducted for the purpose of designing a lightweight and compact tremor suppression device for hand tremor. For example, the placement of the steering motor can be optimized to reduce the size of the MMS; the length of the cylinder, the height of the hemispherical disc and the length of the disc shaft can be miniaturized to reduce the size and weight of the MMS.

REFERENCES

- [1] M. A. Harris, M. Koehoorn, and K. Teschke, "Ongoing challenges to finding people with Parkinson's disease for epidemiological studies: A comparison of population-level case ascertainment methods," *Parkinsonism & Related Disorders*, vol. 17, pp. 464–469, 2011.
- [2] A. Wright Willis, B. A. Evanoff, M. Lian, S. R. Criswell, and B. A. Racette, "Geographic and ethnic variation in Parkinson disease: a population-based study of US Medicare beneficiaries," *Neuroepidemiology*, vol. 34, pp. 143–151, 2010.
- [3] G. W. Duncan, K. T. Khoo, S. Y. Coleman, C. Brayne, A. J. Yarnall, J. T. O'Brien, R. A. Barker, and D. J. Burn, "The incidence of Parkinson's disease in the North-East of England," *Age and Ageing*, vol. 43, pp. 257–263, 2014.
- [4] C. M. Peters, C. E. Gartner, P. A. Silburn, and G. D. Mellick, "Prevalence of Parkinson's disease in metropolitan and rural Queensland: a general practice survey," *Journal of Clinical Neuroscience*, vol. 13, pp. 343–348, 2006.
- [5] C. L. Ma, L. Su, J. J. Xie, J. X. Long, P. Wu, and L. Gu, "The prevalence and incidence of Parkinson's disease in China: a systematic review and meta-analysis," *Journal of Neural Transmission*, vol. 121, no. 2, pp. 123–134, 2014.
- [6] S. K. Van Den Eeden, C. M. Tanner, A. L. Bernstein, R. D. Fross, A. Leimpeter, D. A. Bloch and L. M. Nelson, "Incidence of Parkinson's disease: variation by age, gender, and race/ethnicity," *American Journal of Epidemiology*, vol. 157, pp. 1015–1022, 2003.
- [7] A. E. Spottke, M. Reuter, O. Machat, B. Bornschein, S. von Campenhausen, K. Berger, R. Koehne-Volland, J. Rieke, A. Simonow, D. Brandstaedter, U. Siebert, W. H. Oertel, G. Ulm, and R. Dodel, "Cost of illness and its predictors for Parkinson's disease in Germany," *Pharmacoeconomics*, vol. 23, pp. 817–836, 2005.
- [8] E. R. Dorsey, R. Constantinescu, J. P. Thompson, K. M. Biglan, R. G. Holloway, K. Kieburtz, F. J. Marshall, B. M. Ravina, G. Schifitto, A. Siderowf, and C. M. Tanner, "Projected number of people with Parkinson disease in the most populous nations, 2005 through 2030," *Neurology*, vol. 68, pp. 384–386, 2007.
- [9] M. Guttman, P. M. Slaughter, M. E. Theriault, D. P. DeBoer, and C. D. Naylor, "Burden of Parkinsonism: A population-based study," *Movement Disorders*, vol. 18, pp. 313–319, 2003.
- [10] K. Noyes, H. Liu, Y. Li, R. Holloway, and A. W. Dick, "Economic burden associated with Parkinson's disease on elderly Medicare beneficiaries," *Movement Disorders*, vol. 21, pp. 362–372, 2006.
- [11] A. Kaltenboeck, S. J. Johnson, M. R. Davis, H. G. Birnbaum, C. A. Carroll, M. L. Tarrant, and A. D. Siderowf, "Direct costs and survival of Medicare beneficiaries with early and advanced Parkinson's disease," *Parkinsonism & Related Disorders*, vol. 18, pp. 321–326, 2012.
- [12] S. von Campenhausen, Y. Winter, A. R. e Silva, C. Sampaio, E. Ruzicka, P. Barone, W. Poewe, A. Guekht, C. Mateus, K. P. Pfeiffer, K. Berger, J. Skoupa, K. Bötzel, S. Geiger-Gritsch, U. Siebert, M. Balzer-Geldsetzer, W. H. Oertel, R. Dodel, J. P. Reese, "Costs of illness and care in Parkinson's disease: An evaluation in six countries," *European Neuropsychopharmacology*, vol. 21, pp. 180–191, 2011.
- [13] J. Jankovic, "Parkinson's disease: clinical features and diagnosis," *Journal of Neurology, Neurosurgery & Psychiatry*, vol. 79, pp. 368–376, 2008.
- [14] J. D. Parkes, R. C. Baxter, C. D. Marsden, and J. E. Rees, "Comparative trial of benzhexol, amantadine, and levodopa in the treatment of Parkinson's disease," *Journal of Neurology, Neurosurgery & Psychiatry*, vol. 37, pp. 422–426, 1974.
- [15] A. J. Lees. "Dopamine agonists in Parkinson's disease: a look at apomorphine," *Fundamental &*

Clinical Pharmacology, vol. 7, pp. 121–128, 1993.

- [16] O. Rascol, D. J. Brooks, A. D. Korczyn, P. P. De Deyn, C. E. Clarke, and A. E. Lang, “A five-year study of the incidence of dyskinesia in patients with early Parkinson's disease who were treated with ropinirole or levodopa,” *New England Journal of Medicine*, vol. 342, 1484–1491, 2000.
- [17] A. J. Lees, L. J. Kohout, K. M. Shaw, G. M. Stern, J. D. Elsworth, M. Sandler, and M. B. H. Youdim, “Deprenyl in Parkinson's disease,” *The Lancet*, vol. 310, pp. 791–795, 1977.
- [18] K. Kieburtz, I. Shoulson, S. Fahn, M. McDermott, W. Koller, P. LeWitt, J. Nutt, M. C. Lannon, “Entacapone improves motor fluctuations in levodopa-treated Parkinson's disease patients,” *Annals of Neurology*, vol. 42, pp. 747–755, 1997.
- [19] R. J. Elble and W. C. Koller, *Tremor*. Baltimore, MD: Johns Hopkins University Press, 1990, pp. 54–89.
- [20] K. E. Lyons and R. Pahwa, “Deep brain stimulation and tremor,” *Neurotherapeutics*, vol. 5, pp. 331–338, 2008.
- [21] H. Boecker, A. J. Wills, A. Ceballos-Baumann, M. Samuel, D. G. Thomas, C. D. Marsden, and D. J. Brooks, “Stereotactic thalamotomy in tremor-dominant Parkinson's disease: An H215O PET motor activation study,” *Annals of Neurology*, vol. 41, pp. 108–111, 1997.
- [22] Y. Katayama, T. Kano, K. Kobayashi, H. Oshima, C. Fukaya, and T. Yamamoto, “Difference in surgical strategies between thalamotomy and thalamic deep brain stimulation for tremor control,” *Journal of Neurology*, vol. 252, pp. 17–22, 2005.
- [23] E. D. Flora, C. L. Perera, A. L. Cameron, and G. J. Maddern, “Deep brain stimulation for essential tremor: a systematic review,” *Movement Disorders*, vol. 25, pp. 1550–1559, 2010.
- [24] M. Rosen and B. Aldenstein, “The effect of mechanical impedance on abnormal intention tremor,” in *Proceedings of the 9th Annual Northeast Bioengineering Conference, Elmsford, NY, March, 19–20, 1981*, pp. 187–192.
- [25] M. J. Rosen, A. S. Arnold, I. J. Baiges, M. L. Aisen, and S. R. Eglowstein, “Design of a controlled-energy-dissipation orthosis (CEDO) for functional suppression of intention tremors,” *Journal of Rehabilitation Research and Development*, vol. 32, pp. 1–16, 1995.
- [26] J. Kotovsky and M. J. Rosen, “A wearable tremor-suppression orthosis,” *Journal of Rehabilitation Research and Development*, vol. 35, pp. 373–387, 1998.
- [27] R. C. Loureiro, J. M. Belda-Lois, E. R. Lima, J. L. Pons, J. J. Sanchez-Lacuesta, and W. S. Harwin, “Upper limb tremor suppression in ADL via an orthosis incorporating a controllable double viscous beam actuator,” in *IEEE 9th International Conference on Rehabilitation Robotics, Chicago, Illinois, USA, June 28–July 1, 2005*, pp. 119–122.
- [28] S. S. C. Lavu and A. Gupta, “Active vibration control of essential tremor,” in *Proceedings of the 14th National Conference on Machines and Mechanisms, Durgapur, India, December 17–18, 2009*, pp. 446–449.
- [29] S. Kazi, A. As' Arry, M. M. Zain, M. Mailah, and M. Hussein, “Experimental implementation of smart glove incorporating piezoelectric actuator for hand tremor control,” *WSEAS Transactions on Systems and Control*, vol. 5, pp. 443–453, 2010.
- [30] X. Yu, “Simulation study of tremor suppression and experiment of energy harvesting with piezoelectric materials,” Master's Thesis, University of North Texas, Denton, TX, USA, 2012.
- [31] B. Taheri, D. Case, and E. Richer, “Robust controller for tremor suppression at musculoskeletal level in human wrist,” *IEEE Transactions on Neural Systems and Rehabilitation Engineering*, vol. 22, pp. 379–388, 2014.
- [32] E. Rocon, A. F. Ruiz, and J. L. Pons, “On the use of ultrasonic motors in orthotic rehabilitation of pathologic tremor,” in *Proceedings of ACTUATOR 2004 Conference, Bremen, Germany, June 14–16, 2004*, pp. 387–390.

- [33] E. Rocon, A. F. Ruiz, J. L. Pons, J. M. Belda-Lois, and J. J. Sánchez-Lacuesta, "Rehabilitation robotics: a wearable exo-skeleton for tremor assessment and suppression," in *Proceedings of the IEEE International Conference on Robotics and Automation, Barcelona, Spain, April 18–22, 2005*, pp. 2271–2276.
- [34] E. Rocon, J. A. Gallego, J. C. Moreno, and J. L. Pons, "Wearable Robots in Rehabilitation Engineering Tremor Suppression," in *Rehabilitation Engineering*, edited by Tan Yen Kheng, INTECH Open Access Publisher, 2009. Available: <http://cdn.intechweb.org/pdfs/9316.pdf>
- [35] E. Rocon, J. M. Belda-Lois, A. F. Ruiz, M. Manto, J. C. Moreno, and J. L. Pons, "Design and validation of a rehabilitation robotic exoskeleton for tremor assessment and suppression," *IEEE Transactions on Neural Systems and Rehabilitation Engineering*, vol. 15, pp. 367–378, 2007.
- [36] N. Stone, K. Kaiser, and R. D. White, "Autotuning of a PID controller for an active vibration suppression device for the treatment of essential tremor," in *ASME 2006 International Mechanical Engineering Congress and Exposition. Chicago, Illinois, USA, November 5–10, 2006*, pp. 855–861.
- [37] T. Ando, M. Watanabe, K. Nishimoto, Y. Matsumoto, M. Seki, and M. G. Fujie, "Myoelectric-Controlled Exoskeletal Elbow Robot to Suppress Essential Tremor: Extraction of Elbow Flexion Movement Using STFTs and TDNN," *Journal of Robotics and Mechatronics*, vol. 24, pp. 141–149, 2012.
- [38] B. Taheri, "Real-Time Pathological Tremor Identification and Suppression in Human Arm via Active Orthotic Devices," Ph.D. dissertation, Southern Methodist University, Dallas, TX, USA, 2013.
- [39] G. Herrnstadt and C. Menon, "On-Off Tremor Suppression Orthosis with Electromagnetic Brake," *International Journal of Mechanical Engineering and Mechatronics*, vol. 1, pp. 7–24, 2013.
- [40] A. As'array, M. Z. M. Zain, M. Mailah, and M. Hussein, "Hybrid learning control for improving suppression of hand tremor," in *Proceedings of the Institution of Mechanical Engineers, Part H: Journal of Engineering in Medicine*, vol. 227, pp. 1171–1180, 2013.
- [41] M. Seki, Y. Matsumoto, H. Iijima, T. Ando, Y. Kobayashi, M. G. Fujie, and M. Nagaoka, "Development of robotic upper limb orthosis with tremor suppressibility and elbow joint movability," in *IEEE International Conference on Systems, Man, and Cybernetics, Anchorage, Alaska, USA, October 9–12, 2011*, pp. 729–735.
- [42] B. Taheri, D. Case, and E. Richer, "Theoretical development and experimental validation of an adaptive controller for tremor suppression at musculoskeletal level," in *ASME 2013 Dynamic Systems and Control Conference, Stanford, California, USA, October 21–23, 2013*, pp. V002T22A005–V002T22A012.
- [43] R. J. Elble and W. C. Koller, *Tremor*, Johns Hopkins University Press, 1990.
- [44] A. Anouti and W. C. Koller, "Tremor disorders. Diagnosis and management," *Western Journal of Medicine*, vol. 162, pp. 510–513, 1995.
- [45] G. Deuschl, P. Bain, and M. Brin, "Consensus statement of the Movement Disorder Society on tremor," *Movement Disorders*, vol. 13, pp. 2–23, 1998.
- [46] S. Morrison, G. Kerr, and P. Silburn, "Bilateral tremor relations in Parkinson's disease: Effects of mechanical coupling and medication," *Parkinsonism & Related Disorders*, vol. 14, pp. 298–308, 2008.
- [47] B. Pellegrini, L. Faes, G. Nollo, and F. Schena, "Quantifying the contribution of arm postural tremor to the outcome of goal-directed pointing task by displacement measures," *Journal of Neuroscience Methods*, vol. 139, pp. 185–193, 2004.
- [48] A. P. Bó P. Poignet, F. Widjaja, and W. T. Ang, "Online pathological tremor characterization using extended Kalman filtering," in *Proceedings of the 30th International Conference of the*

- IEEE Engineering in Medicine and Biology Society, Vancouver, BC, Canada, August 20–25, 2008*, pp. 1753–1756.
- [49] K. E. Norman, R. Edwards, and A. Beuter, “The measurement of tremor using a velocity transducer: comparison to simultaneous recordings using transducers of displacement, acceleration and muscle activity,” *Journal of Neuroscience Methods*, vol. 92, pp. 41–54, 1999.
 - [50] D. Case, B. Taheri, and E. Richer, “Design and characterization of a small-scale magnetorheological damper for tremor suppression,” *IEEE/ASME Transactions on Mechatronics*, vol. 18, pp. 96–103, 2013.
 - [51] J. L. Pons, E. Rocon, and J. A. Gallego, “A Wearable Neuroprosthesis for the Suppression of Pathological Tremor”. *IEEE Life Sciences Newsletter*, November, 2012. Available : <http://lifesciences.ieee.org/publications/newsletter/november-2012/211-a-wearable-neuroprosthesis-for-the-suppression-of-pathological-tremor>
 - [52] J. Á. Gallego, E. Rocon, J. M. Belda-Lois, and J. L. Pons, “A neuroprosthesis for tremor management through the control of muscle co-contraction,” *Journal of Neuroengineering and Rehabilitation*, vol. 10, pp. 36–47, 2013.
 - [53] L. P. Maneski, N. Jorgovanović, V. Ilić, S. Došen, T. Keller, M. B. Popović, and D. B. Popović, “Electrical stimulation for the suppression of pathological tremor,” *Medical & Biological Engineering & Computing*, vol. 49, pp. 1187–1193, 2011.
 - [54] A. Gupta, R. Riddell, and R. Sra, “Exoskeleton for Essential Tremor and Parkinson’s Disease,” *U.S. Patent No. 20,150,272,807*. Washington, DC: U.S. Patent and Trademark Office, 2015.
 - [55] D. Zhang and W. T. Ang, (2007, August). “Reciprocal EMG controlled FES for pathological tremor suppression of forearm,” in *proceedings of the 29th Annual International Conference of the IEEE Engineering in Medicine and Biology Society, Lyon, France, August 23–26, 2007*, pp. 4810–4813.
 - [56] F. Widjaja, C. Y. Shee, D. Zhang, W. T. Ang, P. Poignet, A. Bo, and D. Guiraud, “Current progress on pathological tremor modeling and active compensation using functional electrical stimulation,” in *ISG’08: The 6th Conference of the International Society for Gerontechnology, Tuscany, Italy, June 4–6, 2008*, pp. 1–6.
 - [57] A. P. L. B. P. Poignet, D. Zhang, and W. T. Ang, “FES-controlled co-contraction strategies for pathological tremor compensation,” in *IEEE/RSJ International Conference on Intelligent Robots and Systems, St. Louis, Missouri, USA, October 11–15, 2009*. pp. 1633–1638, 2009.
 - [58] D. Zhang, P. Poignet, F. Widjaja, and W. T. Ang, “Neural oscillator based control for pathological tremor suppression via functional electrical stimulation,” *Control Engineering Practice*, vol. 19, pp. 74–88, 2011.
 - [59] A. Prochazka, J. Elek, and M. Javidan, “Attenuation of pathological tremors by functional electrical stimulation I: Method,” *Annals of Biomedical Engineering*, vol. 20, pp. 205–224, 1992.
 - [60] S. Dosen, S. Muceli, J. L. Dideriksen, J. P. Romero, E. Rocon, J. F. Pons, and D. Farina, “Online Tremor Suppression Using Electromyography and Low Level Electrical Stimulation,” *IEEE Transactions on Neural Systems and Rehabilitation Engineering*, vol. 23, pp. 385–395, 2015.
 - [61] C. L. Lynch and M. R. Popovic, “Functional electrical stimulation,” *IEEE Transactions on Control Systems*, vol. 28, pp. 40–50, 2008.
 - [62] S. Tzu, “*The Illustrated Art of War*,” Mineola, New York: Dover Publications, Inc., 2012.
 - [63] P. O. Riley and M. J. Rosen, “Evaluating manual control devices for those with tremor disability,” *Journal of Rehabilitation Research and Development*, vol. 24, pp. 99–110, 1987.
 - [64] J. G. González, J. G. González, and J. C. Cavanaugh, “A new approach to suppressing abnormal tremor through signal equalization,” in *Proceedings of RESNA Annual Conference, Vancouver, BC, Canada, June 9–14, 1995*, pp. 707–709.

- [65] B. Widrow and S. D. Stearns, "Adaptive signal processing," *Englewood Cliffs, NJ: Prentice-Hall, Inc.*, 1985.
- [66] C. A. Vaz and N. V. Thakor, "Adaptive Fourier estimation of time-varying evoked potentials", *IEEE Transactions on Biomedical Engineering*, vol. 36, pp. 448–455, 1989.
- [67] C. Vaz, X. Kong, and N. Thakor, "An adaptive estimation of periodic signals using a Fourier linear combiner," *IEEE Transactions on Signal Processing*, vol. 42, pp. 1–10, 1994.
- [68] C. N. Riviere, R. S. Rader, and N. V. Thakor, "Adaptive cancelling of physiological tremor for improved precision in microsurgery," *IEEE Transactions on Biomedical Engineering*, vol. 45, pp. 839–846, 1998.
- [69] S. Kim and J. McNames, "Tracking tremor frequency in spike trains using the extended Kalman filter," in *27th Annual International Conference of the Engineering in Medicine and Biology Society, Shanghai, China, September 1–4, 2005*, pp. 7576–7579.
- [70] F. Widjaja, C. Y. Shee, W. T. Latt, W. L. Au, P. Poignet, and W. T. Ang, "Kalman filtering of accelerometer and electromyography (EMG) data in pathological tremor sensing system," in *Proceedings of IEEE International Conference on Robotics and Automation, Pasadena, California, USA, May 19–23, 2008*, pp. 3250–3255.
- [71] A. P. L. Bo, P. Poignet, and C. Geny, "Pathological tremor and voluntary motion modeling and online estimation for active compensation," *IEEE Transactions on Neural Systems and Rehabilitation Engineering*, vol. 19, pp. 177–185, 2011.
- [72] B. C. Becker, R. MacLachlan, and C. N. Riviere, "State estimation and feedforward tremor suppression for a handheld micromanipulator with a Kalman filter," in *2011 IEEE/RSJ International Conference on Intelligent Robots and Systems, San Francisco, California, September, 25–30, 2011*, pp. 5160–5165.
- [73] J. Timmer, S. Häfner, M. Lauk, and C. H. Lücking, "Pathological tremors: Deterministic chaos or nonlinear stochastic oscillators?" *Chaos: An Interdisciplinary Journal of Nonlinear Science*, vol. 10, pp. 278–288, 2000.
- [74] J. B. Gao and W. W. Tung, "Pathological tremors as diffusional processes," *Biological Cybernetics*, vol. 86, pp. 263–270, 2002.
- [75] W. Nho, "Development and evaluation of enhanced weighted frequency Fourier linear combiner algorithm using bandwidth information in joystick operation," Ph.D. dissertation, University of Pittsburgh, Pittsburgh, PA, USA, 2006.
- [76] K. C. Veluvolu, U. X. Tan, W. T. Latt, C. Y. Shee, and W. T. Ang, "Bandlimited multiple Fourier linear combiner for real-time tremor compensation," in *29th Annual International Conference of the Engineering in Medicine and Biology Society, Lyon, France, August 23–26, 2007*, pp. 2847–2850.
- [77] STMicroelectronics, "Tilt measurement using a low-g 3-axis accelerometer", *STMicroelectronics*, Doc ID 17289 Rev 1, 2010. [Online]. Available: <http://www.st.com>.
- [78] Google. (2012, December). Android SDK [Online]. Available: <http://developer.android.com/sdk/index.html>
- [79] D. E. Vaillancourt and K. M. Newell, "The dynamics of resting and postural tremor in Parkinson's disease," *Clinical Neurophysiology*, vol. 111, pp. 2046–2056, 2000.
- [80] J. M. Belda-Lois, J. Sanchez-Lacuesta, M. J. Vivas-Broseta, E. Rocon, L. Bueno, and J. L. Pons, "Tremor movement analysis techniques: an approach towards ambulatory systems," *Assistive Technology-Shaping the Future*, vol. 11, pp. 827–831, 2003.
- [81] M. M. Sturman, D. E. Vaillancourt, L. V. Metman, R. A. Bakay, and D. M. Corcos, "Effects of subthalamic nucleus stimulation and medication on resting and postural tremor in Parkinson's disease," *Brain*, vol. 127, pp. 2131–2143, 2004.

- [82] A. C. Leal, "Neuroengineering Contributions in Parkinsonic Tremor Characterization Using Accelerometry and Surface Electromyography," Master's thesis, The University of Coimbra, Coimbra, Portugal, 2015.
- [83] J. A. Gallego, E. Rocon, J. O. Roa, J. C. Moreno, and J. L. Pons, "Real-time estimation of pathological tremor parameters from gyroscope data," *Sensors*, vol. 10, pp. 2129–2149, 2010.
- [84] R. E. Kalman, "A new approach to linear filtering and prediction problems," *Journal of Fluids Engineering*, vol. 82, pp. 35–45, 1960.
- [85] C. N. Riviere, S. G. Reich, and N. V. Thakor, "Adaptive Fourier modeling for quantification of tremor," *Journal of Neuroscience Methods*, vol. 74, pp. 77–87, 1997.
- [86] W. M. Cheung and W. H. Liao, "Continuous variable transmission and regenerative braking devices in bicycles utilizing magnetorheological fluids," in *Proceedings of SPIE 8688, Active and Passive Smart Structures and Integrated System*, 2013, pp. 868810-1–868810-12.
- [87] J. T. Belter and A. M. Dollar, "A passively adaptive rotary-to-linear continuously variable transmission," *IEEE Transactions on Robotics*, vol. 30, pp. 1148–1160, 2014.
- [88] J. Sun, W. Fu, H. Lei, E. Tian, and Z. Liu, "Rotational swashplate pulse continuously variable transmission based on helical gear axial meshing transmission," *Chinese Journal of Mechanical Engineering*, vol. 25, pp. 1138–1143, 2012.
- [89] Y. Q. Chen, P. K. Wong, Z. C. Xie, H. W. Wu, K. U. Chan, and J. L. Huang, "Modelling of a novel dual-belt continuously variable transmission for automobiles," *World Academy of Science Engineering and Technology*, vol. 70, pp. 1157–1161, 2012.
- [90] H. Yamada, "A Radial Crank-type continuously variable transmission driven by two ball screws," in *Proceedings of IEEE International Conference on Robotics and Automation, St. Paul, Minnesota, USA, May 14–18, 2012*, pp. 1982–1987.
- [91] X. F. Wang and W. D. Zhu, "Design, modeling, and simulation of a geared infinitely variable transmission," *Journal of Mechanical Design*, vol. 136, 071011-1–071011-9, 2014.
- [92] D. Rockwood, N. Parks, and D. Garmire, "A continuously variable transmission for efficient urban transportation," *Sustainable Materials and Technologies*, vol. 1, pp. 36–41, 2014.
- [93] N. Sclater and N. P. Chironis, *Mechanisms and Mechanical Devices Sourcebook*. New York: McGraw-Hill, 2001.
- [94] C. Moore, M. Peshkin, and J. E. Colgate, "Design of a 3R cobot using continuous variable transmissions," in *Proceedings of IEEE International Conference on Robotics and Automation, Detroit, Michigan, USA, May 10–15, 1999*. vol. 4, pp. 3249–3254.
- [95] M. Peshkin, J. E. Colgate, W. Wannasuphoprasit, C. Moore, R. B. Gillespie, and P. Akella, "Cobot architecture," *IEEE Transactions on Robotics and Automation*, vol. 17, pp. 377–390, 2001.
- [96] E. L. Faulring, T. Moyer, J. Santos-Munne, A. Makhlin, J. E. Colgate, and M. Peshkin, "Continuously Variable Transmission with Multiple Outputs," *U.S. Patent No. 8,251,863*. Washington, DC: U.S. Patent and Trademark Office, 2012.
- [97] J. M. Belda-Lois, E. Rocon, J. J. Sanchez-Lacuesta, A. F. Ruiz, and J. L. Pons, "Estimation of the biomechanical characteristics of tremorous movements based on gyroscopes," in *8th European Conference for the Advancement of Assistive Technology in Europe, Assistive Technology from Virtuality to Reality, Lille, France, September 6–9, 2005*, pp. 138–1425.
- [98] J. W. Hurst, "The Role and Implementation of Compliance in Legged Locomotion," Ph.D. dissertation. Carnegie Mellon University, Pittsburgh, Pennsylvania, USA, 2008.
- [99] A. D. Deshpande, R. Balasubramanian, J. Ko, and Y. Matsuoka, "Acquiring variable moment arms for index finger using a robotic testbed," *IEEE Transactions on Biomedical Engineering*, vol. 57, pp. 2034–2044, 2010.

- [100] A. Gupta and M. K. O'Malley, "Design of a haptic arm exoskeleton for training and rehabilitation," *IEEE/ASME Transactions on Mechatronic*, vol. 11, pp. 280–289, 2006.
- [101] C. Majidi, R. E. Groff, Y. Maeno, B. Schubert, S. Baek, B. Bush, R. Maboudian, N. Gravish, M. Wilkinson, K. Autumn, and R. S. Fearing, "High friction from a stiff polymer using microfiber arrays," *Physical Review Letters*, vol. 97, pp. 076103-1–076103-4, 2006.
- [102] L. Ge, S. Sethi, L. Ci, P. M. Ajayan, and A. Dhinojwala, "Carbon nanotube-based synthetic gecko tapes," in *Proceedings of the National Academy of Sciences*, vol. 104, pp. 10792–10795, 2007.
- [103] L. Shen, N. J. Glassmaker, A. Jagota, and C. Y. Hui, "Strongly enhanced static friction using a film-terminated fibrillar interface," *Soft Matter*, vol. 4, pp. 618–625, 2008.

Appendix A

Software Development for Data Acquisition

A customized graphical user interface (GUI) was developed to manage data transfer from the sensing devices to a PC. The function of the software is given below:

1. To collect inertial information from 5 IMUs, position information from an Aurora system and EMG information from a Myo (Thalmic Labs Inc.) arm band (the EMG data were not studied in this work).
2. To synchronize all data to the same timestamp.
3. To include all five tasks with visual instructions.
4. To count time duration for each task.

The GUI was developed in C++ using windows form in Visual Studio 2013. A screen shot of the GUI is shown in Fig. A.1. Prior to the start of data collection, an initialization process must be performed to set the sensing system to the ready state. After each task, a folder labeled with the task number and patient number is created for each data file.

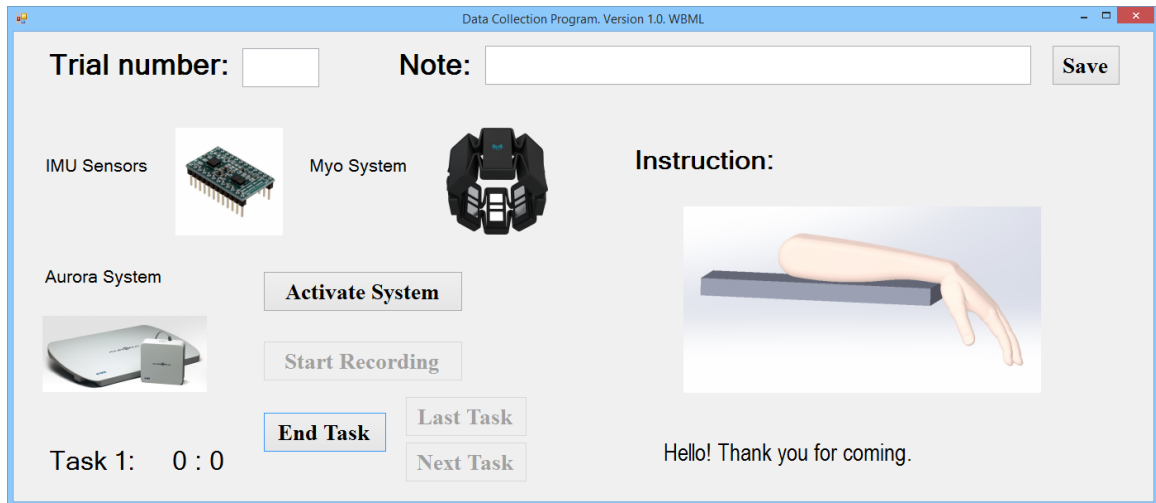


Figure A.1: Graphical user interface for hand tremor data acquisition.

Appendix B

Permissions and Approvals

The following forms and approval are presented in this Appendix:

- Ethics approval for the PD hand tremor assessment from the Western University Health Science Research Ethics Board (HSREB)
- Consent form for the participant of the tremor assessment study



**Western
Research**

Research Ethics

**Western University Health Science Research Ethics Board
HSREB Amendment Approval Notice**

Principal Investigator: Dr. Mary Jenkins

Department & Institution: Schulich School of Medicine and Dentistry/Clinical Neurological Sciences, London Health Sciences Centre

Review Type: Expedited

HSREB File Number: 106172

Study Title: Assessment of Hand Tremor

Sponsor:

HSREB Amendment Approval Date: June 17, 2015

HSREB Expiry Date: February 20, 2016

Documents Approved and/or Received for Information:

Document Name	Comments	Version Date
Instruments	Revised list of instruments	2015/05/20
Revised Letter of Information & Consent		2015/05/20
Revised Western University Protocol		2015/05/20

The Western University Health Science Research Ethics Board (HSREB) has reviewed and approved the amendment to the above named study, as of the HSREB Initial Approval Date noted above.

HSREB approval for this study remains valid until the HSREB Expiry Date noted above, conditional to timely submission and acceptance of HSREB Continuing Ethics Review.

The Western University HSREB operates in compliance with the Tri-Council Policy Statement Ethical Conduct for Research Involving Humans (TCPS2), the International Conference on Harmonization of Technical Requirements for Registration of Pharmaceuticals for Human Use Guideline for Good Clinical Practice Practices (ICH E6 R1), the Ontario Personal Health Information Protection Act (PHIPA, 2004), Part 4 of the Natural Health Product Regulations, Health Canada Medical Device Regulations and Part C, Division 5, of the Food and Drug Regulations of Health Canada.

Members of the HSREB who are named as Investigators in research studies do not participate in discussions related to, nor vote on such studies when they are presented to the REB.

The HSREB is registered with the U.S. Department of Health & Human Services under the IRB registration number IRB 00000949.



LAWSON
HEALTH RESEARCH INSTITUTE



Letter of Information

Title: Assessment of Hand Tremor.

You are invited to participate in a research study of the dynamic characteristics of hand tremor in individuals with Parkinson's disease. This information will be used to identify the characteristics of Parkinson's tremor in order to develop a tremor suppression glove. This study is being conducted by the following researchers:

Dr. Mary Jenkins, MD, FRCPC (Principal Investigator)

Associate Professor, Department of Clinical Neurological Sciences
The University of Western Ontario
University Hospital, 339 Windermere Road, London, Ontario, N6A 5A5

Dr. Ana Luisa Trejos, Ph.D. (Co-Investigator)

Assistant Professor, Department of Electrical and Computer Engineering
The University of Western Ontario, London, Ontario, N6A 5B9
Associate Scientist, Canadian Surgical Technologies & Advanced Robotics (CSTAR)
Lawson Health Research Institute, 339 Windermere Road, London, Ontario, N6A 5A5

Dr. Michael Naish, Ph.D. (Co-Investigator)

Canadian Surgical Technologies & Advanced Robotics, Lawson Health Research Institute
Department of Mechanical and Materials Engineering, Department of Electrical and Computer Engineering, Faculty of Engineering
The University of Western Ontario

Mr. Yue Zhou (Student)

MESC student
Department of Electrical and Computer Engineering
Faculty of Engineering
The University of Western Ontario

Details of the Study:

The most obvious symptoms of Parkinson's disease (PD) are motion-related. These include tremor, rigid muscles, slowness of movement and difficulty with walking and gait. Tremor, among all of these symptoms, significantly affects patients' daily life, such as difficulty with eating and writing. Based on the level of the hand tremor that occurs at your hand, we invite you

Please Initial: _____



to participate in our study. The intent of this study is to develop a better understanding of the characteristics of tremor motion. With this knowledge we hope to design a device in the near future that can suppress (stop) hand tremor in individuals with PD.

No personal information will be collected during the experiments. The experiment is expected to take no more than 1.5 hours. An evaluation of the severity of the disease will be performed at the beginning. Then you will be asked to perform 5 different tasks: i) keep one arm at rest on a table, ii) maintain the hand 45° to the table, iii) reach for an object by moving the wrist, iv) move an object from one position to another position by moving the wrist, and v) draw a spiral on a tablet. A tracking device will be used to acquire data during each task. You will need to wear this device during the whole experiment.

While you perform the tasks, software will be used to record the acceleration, position, electromyography (EMG) signals of your hand and video images (of the device and hands only) so that we can relate the information recorded to the steps required to complete each task. The results from these experiments will be used to perform a thorough analysis to assess the characteristics of the tremor.

You do not waive any legal rights by signing the consent form. Participation in this study is voluntary. You may refuse to participate, refuse to answer any questions or withdraw from the study at any time with no effect on your health care.

Risks:

You may experience slight discomfort caused by the straps which will be used to fix your arm on the table.

Benefits:

Although you may not benefit directly from this study, your participation may contribute to our basic knowledge of tremor feature and how to incorporate this knowledge into improving the treatment of tremor in Parkinson's patients. A potential benefit may come at a future date, when a wearable device that suppresses hand tremor may become available. This device will be an adjunct treatment for people with Parkinsonian tremor, that does not improve with medication.

Confidentiality:

All data will be stored on a password protected personal computer (University of Western Ontario,). Hardcopies of any documents will be stored in locked cabinets in . The only documents containing your name will be the Consent Forms, which will not be linked to any of the recorded data. Access to records and

Please Initial: _____



data is limited to authorized persons. Your anonymity will be protected at all times by using alphanumeric codes when analyzing your experimental data.

This project is supported by a Discovery Grant of the Natural Sciences and Engineering Research Council (NSERC) of Canada, by the Western Strategic Support for NSERC Success Grant and by the Academic Development Fund, Western University. No commercial interest is stemming out of this project currently.

If you have any questions or concerns regarding participation in our study, please contact Dr. Jenkins or Dr. Ana Luisa Trejos at

If you have any questions about the conduct of this study or your rights as a research subject you may contact Dr. David Hill, Scientific Director, Lawson Health Research Institute at . A copy of this information package is yours to keep for your personal records.

Please Initial: _____



CONSENT FORM

Title of Research: Assessment of Hand Tremor

Principal Investigator: Dr. Mary Jenkins

Co-Investigators: Dr. Ana Luisa Trejos, Dr. Michael Naish

Collaborators: Yue Zhou

For the Participant:

I have read and understand the above information describing this study. I have had the purposes, procedures and technical language of this study explained to me. I have been given sufficient time to consider the above information and to seek advice if I chose to do so. I have had the opportunity to ask questions which have been answered to my satisfaction. I am voluntarily signing this form. I will receive a copy of this consent form for my information.

If at any time I have further questions, problems or adverse events, I can contact Dr. Mary Jenkins, the principal investigator of the project, at _____ or any of the investigators and collaborators on the project.

If I have any questions about your rights as a research participant or the conduct of this study, I may contact The Office of Research Ethics

By signing this consent form, I am indicating that I agree to participate in this study.

Name of Participant
 (Please print)

Signature of Participant

Date

Name of Person Obtaining
Informed Consent

Signature of Person Obtaining
Informed Consent

Date

Curriculum Vitae

Name: Yue Zhou

Post-secondary Education and Degrees: The University of Tianjin Polytechnic University
Tianjin, China
2007–2011 B.Eng. in Automation.

The University of Western Ontario
London, Ontario, Canada
2014–2015 M.E.Sc. in Electrical and Computer Engineering.

Related Work Experience Research Assistant
The University of Western Ontario
2014–2015

Teaching Assistant
The University of Western Ontario
2014–2015

Submitted Publications:

Y. Zhou, M. E. Jenkins, M. D. Naish, and A. L. Trejos, “The Measurement and Analysis of Parkinsonian Hand Tremor,” submitted to *International Conference on Biomedical and Health Informatics*, Las Vegas, Nevada, USA, February 24–27, 2016.